UNIVERSIDADE FEDERAL DE SANTA CATARINA
CAMPUS FLORIANÓPOLIS
PROGRAMA DE PÓS-GRADUAÇÃO EM CIÊNCIA E ENGENHARIA DOS MATERIAIS

Bruno Lessmann Fertig

On the Use of HDDR Powder Obtained from Nd-Fe-B End-of-Life Magnets as Raw Material for Laser Powder Bed Fusion

Florianópolis
2024

Bruno Lessmann Fertig

On the Use of HDDR Powder from Nd-Fe-B End-of-Life Magnets as Raw Material for Laser Powder Bed Fusion

Dissertação submetida ao Programa de Pós-Graduação em Ciência e Engenharia de Materiais da Universidade Federal de Santa Catarina para a obtenção do título de Mestre em Ciência e Engenharia de Materiais.

Orientador: Prof. Paulo Antônio Pereira Wendhausen, Dr.
Coorientador: Prof. Leonardo Ulian Lopes, Dr.

Florianópolis
2024

Fertig, Bruno Lessmann
On the Use of HDDR Powder from Nd-Fe-B End-of-Life Magnets as Raw Material for Laser Powder Bed Fusion / Bruno Lessmann Fertig ; orientador, Paulo Antônio Pereira Wendhausen, coorientador, Leonardo Ulian Lopes, 2024.
114 p.

Dissertação (mestrado) - Universidade Federal de Santa Catarina, Centro Tecnológico, Programa de Pós-Graduação em Ciência e Engenharia de Materiais, Florianópolis, 2024.

Inclui referências.

1. Ciência e Engenharia de Materiais. 2. Nd-Fe-B magnets. 3. Recycling. 4. Laser Powder Bed Fusion (LPBF). I. Wendhausen, Paulo Antônio Pereira . II. Lopes, Leonardo Ulian . III. Universidade Federal de Santa Catarina. Programa de Pós-Graduação em Ciência e Engenharia de Materiais. IV. Título.

Bruno Lessmann Fertig

On the Use of HDDR Powder Obtained from Nd-Fe-B End-of-Life Magnets as Raw Material for Laser Powder Bed Fusion

O presente trabalho em nível de Mestrado foi avaliado e aprovado, em 16 de Julho de 2024, pela banca examinadora composta pelos seguintes membros:

Prof. João Batista Rodrigues Neto, Dr.
Universidade Federal de Santa Catarina

Prof. Sergio Michielon de Souza, Dr.
Universidade Federal do Amazonas

Fernando Maccari, Dr.
Technische Universität Darmstadt

Certificamos que esta é a versão original e final do trabalho de conclusão que foi julgado adequado para obtenção do título de Mestre em Ciência e Engenharia dos Materiais.

Documento assinado digitalmente
Aloisio Nelmo Klein
Data: 12/08/2024 20:01:50-0300
CPF: ***.316.770-**
Verifique as assinaturas em https://v.ufsc.br
ICP-Edu

Coordenação do Programa de Pós-Graduação

Documento assinado digitalmente
Paulo Antonio Pereira Wendhausen
Data: 15/08/2024 09:53:26-0300
CPF: ***.380.839-**
Verifique as assinaturas em https://v.ufsc.br
ICP-Edu

Prof. Paulo Antônio Pereira Wendhausen, Dr.
Orientador

Florianópolis, 2024

ACKNOWLEDGEMNETS

First, I would like to express my gratitude to Prof. Dr. Paulo A. P. Wendhausen. His guidance and support were crucial for my work development at the Magnetic Materials Laboratory (MAGMA). His constructive suggestions and criticisms significantly influenced my research direction, contributing greatly to my professional and personal growth. My co-advisor, Prof. Dr. Leonardo U. Lopes, deserves special thanks for the productive partnership over these years. His availability and assistance were crucial to the development of this work.

I am grateful to the Brazilian research agencies that have supported this work: FAPESC, CNPq, and FINEP. Special thanks to Coordenação de Aperfeiçoamento de Pessoal de Nível Superior (CAPES) for the master's scholarship grant.

To Prof. Sérgio M. de Souza, coordinator of the Mineração urbana, reciclagem de ímãs permanentes de Terras Raras project (CNPq), I thank you for the opportunity to become more deeply involved with the subject and for the fruitful interactions that we had in the past years.

I express my gratitude to the Programa de Pós-Graduação em Ciência e Engenharia de Materiais at UFSC, represented by our secretary Rogério Campos, for the efficiency, agility, and willingness to assist postgraduate students.

To the colleagues at MAGMA who contributed to the development of this work, I thank you for the partnership and support over these years. Especially to Msc. Marcelo Rosa, for the constant collaboration and valuable contributions.

I thank the Institute of Technological Research (IPT) for the analyses of residual oxygen, carbon, and hydrogen content carried out throughout the work.

To Prof. Dr. Oliver Gutfleisch, from the Functional Materials Laboratory at the Technical University of Darmstadt, I thank you for the cordial reception and the opportunity to carry out the MOKE characterizations. Especially to Dr. Fernando Maccari, for all the assistance and companionship during this period.

I offer special thanks to my parents, who provided great understanding, encouragement, and support. Your help has stood by me from the very beginning of this journey.

Last but not least, I thank my best friend and fiancée, Nicolly Poletti. You have been by my side in all moments, whether they were of tears or smiles. You have been my greatest encourager and supporter. Thank you very much for your affection, care, patience, joy, and dedication.

AGRADECIMENTOS

Primeiro, gostaria de expressar minha gratidão ao Prof. Dr. Paulo A. P. Wendhausen. Sua orientação e apoio foram cruciais para o desenvolvimento do meu trabalho no Laboratório de Materiais Magnéticos (MAGMA). Suas sugestões e críticas construtivas influenciaram significativamente a direção da minha pesquisa, contribuindo muito para o meu crescimento profissional e pessoal. Meu coorientador, Prof. Dr. Leonardo U. Lopes, merece agradecimentos especiais pela parceria produtiva ao longo desses anos. Sua disponibilidade e assistência foram essenciais para o desenvolvimento deste trabalho.

Agradeço às agências de pesquisa brasileiras que apoiaram este trabalho: FAPESC, CNPq e FINEP. Agradecimentos especiais à Coordenação de Aperfeiçoamento de Pessoal de Nível Superior (CAPES) pela concessão da bolsa de mestrado.

Ao Prof. Sérgio M. de Souza, coordenador do projeto Mineração urbana, reciclagem de ímãs permanentes de Terras Raras (CNPq), agradeço pela oportunidade de me envolver mais profundamente com o tema e pelas interações frutíferas que tivemos nos últimos anos.

Expresso minha gratidão ao Programa de Pós-Graduação em Ciência e Engenharia de Materiais da UFSC, representado pelo nosso secretário Rogério Campos, pela eficiência, agilidade e disposição para auxiliar os estudantes de pós-graduação.

Aos colegas do MAGMA que contribuíram para o desenvolvimento deste trabalho, agradeço pela parceria e apoio ao longo desses anos. Especialmente ao Msc. Marcelo Rosa, pela constante colaboração e valiosas contribuições.

Agradeço ao Instituto de Pesquisas Tecnológicas (IPT) pelas análises de teor residual de oxigênio, carbono e hidrogênio realizadas ao longo do trabalho.

Ao Prof. Dr. Oliver Gutfleisch, do Laboratório de Materiais Funcionais da Universidade Técnica de Darmstadt, agradeço pela cordial recepção e oportunidade de realizar as caracterizações MOKE. Especialmente ao Dr. Fernando Maccari, por toda a assistência e companheirismo durante este período.

Ofereço agradecimentos especiais aos meus pais, que me proporcionaram grande compreensão, incentivo e apoio. Sua ajuda esteve ao meu lado desde o início desta jornada.

Por último, mas não menos importante, agradeço à minha melhor amiga e noiva, Nicolly Poletti. Você esteve ao meu lado em todos os momentos, sejam eles de lágrimas ou sorrisos. Você tem sido minha maior incentivadora e apoiadora. Muito obrigado pelo seu carinho, cuidado, paciência, alegria e dedicação.

ABSTRACT

The recycling of Nd-Fe-B magnets has garnered increasing attention due to the substantial volume of End-of-Life magnets, particularly from electric motors and wind generators. These magnets are highly valued for their rare earth element content, which is in significant demand for various technological applications. Recycling Nd-Fe-B magnets is a vital strategy for addressing resource scarcity and environmental sustainability challenges. Hydrogen-based methods, such as Hydrogen Decrepitation (HD), have been investigated for recycling these magnets by transforming them into powder suitable for reuse. Previous studies have examined reprocessing this powder into new, fully dense magnets. However, this approach can present certain drawbacks concerning the quality of the final magnets. The use of recycled powder as raw material for Additive Manufacturing (AM) to produce bonded magnets has not been extensively explored. Laser Powder Bed Fusion (LPBF) offers sustainable production methods with minimal waste during processing. Nonetheless, preparing recycled raw material for LPBF presents challenges due to its diminished magnetic properties following HD processing. Therefore, further development of the recycled powder is necessary to optimize its magnetic properties. This study investigates the use of hydrogen processing to prepare suitable recycled powders for LPBF. The process includes HD to transform the bulk End-of-Life magnet into powder, followed by Hydrogenation, Disproportionation, Desorption, Recombination (HDDR) to enhance coercivity and remanence values, thereby making it a suitable raw material for LPBF. Despite existing research on these processes, their specific roles in preparing recycled raw material for LPBF have not been thoroughly described. Additionally, this study examines the characteristics of recycled HDDR powder for producing bonded magnets through AM. Recycled HDDR powder with coercivity values up to 850 kA/m was successfully produced and incorporated into the feedstock composition for LPBF. The microstructure and magnetic properties of the printed bonded magnets are analyzed and compared with previous works in the literature. The findings of this study have significant implications for the production of recycled Nd-Fe-B bonded magnets using LPBF. Utilizing HDDR-processed rare earth powders as feedstock has the potential to reduce dependency on costly rare earth components and provide a more environmentally friendly approach to producing high-performance magnets.

Key words: Nd-Fe-B magnets; Recycling; Hydrogen Decrepitation (HD); Hydrogenation, Disproportionation, Desorption, Recombination (HDDR); Laser Powder Bed Fusion (LPBF).

RESUMO EXPANDIDO EM PORTUGUÊS

Introdução e Objetivos

Elementos de Terras Raras (ETR) são vitais em ímãs de alto desempenho, como em ligas à base de Nd-Fe-B, usadas em sistemas de energia renovável, veículos elétricos e eletrônicos. A demanda global por ETR está aumentando, mas a escassez de oferta e as flutuações de preços representam riscos. Tensões geopolíticas podem interromper cadeias de suprimento, destacando a necessidade de estratégias eficazes de gestão. A dominância da China no mercado de ETR levanta preocupações de dependência, levando a um impulso global por alternativas como reciclagem e reprocessamento de ímãs de TR.

Reutilizar ímãs em fim de vida melhora a sustentabilidade da cadeia de suprimentos ao reaproveitá-los para outras aplicações. No entanto, a reutilização direta é difícil devido aos requisitos de desmontagem e possíveis danos durante a desmagnetização térmica. O reprocessamento é uma opção mais viável, com métodos como a refusão da liga ou difusão redução com cálcio. O processo de Decrepitação por Hidrogênio (HD), que transforma ímãs Nd-Fe-B em fim de vida em pó sob uma atmosfera de hidrogênio, é particularmente eficiente para reciclagem e reutilização. O pó de Nd-Fe-B pode ser reprocessado em um novo ímã sinterizado usando técnicas convencionais de metalurgia do pó ou um método inovador aproveitando sua forma em pó. Com propriedades adequadas, ele serve como um material ideal para a tecnologia de Fusão em Leito de Pó a Laser (FLPL), um processo de Manufatura Aditiva (MA) que minimiza o desperdício e promove a produção eficiente de componentes. Um grande desafio na preparação de matérias-primas recicladas para FLPL é alcançar o máximo produto energia dos ímãs Nd-Fe-B. Isso envolve uma combinação entre elevadas propriedades intrínsecas da fase ferromagnética e uma microestrutura adequada resultante de algum processamento. Após o processo HD, os valores de propriedades magnéticas das partículas recicladas são baixas, limitando seu uso direto em FLPL. Etapas adicionais de processamento são necessárias para melhorar a coercividade e remanência no pó. Um método para ajustar as propriedades magnéticas é controlando a microestrutura através de técnicas específicas de processamento. O processo de Hidrogenação, Desproporção, Dessorção, Recombinação (HDDR) refina efetivamente os grãos da fase ferromagnética dura e promove alta coercividade no pó.

Este estudo examina a preparação e avaliação de pós reciclados de Nd-Fe-B para FLPL. Propõe um método para gerar matéria-prima reciclada a partir de ímãs de Nd-Fe-B em fim de vida utilizando dois processos por hidrogênio (HD e HDDR). Embora esses processos sejam amplamente documentados na literatura, sua aplicação na preparação de matéria-prima reciclada especificamente para FLPL não foi anteriormente explorada. Além disso, o estudo investiga a utilização desse material reciclado em FLPL e avalia como as propriedades do pó HDDR influenciam a produção de ímãs compósitos feitos por MA.

Metodologia

Neste estudo, foram utilizados pós ferromagnéticos à base de Nd-Fe-B e um sistema de ligante composto por poliamida 12 (PA-12). Esses pós ferromagnéticos foram obtidos a partir de ímãs em fim de vida (classe N42) que foram previamente utilizados em turbinas eólicas. O sistema de ligante PA-12 utilizado neste estudo foi obtido da classe DuraForm PA2200, que é fabricada pela 3Dsystems, um conhecido fornecedor de matérias-primas para impressão 3D. A escolha da PA-12 foi baseada em suas propriedades tecnológicas e térmicas, que a tornam adequada

para o processamento a laser. A metodologia para o processamento utilizada neste trabalho envolve três etapas principais, sendo estas a produção do pó ferromagnético, produção da carga de impressão e impressão de ímãs compósitos. A etapa inicial envolve a transformação do ímã em fim de vida em um pó friável com propriedades tecnológicas adequadas para utilização em FLPL. O pó resultante deve exibir altos valores de coercividade, tornando-o adequado para a produção de ímãs compósitos. Este processo de transformação emprega duas técnicas de processamento por hidrogênio: Decrepitação por Hidrogênio (HD) e Hidrogenação, Desproporção, Dessorção, Recombinação (HDDR). Esses métodos são utilizados tanto na pulverização quanto no endurecimento magnético do pó. Durante a etapa de produção da carga de impressão, o pó ferromagnético derivado do processo anterior é combinado com Poliamida 12 (PA-12) em diferentes frações volumétricas (30, 45, e 60% vol. PA-12). Esta combinação é utilizada para investigar e analisar várias composições de matéria-prima e sua influência nas propriedades finais dos ímãs compósitos impressos. Na etapa final, ímãs compósitos são produzidos usando uma máquina protótipo de manufatura aditiva por FLPL. Após a produção, os ímãs compósitos reciclados de Nd-Fe-B são submetidos a análises de microestrutura e avaliação de suas propriedades magnéticas

Resultados e Discussão

A análise microestrutural do ímã em fim de vida revelou características sobre seus constituintes e integridade. Através da microscopia eletrônica de varredura, fases distintas dentro do ímã foram reveladas, dentre estas a fase $Nd_2Fe_{14}B$ (φ) e a fase rica em Nd. A integridade microestrutural do ímã em fim de vida, incluindo a preservação da fase φ, foi confirmada através da análise da estrutura do domínio magnético. Os padrões labirínticos observados nas estruturas de domínio magnético tanto do ímã em fim de vida quanto de um ímã comercialmente disponível indicam a retenção de características críticas necessárias para ímãs de Nd-Fe-B reprocessados de alta qualidade. No entanto, o processo de reciclagem pode introduzir desafios relacionados à absorção de carbono e oxigênio, que podem impactar negativamente as propriedades magnéticas, especialmente em ímãs de Nd-Fe-B sinterizados. Os níveis iniciais mais altos de oxigênio e carbono em ímã em fim de vida, agravados por possíveis aumentos durante o reprocessamento, exigem consideração cuidadosa para manter e otimizar as propriedades magnéticas em ímãs reciclados.

A caracterização magnética do pó decrepitado fornece informações sobre suas propriedades e potenciais aplicações em processos de MA. As propriedades magnéticas subótimas do pó, indicadas por seus baixos valores de remanência (0,18 T) e coercividade (70 kA/m), ressaltam a importância de entender os fatores que influenciam essas baixas propriedades. A presença de hidrogênio em solução sólida e a formação de α-Fe durante o processo HD contribuem para a coercividade reduzida do pó. A análise microestrutural revela a presença de grãos poliédricos originados da fase φ, bem como fissuras e irregularidades induzidas pelo processo HD. Essas características afetam as propriedades tecnológicas do pó, como fluidez e densidade de empacotamento, que são críticas para processos de manufatura aditiva como FLPL. Para garantir a adequação do pó HD para aplicações am MA, processos de peneiramento são realizados para atingir a distribuição de tamanho de partículas recomendada. Apesar da mínima coercividade dentro da faixa de tamanho desejada, o pó pode passar por processamento adicional, como HDDR, para ajustar sua coercividade conforme necessário.

A otimização do tratamento HDDR focou principalmente na variação da temperatura de patamar, pois foi identificada como o fator mais influente na determinação dos valores de coercividade. As curvas de desmagnetização das amostras processadas em diferentes

temperaturas de HDDR revelaram um aumento significativo nos valores de coercividade com patamares de temperatura mais elevados. O processamento a 940 °C resultou em um valor de coercividade de 850 kA/m, representando uma melhoria substancial em relação ao pó HD inicial. A comparação com pós comercialmente disponíveis demonstrou que o pó HDDR alcançou valores de coercividade comparáveis aos padrões da indústria. Isso sugere a viabilidade de usar matérias-primas recicladas para produzir ímãs compósitos usando FLPL. A análise microestrutural revelou que o processo HDDR manteve o aspecto geral do pó enquanto refinava a estrutura do grão. A morfologia irregular das partículas após o processamento HDDR pode impactar propriedades tecnológicas como fluidez e densidade de empacotamento, críticas para FLPL. A diminuição do conteúdo de hidrogênio após o processamento HDDR indica recombinação e remoção bem-sucedidas do hidrogênio, essenciais para restaurar a fase $Nd_2Fe_{14}B$ e alcançar os valores de coercividade desejados. Embora um aumento no conteúdo de oxigênio tenha sido observado após o processamento HDDR, isso não prejudicou significativamente a rota de reprocessamento escolhida neste estudo.

A seção final deste estudo envolveu o uso do pó reciclado desenvolvido em FLPL para fabricar ímãs compósitos impressos. Em relação à caracterização geométrica dos ímãs obtidos, os valores de densidade e porosidade variaram significativamente dependendo da fração volumétrica de ligante polimérico (PA-12) na carga de impressão, com concentrações mais altas resultando em ímãs mais densos e com menor porosidade. A imagem de MEV forneceu confirmação visual das características microestruturais, revelando a presença de poros e a distribuição das partículas HDDR dentro da matriz polimérica.

Em relação às propriedades magnéticas dos ímãs impressos, a diminuição observada nos valores de coercividade em relação ao pó HDDR foi atribuída à rotação das partículas HDDR durante a magnetometria, facilitada pela ligação incompleta entre as partículas ferromagnéticas e a matriz de PA-12. Os resultados também sugerem a possibilidade de mudanças microestruturais nas partículas ferromagnéticas afetadas pelo laser durante o processo de FLPL, potencialmente explicando a diminuição observada na coercividade. Mais pesquisas são necessárias para elucidar a relação entre variáveis de processamento e coercividade, particularmente no que diz respeito às características únicas do pó HDDR derivado de ímãs em fim de vida.

Considerações Finais

As comparações com a literatura existente evidenciam a competitividade dos ímãs compósitos desenvolvidos neste estudo, especialmente considerando o uso de pó HDDR reciclado proveniente de ímãs em fim de vida. O estudo demonstrou que os ímãs fabricados por impressão 3D, mesmo sem a otimização dos parâmetros de processamento, apresentaram valores de coercividade comparáveis aos obtidos com o uso de pó comercial esférico de Nd-Fe-B. Esses resultados destacam o potencial dos materiais reciclados para aplicações em MA.

Uma característica notável do material particulado derivado da reciclagem e reutilização de ímãs em fim de vida é sua capacidade de criar pós com textura cristalográfica através do processo de HDDR. Especificamente, o processo d-HDDR produz pós anisotrópicos que podem ser alinhados durante ou após o processamento a laser em MA. Este alinhamento facilita a potencial otimização dos valores de remanência dos ímãs reciclados produzidos por FLPL.

FIGURE LIST

TABLE LIST

ACRONYMS LIST

BSE - Backscattered electrons

SE - Secondary Electrons

LPBF - Laser Powder Bed Fusion

SLS - Selective Laser Sintering

HS - Hatch spacing

LASER - Light Amplification by Stimulated Emission of Radiation

LP - Laser power

LS - Laser scan speed

LT - Layer thickness

STL - Standard Tesselation Language

AM - Additive Manufacturing

SEM - Scanning Electron Microscopy

PA-12 - Polyamide-12

HD - Hydrogen Decrepitation

HDDR - Hydrogenation, Disproportionation, Desorption, Recombination

REEs - Rare-Earth Elements

SYMBOLS LIST

B – Magnetic Induction

M – Magnetization

J – Magnetic Polarization

H – Applied Magnetic Field

μ – Permeability

μ_0 – Permeability of free space

H_A – Anisotropy Field

H_{cb} – Inductive Coercivity

H_{cj} – Intrinsic Coercivity;

B_r – Remanence;

$(BH)_{max}$ – Maximum energy product;

Nd-Rich – Neodymium rich phase;

ρ – Density

φ – $Nd_2Fe_{14}B$ phase

SUMMARY

1 INTRODUCTION AND OBJECTIVES

In the context of the rapidly advancing technological landscape, the significance of rare-earth elements (REEs) in the fabrication of high-performance permanent magnets cannot be overstated. These magnets, predominantly comprising neodymium-iron-boron (Nd-Fe-B) alloys, serve as essential components underpinning a wide array of contemporary technological advancements. Their applications extend from renewable energy systems, such as wind turbines and electric vehicles, to consumer electronics including smartphones and laptops [1].

The escalating global demand for rare-earth materials presents a substantial challenge, primarily due to the heightened risk of supply scarcity and price volatility, which can destabilize economic conditions. Additionally, the supply chain for these elements is vulnerable to disruptions caused by geopolitical tensions and international trade disputes [2]. These factors collectively necessitate the development of effective strategies to manage the supply and demand of these critical components, thereby ensuring the continued progress and development of a technology-dependent society.

China is currently the world's predominant source of REEs, notably Nd, Pr, and Dy. This monopolistic control by a single nation over such critical resources has raised significant concerns regarding global dependence. The implications of this dependency are extensive, necessitating a concerted global response. Consequently, there has been a substantial surge in the exploration of alternative solutions aimed at mitigating this reliance. These strategies encompass the discovery of new reserves and the advancement of technologies capable of efficiently recycling these elements. Recent years have witnessed a marked increase in research activities dedicated to the recycling and reprocessing of rare earth-based magnets. This trend is a global phenomenon, reflecting a collective endeavor to tackle this critical issue [3, 4].

Permanent magnets based on rare-earth alloys contain a significant proportion of REEs, comprising approximately 30% of their composition [5]. This substantial presence of REEs in permanent magnets presents an opportunity for these materials to serve as a secondary source of rare-earth elements. Despite the vast potential of REE recovery, the current recycling rates remain alarmingly low, at less than 1% [6]. Several factors contribute to this low recycling rate, including inadequate logistics for the collection of REE-containing products, limited information regarding the quantities of available RE materials for recycling, and product designs that do not facilitate easy recycling.

Given the economic significance of REEs and the considerable risks associated with their supply chain, the European Commission has classified REEs as critical elements [2, 6]. This classification highlights the urgency and importance of improving recycling rates and developing more sustainable practices in the utilization of REEs. Increasing the efficiency of REE recycling processes is essential to ensure a stable and secure supply of these critical materials, which are vital for numerous technological applications.

A promising strategy for enhancing supply chain sustainability is the reuse of End-of-Life magnets. This approach involves repurposing used magnets for different components or applications. However, direct reuse is challenging due to the need for disassembly, which often requires high temperatures for thermal demagnetization [7]. This process can potentially damage the magnet's coating or degrade its performance [8], making direct reuse less ideal. Consequently, reprocessing has emerged as a more viable strategy. Various methods for reprocessing have been documented in the literature, ranging from direct remelting of the alloy [9] to reduction diffusion with calcium [10]. Despite these approaches, they have been found to be less efficient compared to those involving hydrogen [11, 12]. Among these, the Hydrogen Decrepitation (HD) process, which is conducted under a hydrogen atmosphere, is particularly noteworthy. This method transforms Nd-Fe-B End-of-Life magnets into powder, facilitating their recycling and reuse.

The Nd-Fe-B powder can be reprocessed into a new sintered magnet through conventional powder metallurgy techniques [13]. Alternatively, it can be utilized in a novel processing method that capitalizes on its powder form. When prepared with the appropriate technological and magnetic properties, the powder serves as an ideal raw material for Laser Powder Bed Fusion (LPBF) technology [14, 15]. This Additive Manufacturing (AM) approach offers significant advantages, including minimal material waste, thereby promoting a sustainable and efficient production method [16].

A significant challenge in the preparation of recycled raw materials for LPBF is achieving the high maximum energy product characteristic of Nd-Fe-B magnets. This development involves a complex interplay of factors, including the intrinsic properties of the ferromagnetic phase and the microstructure resulting from processing. Following the HD process, the magnetic properties of the decrepitated particles are notably low. This limitation restricts the direct application of the HD product in LPBF processing. Consequently, additional strategic processing steps are essential to enhance the coercivity and remanence values in the powder [17].

A viable method to tailor magnetic properties involves controlling the microstructure resulting from specific processing techniques. One effective strategy for refining the grains of the hard ferromagnetic phase and simultaneously promoting high coercivity values in the powder is the Hydrogenation, Disproportionation, Desorption, Recombination (HDDR) process [18, 19].

This study examines the preparation and evaluation of recycled Nd-Fe-B powders for LPBF. It proposes a method to generate recycled raw material from End-of-Life Nd-Fe-B magnets by employing two hydrogen-based processes (HD and HDDR). Although these processes are extensively documented in the literature [11, 12, 20, 21], their application in preparing recycled raw material specifically for LPBF has not been previously explored. Furthermore, the study will investigate the utilization of this recycled material in LPBF and assess how the properties of HDDR powder influence the production of bonded magnets.

To achieve the research goals, the following specific objectives were established:

- To utilize HD to transform the End-of-Life bulk magnet into a friable powder.
- To assess the suitability of HD powder as a feedstock for LPBF by performing a sieving process using a 106 μm sieve. This procedure follows established literature insights [22 – 24] to ensure adherence to recommended particle size and distribution standards.
- To generate high coercive powder through the Hydrogenation, Disproportionation, Desorption, Recombination (HDDR) process.
- To identify the optimal set of HDDR processing parameters that yield a coercivity value of approximately 800 kA/m for the powder. This target is based on findings from prior optimizations in other studies [25, 26], demonstrating the feasibility of using the produced recycled material in LPBF processes.
- To manufacture bonded magnets employing the LPBF additive manufacturing technique.
- To characterize the as-printed bonded recycled magnets in terms of their microstructural and magnetic properties.

2 FUNDAMENTATION

This chapter is systematically structured into three primary sections:

- Section 2.1 delves into the fundamental properties of ferromagnetic materials. This section also provides a comprehensive analysis of permanent magnets, elaborated further in subsection 2.1.1.
- Section 2.2 is dedicated to the processing techniques of permanent magnets, with a particular emphasis on Nd-Fe-B based magnets. It starts with an exploration of sintered Nd-Fe-B magnets in section 2.2.1, followed by a detailed examination of bonded magnets in section 2.2.2. This includes an account of the production methods for ferromagnetic particles, focusing on Rapid Solidification (subsection 2.2.2.1) and Hydrogenation, Disproportionation, Desorption, Recombination (HDDR) processes (subsection 2.2.2.2). The section concludes with an overview of the current recycling practices for Nd-Fe-B magnets, detailed in subsection 2.2.3.
- The final section, Section 2.3, addresses the advancements in additive manufacturing. Section 2.3.1 highlights various additive manufacturing technologies, while section 2.3.2 explores the state-of-the-art developments in the additive manufacturing of Nd-Fe-B bonded magnets.

2.1 FERROMAGNETIC MATERIALS

At the core of magnetic behavior there is the idea of magnetic dipoles, similar to their electric counterparts. These magnetic dipoles, visualized as small bar magnets with both north and south poles for example, can align themselves when exposed to a magnetic field. This alignment happens because of the torque exerted on the dipoles, making them orient themselves in a particular direction with respect to the magnetic field [27]. In a ferromagnetic solid like α -Fe, for example, each atom represents such a dipole. The way these intrinsic dipoles respond under the influence of an external magnetic field dictates the magnetic behavior of the solid.

The origin of these intrinsic dipoles is related to the magnetic moments of individual electrons. These magnetic moments come from the combined effects of the orbital motion and spin of electrons within an atom. When electrons move in their orbits around the nucleus, they create a small magnetic field. The inherent spin of electrons also adds to their magnetic moment,

aligning along their axis of rotation. These magnetic moments are important for the overall magnetic behavior of materials and affect their magnetic properties on a larger scale [27].

The magnetic induction (B), magnetization (M), and magnetic polarization (J) are fundamental concepts in the study of magnetic and electric fields within materials. Magnetic induction, also known as magnetic flux density, represents the intensity of the magnetic field within a material. The relationship between magnetic induction (B) and the externally applied magnetic field (H) is described by the Equation 1 [28],

$$B = \mu \times H \qquad \text{(Eq. 1)}$$

where μ denotes the magnetic permeability of the medium, which is quantified in units such as webers per ampere-meter (Wb/A·m) or henries per meter (H/m). This parameter characterizes the medium's ability to transmit and amplify the magnetic field [29, 30]. Magnetic induction (B) is measured in Tesla (T), while the applied magnetic field (H) is quantified in kiloamperes per meter (kA/m).

Magnetization represents the magnetic moment per unit volume of a material. For a uniformly magnetized ferromagnetic bar, the relationship between magnetic induction (B), applied magnetic field (H), and magnetization (M) is given by Equation 2,

$$B = \mu_0 \times (H + M) \qquad \text{(Eq. 2)}$$

where μ0 represents the permeability constant of free space. Within a magnet, the H-field, which is oriented oppositely to the magnetization (M), is termed the demagnetizing field. Conversely, outside the magnet, this field is referred to as the stray field. Additionally, magnetic polarization (J), a term frequently used by electrical engineers, is defined by the Equation 3 [28].

$$J = \mu_0 \times M \qquad \text{(Eq. 3)}$$

This leads to the relationship expressed in Equation 4.

$$B = \mu_0 \times H + J \qquad \text{(Eq. 4)}$$

Paramagnetic materials display unique properties because they have unpaired electron spins in their crystalline structure. These unpaired electrons form atomic magnetic dipoles, acting like tiny magnets within the material. Without an external magnetic field, these dipoles are randomly oriented, resulting in a cancellation of magnetic moments and no overall magnetization of the material. However, when an external magnetic field is applied, these dipoles weakly align themselves with the field's direction due to the interaction between the magnetic moments and the external field, which exerts a torque on the atomic dipoles. Consequently, the material becomes weakly magnetized towards the applied field, showing a slight attraction to it. Once the external magnetic field is removed, the dipoles lose their alignment and return to their random orientation, causing the material to return to its original state with no net magnetization [29].

Different to a paramagnetic substance, an important characteristic of ferromagnetic materials is their capacity for long-range magnetic order, which is observed in a substantial majority of magnetic moments pointing in the same direction within smaller volumes known as domains. These domains, as depicted in Figure 1, represent regions where multiple magnetic moments are predominantly oriented in one direction. This alignment of magnetic moments within domains is a key property of ferromagnetic materials and plays a crucial role in their magnetic behavior [27].

Figure 1 – Schematic domain structure of a typical unmagnetized magnet

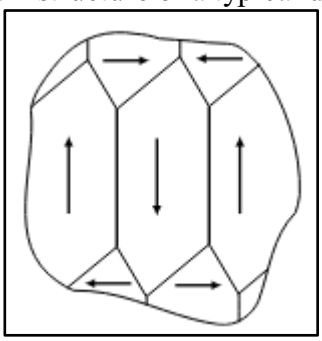

Source: [29]

The hysteresis graph effectively illustrates the interaction between an applied magnetic field (H) and the magnetic induction (B) of a ferromagnet, as demonstrated in Figure 2. This graph visually depicts the material's response to variations in the external magnetic field. Upon the application of an external field, the magnetic domains within the ferromagnetic material progressively align in the direction of the field until they reach a state of saturation. At

saturation, further increases in the external field do not result in additional alignment of the domains.

Figure 2 - Hysteresis loop of a ferromagnetic material illustrating the relationship between applied magnetic field (H) and magnetic induction (B), including domain alignment and saturation points

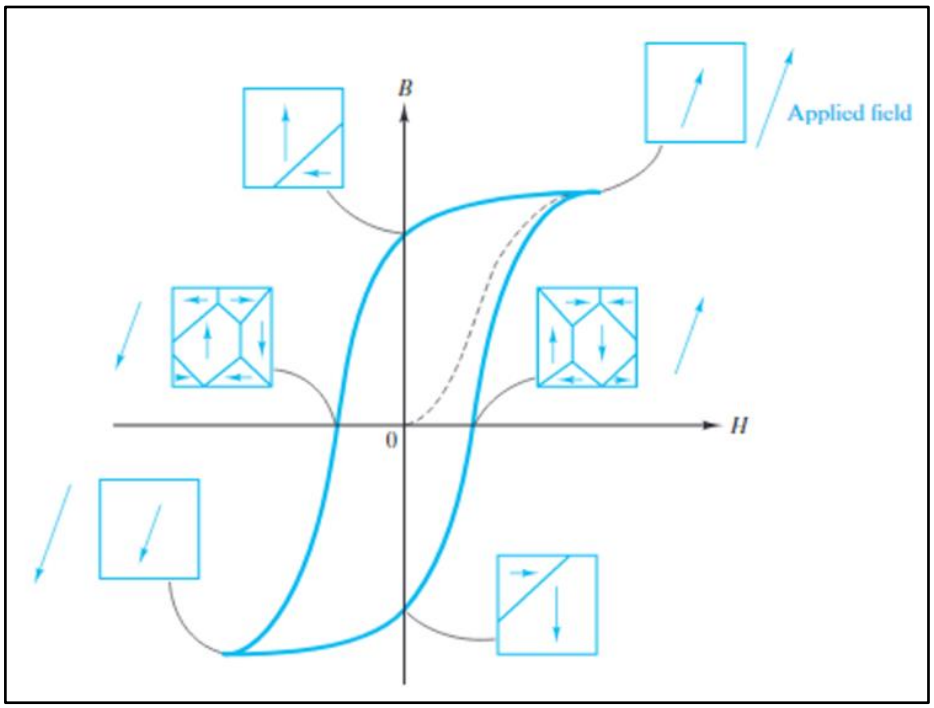

Source: [30]

Notably, when the external field is reduced to zero, the domains do not completely randomize due to the material's coercivity, which is a measure of its resistance to demagnetization. Coercivity prevents the full misalignment of domains in the absence of an external field. When the external field is reversed, the domains begin to reorient in the opposite direction. This reorientation process persists until the material's internal magnetic reaches zero, resulting in demagnetization. The coercivity value is a critical parameter, representing the minimum external field strength required to reduce the material's overall magnetization to zero [29, 30].

Figure 3 presents a visual representation of (a) a complete hysteresis curve, illustrating the responses of both magnetization (M) and magnetic induction (B). The induction, B, corresponds to the magnetic flux density and is represented as M - H. Additionally, (b) depicts the demagnetization curve, which is the second quadrant of a full loop hysteresis curve for a

permanent magnet. This section of the curve is crucial as it demonstrates the calculation of the maximum energy product, represented by the shaded area under the B curve [31].

Figure 3 –Complete hysteresis loop and demagnetization curve for a permanent magnet: (a) Full hysteresis curve illustrating the responses of both magnetization (M) and magnetic induction (B). (b) Demagnetization curve, which is the second quadrant of a full loop hysteresis curve for a permanent magnet.

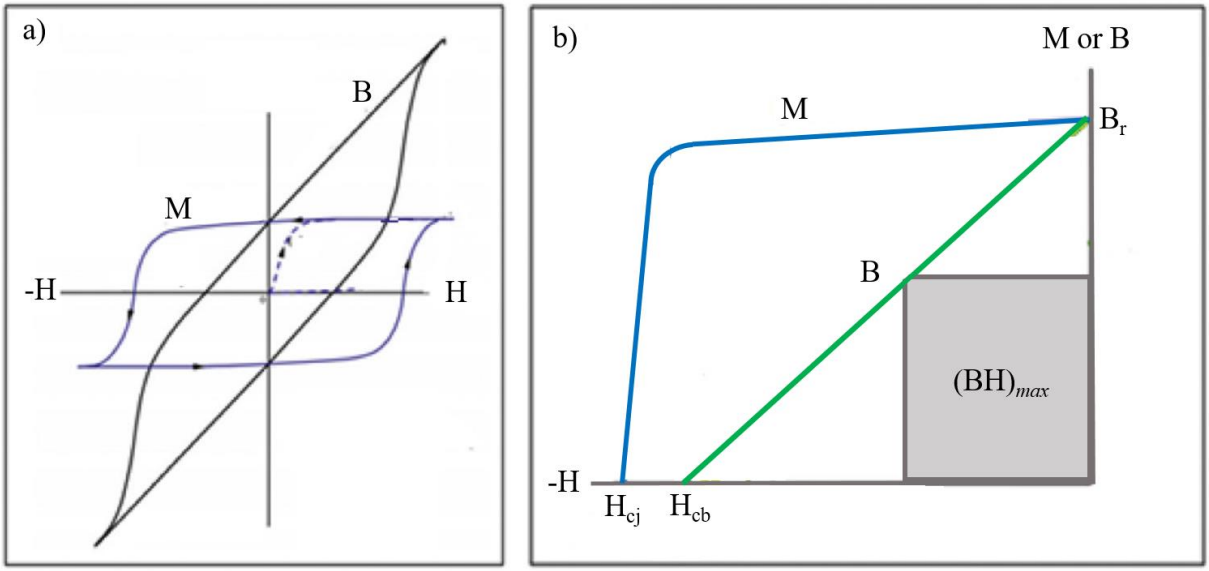

Source: Adapted from [31]

In Fig. 3 (a), the B curve illustrates the external magnetic flux density (B) as a function of the applied magnetic field (H). Notably, this curve does not exhibit saturation and continues to increase linearly with the applied field. In contrast, the M curve represents the internal magnetization (M) of the material. Unlike the B curve, the M curve reaches saturation, attaining a maximum value when all magnetic domains within the material are aligned.

The majority of essential information is derived from the second quadrant of the hysteresis loop, illustrated in Fig. 3(b). This quadrant reveals the values of residual magnetization, or remanence (B_r), intrinsic coercivity (H_{cj}), and inductive coercivity (H_{cb}). Additionally, it illustrates the calculation of the maximum energy product ($(BH)_{max}$), which is a critical parameter for the evaluation of permanent magnets.

Coercivity quantifies a magnet's resistance to demagnetization. Intrinsic coercivity (H_{cj}) refers to the strength of the opposing magnetic field required to reduce the internal magnetization (M) to zero. Inductive coercivity (H_{cb}) measures the opposing field strength

necessary to reduce the external flux density (B) to zero. Typically, H_{cb} is less than H_{cj} due to the impact of external factors [31].

Materials that show properties with easy demagnetization are classified as soft magnetic materials. Hard magnetic materials, which include permanent magnets, are characterized by their ability to retain magnetization even in the absence of an external magnetic field. This property of retaining magnetization is related to an intrinsic property of the ferromagnetic substance called anisotropy field (H_A). For example, a magnet with hard magnetic properties based on Nd-Fe-B, whose main ferromagnetic phase is $Nd_2Fe_{14}B$, has a H_A of nearly 6000 kA/m, while for α-Fe, it is only 40 kA/m [32].

Remanence (B_r) is the residual magnetization left in a material after the external magnetic field is removed. It is identified at the point on the vertical axis where the B curve intersects after reducing the field to zero [29]. Moreover, an additional property used for classifying ferromagnetic materials is the maximum energy product $(BH)_{max}$. This value can be measured using the hysteresis loop and is determined by the largest square that can be found within the second quadrant of the B curve [33]. In practical terms, $(BH)_{max}$ signifies the maximum magnetic energy stored within each unit volume of the material, measured in kilojoules per cubic meter (kJ/m^3) in SI units or mega gauss-oersteds (MGOe) in CGS units.

2.1.1 Permanent Magnets

Permanent magnets are named so because they can maintain a high remanent magnetic induction (B_r) without the need for an external magnetic field (H). This allows permanent magnets to induce magnetic flux in a circuit without the input of electrical currents, such as in electromagnets. A wide range of compounds can be used for the fabrication of permanent magnets, and each one will have specific properties suitable for different applications.

Permanent magnets are characterized by their magnetic properties, namely remanence (B_r), coercivity (H_{cj}), and maximum energy product $(BH)_{max}$. Nd-Fe-B magnets have the highest $(BH)_{max}$ value among all other commercially available options. Figure 4 shows the evolution of the maximum product energy of permanent magnets throughout their development. It is possible to observe that during the 1920s, steels with a $(BH)_{max}$ of about 20 kJ/m^3 were used, and after the mid-20^{th} century, ferrites were developed with a $(BH)_{max}$ of 40 kJ/m^3 [34].

Figure 4 – The evolution of the maximum energy product of permanent magnets in function of the years

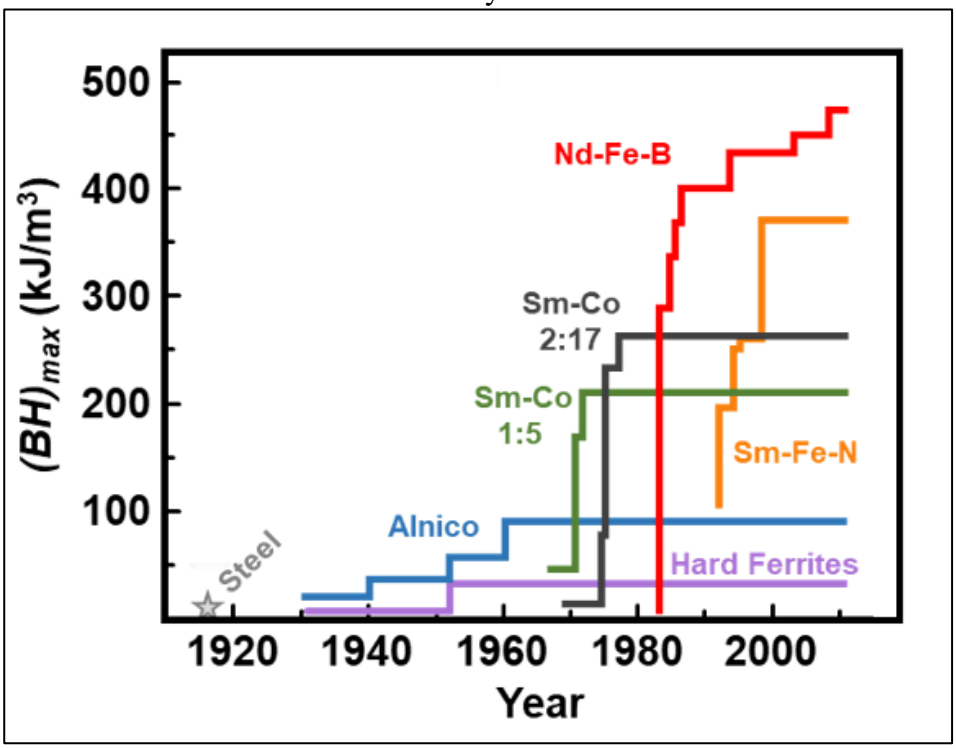

Source: Adapted from [35]

In the 1960s, the hexagonal $SmCo_5$ compound with a $CaCu_5$-type structure appeared as the first rare-earth high-performance magnets [32]. The compound has magnetic properties that make it suitable for use in permanent magnets, including a large uniaxial magnetocrystalline anisotropy (H_A ~ 40 T), a relatively high saturation magnetization (M_s ~ 1.14 T), and a high Curie temperature (T_c = 720°C). The $(BH)_{max}$ of this type of magnet reached 160 kJ/m^3. In 1967, the first permanent magnet based on rare earth alloys was made using the composition of $SmCo_{17}$. In 1973, a more developed form of this alloy was used with the composition Sm_2Co_{17}. However, Samarium and Cobalt are not desirable elements for large scale use due to their high cost and low availability. Therefore, during the 1970s, rare earth magnets based on iron systems were investigated as a potential alternative to the Sm-Co alloy [36].

In 1983, Sagawa from Sumitomo Special Metals Co. pioneered a new age of permanent magnet technology by developing a ternary compound, $Nd_2Fe_{14}B$. This compound was used to develop magnets with a $(BH)_{max}$ greater than 288 kJ/m^3, and later, values as high as 400 kJ/m^3 were achieved. The intrinsic magnetic properties of the $Nd_2Fe_{14}B$ phase are M_s = 1.6 T, H_A ~ 6000 kA/m, and T_c ~ 310 ºC. The development of magnets based on the body-centered

tetragonal $Nd_2Fe_{14}B$ phase was the result of joint efforts by Croat *et al*. [37, 38], who used melt-spinning, and Sagawa *et al*. [39 - 41], who used powder-metallurgy techniques [32].

Permanent magnets rely on rare-earth elements to achieve high levels of magnetocrystalline anisotropy, which is crucial for defining a preferred direction of magnetization within the material's crystallographic structure. In transition metals like iron, cobalt, and nickel, the coupling of orbital spins from 3d electrons is relatively weak. However, incorporating rare-earth elements introduces a strong magnetocrystalline anisotropy field due to the intense 4f electron spins [33]. This results in significantly enhanced magnetic properties. Specifically, in the $Nd_2Fe_{14}B$ compound, the majority of its intrinsic magnetocrystalline anisotropy is attributed to the crystal field splitting of the rare-earth 4f electron levels [37]. This splitting creates a strong directional preference for magnetization, contributing to the superior performance of these compounds.

The significant growth in applications began in 1995 with the first use of Nd-Fe-B sintered magnets in servo systems, compressors, lifting devices, Electric Power Steering (EPS) in automobiles, and driving units in hybrid vehicles. This growth is due to advancements in Nd-Fe-B sintered magnets in the following areas: (1) improved thermal stability with higher value of coercivity, (2) enhanced corrosion resistance through microstructural studies and surface coating technologies, and (3) increased benefits from high-performance magnets, such as electric power savings [32].

Apart from motor applications, permanent magnets have various uses in academic and military research, energy labs, and medical industries like Magnetic Resonance Imaging (MRI), hematology labs, and magnetic hyperthermia techniques. There are about 160 magnets used daily for different purposes, including refrigerator magnets, kitchen appliances, televisions, telephones, watches, computers, and audio systems, as well as in microelectronics. Additionally, around 100 magnets are used in the automobile industry. Therefore, permanent magnets are crucial for many important modern inventions [42].

The increasing demand for energy conversion has led to a rise in the production volume of magnetic components. The wind energy sector is growing faster than other sectors of renewable energy. For example, a generator unit with 3 MW uses approximately 1.5 tons of permanent magnets, and the cost of the magnetic component makes up a significant proportion of the total cost. In the transportation sector, according to Toyota, each Prius model uses a motor with 1.3 kg of Nd-Fe-B based magnets [34].

Rare-earth magnets have enabled the miniaturization of countless devices and the development of highly efficient motors and generators. These magnets are stronger than

conventional magnets made of ferrites or Alnico. Magnetism and magnetic materials have played an important role in modern science and technology since the discovery of the naturally occurring mineral magnetite (Fe_3O_4). The magnetic strength of a material is quantified by the maximum product energy. A higher $(BH)_{max}$ value indicates a stronger magnet, enabling the use of smaller magnets to achieve the same magnetic performance as larger magnets with a lower $(BH)_{max}$. Consequently, materials with a high $(BH)_{max}$ are advantageous in technological applications, as they allow for the design of compact, yet highly efficient, magnetic components [1].

2.2 PROCESSING Nd-Fe-B BASED MAGNETS

2.2.1 Sintered Magnets

Nd-Fe-B magnets must exhibit optimal properties for effective use in technological applications, which are intrinsically linked to their microstructural development during specific fabrication processes. Achieving these properties involves the development of coercivity mechanisms that enhance resistance to demagnetization. This is accomplished by introducing defects in the microstructure to hinder the movement of domain walls. Consequently, a well-engineered microstructure creates kinetic barriers that stabilize the magnetized state, preventing demagnetization processes such as the nucleation of reverse domains or magnetic decoupling [43, 44].

High-performance Nd-Fe-B magnets are fabricated through the sintering of magnetically aligned powders of Nd-Fe-B alloy, with a composition slightly enriched in Nd relative to the stoichiometric $Nd_2Fe_{14}B$ phase. To achieve a high $(BH)_{max}$, it is essential to maximize the remanence of the magnets. This necessitates minimizing the presence of minor non-ferromagnetic phases and ensuring full alignment of the easy axis of magnetization with the magnetization direction. Currently, powder metallurgy is the preferred processing method for manufacturing these magnets, as it allows for precise modification and control of the microstructure, thereby optimizing the magnetic properties [45]. Figure 5 provides a detailed overview of the powder metallurgy process used in the production of Nd-Fe-B sintered magnets.

Figure 5 – Overview of the steps involved in powder metallurgy processing for Nd-Fe-B sintered magnet fabrication

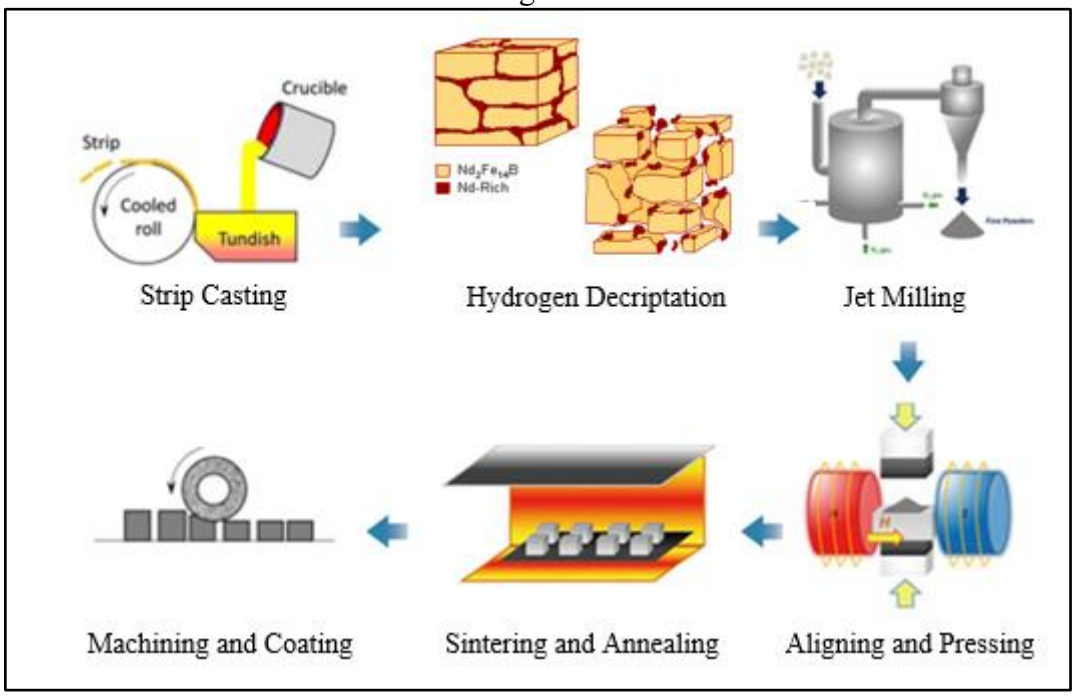

Source: Adapted from [46]

The $Nd_2Fe_{14}B$ compound is formed by a peritectic reaction between Fe and a liquid phase. During the casting process of Nd-Fe-B magnets, Fe precipitates as a primary phase from a molten alloy and tends to become a nucleation site for reverse domains. To fabricate high-performance magnets, the precipitation of primary Fe should be inhibited during the ingot fabrication process. Strip casting is a well-known process for preparing Nd-Fe-B ingots, as it can move the composition close to the stoichiometric composition without any precipitation of the Fe primary phase. The ingots prepared by Strip Casting consist of a columnar structure made up of a $Nd_2Fe_{14}B$ phase and a Nd-rich phase. The width of the columnar structure is around 4-6 μm, which is comparable to the particle size of fine powders after a milling process [32].

The coarse grinding of Nd-Fe-B ingots is achieved through a hydrogen-based process known as Hydrogen Decrepitation (HD). This method involves exposing Nd-Fe-B cast alloys to hydrogen, which disintegrates them into friable powders, making it significantly easier than mechanical pulverization [32]. Decrepitation occurs due to substantial volume expansions during hydrogen absorption in specific phases: 4.8% for $Nd_2Fe_{14}BH_{2.7}$ and 16.4% for NdH_3 [47]. Cracks in Nd-Fe-B alloys predominantly form at the interface between $Nd_2Fe_{14}B$ and Nd-rich phases following the HD process. Research indicates that HD is an effective and

economical additional step in the powder metallurgy route for producing sintered Nd-Fe-B permanent magnets [48].

The fabrication of fine powders is achieved using a jet mill, a widely adopted method due to its ability to grind friable or crystalline materials to a particle size of 3-5 μm, resulting in a very narrow size distribution [32]. The fine powder produced is then placed into molds and subjected to pulse magnetization to align the monocrystalline particles. The applied magnetic field orients the particles' easy magnetization axis, creating a crystallographic texture. This alignment produces anisotropic magnets with enhanced remanence and maximum energy product. Finally, the mold undergoes isostatic pressing to ensure sufficient mechanical strength for handling and subsequent furnace placement.

Following this, thermal cycles comprising sintering and heat treatment are employed. Sintering, a key process in powder metallurgy, transforms aggregated powder into densified blocks through diffusive atomic transport mechanisms at temperatures below the melting point of the primary constituent. This process reduces the system's free energy by decreasing the material's surface energy. During sintering, grain boundaries and necks form, leading to the densification of the part. The process is influenced by variables such as temperature, duration, sintering atmosphere, and the characteristics of the raw material, including powder size distribution and mean powder size. These factors are crucial in achieving full density and determining the final properties of the part. Smaller powder sizes result in larger surface areas and increased contact between particles, thereby enhancing the sintering mechanisms during the process [49].

Liquid Phase Sintering (LPS) plays a crucial role in the processing of Nd-Fe-B based magnets. LPS offers several advantages, including an increased sintering rate, near-total densification, and reduced sintering times, provided the liquid phase enhances wettability. The stages of LPS begin with the rearrangement of particles due to the penetration of molten material between solid phases, driven by capillary forces. This results in particle slipping and rapid densification, depending on the amount of liquid phase present. Additionally, material transport occurs through the liquid phase via diffusion mechanisms, followed by size accommodation and grain growth [50].

However, the Nd-rich phase is non-magnetic and prone to oxidation. This oxidation leads to the precipitation of soft magnetic phases, such as α-Fe, on the surface of the primary phases, which reduces coercivity. To produce high-performance Nd-Fe-B magnets, the atmosphere during sintering and annealing must be strictly controlled to prevent air exposure from crushing to annealing. Consequently, the volume fraction of the Nd-rich phase should be

minimized, and the composition of the sintered magnets should closely match the stoichiometric composition of $Nd_2Fe_{14}B$. [32].

Conventional sintered magnets are composed of two main phases: $Nd_2Fe_{14}B$ and Nd-rich. The coercivity mechanism in these magnets is typically attributed to the nucleation of reverse domains originating from defects on the surface of $Nd_2Fe_{14}B$ grains [32]. The Nd-rich phase transitions to a liquid phase at temperatures above 665°C and is present along grain boundaries, which smooths the surface of $Nd_2Fe_{14}B$ grains and reduces the number of nucleation sites. A microstructure featuring a thin layer of Nd-rich phase distributed along each grain boundary can enhance magnetic properties, particularly coercive force. This enhancement occurs because the Nd-rich phase decouples the primary ferromagnetic phases, thereby influencing the interactions between Nd-Fe-B grains and preventing the nucleation of reverse domains.

Figure 6 depicts the typical microstructure of sintered magnets in their as-sintered and annealed state. The grains of the primary $Nd_2Fe_{14}B$ phase are visible, exhibiting a uniform grey contrast. The brightly imaged regions at the triple junctions of the grain boundaries correspond to the Nd-rich phases, which can be either metallic dhcp-Nd or amorphous. These phases create different contrasts in the back-scattered electron (BSE) image obtained through scanning electron microscopy (SEM). Additionally, a thin, continuous layer is observable along the grain boundaries [45, 51].

Figure 6 – A typical SEM image (BSE mode) of Nd-Fe-B magnet microstructure in as-sintered and annealed condition

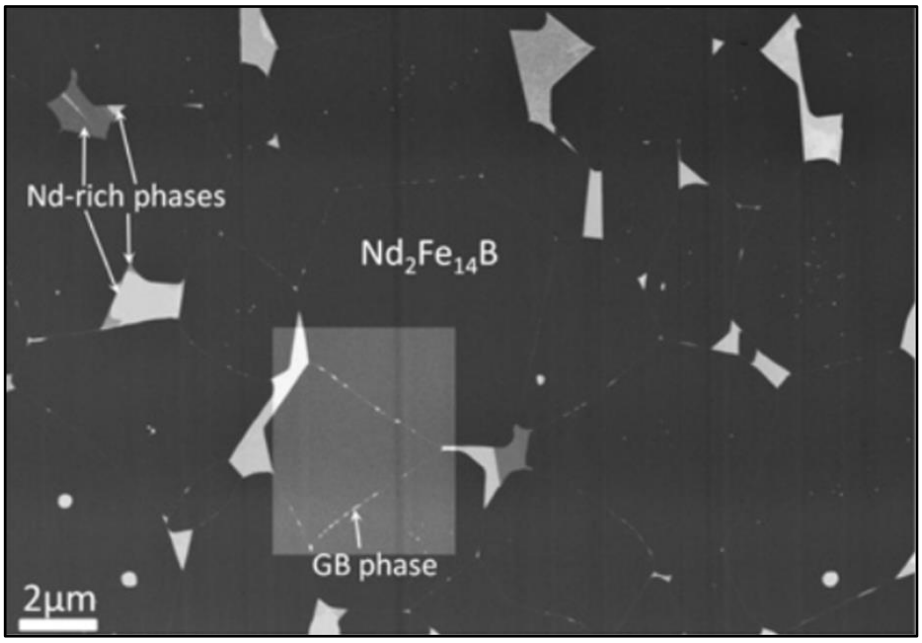

Source: [45]

Powder metallurgy is an efficient method for producing low-geometrical-complexity parts. However, as the magnet format becomes more complex, the cost of producing the component tends to increase. This is due to the low workability of the alloy, which makes the material brittle and increases its hardness. As a result, post-processing to adjust the final dimensions of the part is not desirable. Additionally, producing scrap from the raw material presents a problem, as the chip has low reprocessability. If the component contains rare earth elements in its composition, the final cost is directly affected, further increasing the waste of materials with added value.

2.2.2 Bonded Magnets

New alternatives are being developed for processing Nd-Fe-B-based magnets, opening up possibilities for a wide range of applications. In certain applications, the required complexity of shape makes it impossible to use magnets in their traditional form. Therefore, bonded magnets manufactured using die compaction, injection molding, or more recently, additive manufacturing, are used as alternatives to traditional processing routes.

Bonded magnets consist of two main components: a polymeric binder and a load of powder with ferromagnetic properties. Flexible magnets typically use nitrile rubber or vinyl as binders, while rigid magnets use nylon, PPS, polyester, Teflon, or epoxy resins. Thermoplastic binders can be processed and formed through calendering or extrusion, or molded into various complex shapes using injection molding [52].

In the next two subsections, two well-known processing routes for producing powder with high magnetic properties for bonded magnet fabrication are explored: 2.2.2.1 Rapid Solidification and 2.2.2.2 HDDR.

2.2.2.1 Rapid Solidification

Producing a bonded magnet presents significant challenges, as magnetic hardening cannot be achieved through the sintering of fine powders, unlike in the case of sintered Nd-Fe-B magnets. Consequently, an alternative processing route was developed to produce ferromagnetic powders with high magnetic property values. This involves the production of Nd-Fe-B based raw material using rapid solidification.

The melt spinning technique enables the rapid solidification of a nanocrystalline structure with grain sizes ranging from 20 to 50 nm [37, 38, 53]. However, due to the random orientation of these grains, the maximum energy-product of melt-spun Nd-Fe-B magnets cannot be treated in the same manner as anisotropic magnets. Their isotropic nature makes melt-spun Nd-Fe-B magnets suitable primarily for low-cost, low-performance bonded magnet applications. Over the past decade, rapidly solidified permanent magnets have garnered increased attention due to their significantly simpler processing routes. These routes are less time-consuming and complex compared to the extensive heat treatment and solution treatment typically required to achieve high coercivity in bulk rare-earth permanent magnets [42].

In 1986, General Motors provided a subsidy to Magnequench and helped pioneer the use of melt spinning to produce isotropic powder for creating bonded magnets through compression and molding injection. This process involves melting an alloy or its constituent elements in a vacuum or inert gas and then jetting the material through a hole towards a copper wheel or disc cooled with water. Rapid cooling rates of up to 1,000,000 °C/min can be achieved, resulting in an alloy with very small grains [54]. Processing bonded magnets has the advantage of manufacturing near-net-shape parts, which means little to no post-processing operation is necessary for dimensional adjustment.

However, the raw material produced by the melt spinning technique is not limited to the fabrication of bonded magnets. Recent advancements in hot-pressed, anisotropic, fully dense magnets have enabled the use of melt-spun ribbons for high-performance anisotropic magnets [45]. Anisotropic bulk magnets can be produced through hot-pressing and subsequent die-upsetting of rapidly solidified nanocrystalline alloys [54]. This method yields a coercivity of approximately 900 kA/m and a maximum energy product of 320 kJ/m^3, which are comparable to those of sintered Nd-Fe-B magnets. However, due to the typical grain size of 250 nm in the planar direction and 100 nm in the normal direction, the maximum coercivity of anisotropic hot-deformed magnets is limited to about 1300 kA/m [55].

Melt spinning is the most commonly used rapid solidification technique for processing rare-earth permanent magnet alloy systems. While the atomization technique provides a high production rate and uniform spherical particle morphology, it cannot provide the necessary compositional changes due to the lower cooling rate involved [56]. Atomization involves using high-pressure fluid jets to break up a molten metal stream into very fine droplets, which eventually solidify into fine particles. This versatile method is commonly used for powder production. In conventional atomization, a liquid metal is poured through a tundish with a nozzle at its base. The tundish acts as a reservoir, supplying a constant, controlled flow of metal

into the atomizing chamber. As the metal stream exits the tundish, it is struck by a high-velocity stream of the atomizing medium (water, air, or an inert gas). The molten metal stream is disintegrated into fine droplets, which solidify during their fall through the atomizing tank. The resulting particles are collected at the bottom of the tank [42].

2.2.2.2 Hydrogenation, Disproportionation, Desorption, Recombination (HDDR)

The Hydrogenation, Disproportionation, Desorption, Recombination (HDDR) process is a well-known processing route for achieving a refined grain structure in rare-earth transition metal alloys, especially in Nd-Fe-B alloys. This process is simple and mainly based on hydrogen-induced phase transformation, which can produce highly coercive $Nd_2Fe_{14}B$ powders. These powders can be used to produce bonded magnets as well as fully dense hot-pressed magnets [42]. The process involves a heat treatment with high-pressure H_2 to obtain isotropic or anisotropic nanocrystalline powders. It is based on the disproportionation of $Nd_2Fe_{14}B$ into Fe-α, NdH_2, and Fe_2B and this is followed by recombination of the three phases under low pressure to create a new microstructure that is near single domain. These unique microstructural features suggest that HDDR powders have the potential to be used for the development of high coercivity and remanence Nd-Fe-B magnets [45].

The HDDR process was first developed by Takeshita and Nakayama at Mitsubishi Materials in Japan in 1989 for the production of coercive powder via a "Hydrogenation-Dehydrogenation Treatment" [57]. McGuinness *et al*. later explained the process in terms of the "Hydrogenation, Disproportionation, Desorption, Recombination (HDDR) reaction" [58]. The process quickly gained international recognition, prompting research at many scientific institutions worldwide. Significant research includes studies by Gutfleisch *et al*. [53, 59 - 61]. Since then, bonded Nd-Fe-B magnets using HDDR powders have been reported to have a high $(BH)_{max}$ of 200 kJ/m³ and a maximum operating temperature of 130°C [32].

During the first stage of HDDR process, hydrogen is absorbed by the Nd-rich material at the grain boundaries, forming $NdH_{2.7}$. This process is commonly known as Hydrogen Decrepition (HD). Afterwards, the hydrogen is absorbed by the $Nd_2Fe_{14}B$ matrix phase. These absorption processes cause the material to decrepitate due to the large differential volume expansion of the phases present [2, 17]. However, to avoid the HD stage, hydrogen can be introduced at elevated temperature to cause the disproportionation of the material without the cracking that is introduced by HD. This is known as solid HDDR (s-HDDR) [60, 62].

During the HDDR process, hydrogen is continuously released from the material until it reaches approximately 650°C. In a near-stoichiometric $Nd_2Fe_{14}B$ alloy, if the temperature and kinetics enable metal diffusion, nearly all the hydrogen is degassed from the matrix phase before the disproportionation reaction begins. This reaction is driven by two processing parameters: temperature and hydrogen pressure. It results in a finely divided mixture of $NdH_{2.7}$, Fe_2B, and α-Fe phases, producing a colony-type structure with $NdH_{2.7}$ rods embedded in an α-Fe matrix with an average grain size of 100 nm, and randomly distributed Fe_2B grains [62].

The initial stages of the disproportionation reaction in $Nd_2Fe_{14}B$ start at the Nd-rich grain boundary, which serves as a fast diffusion path for hydrogen, and then proceed towards the center of the original grains. Figure 7 provides a schematic illustration of how the disproportionation occurs. It shows the original Nd-Fe-B grains, the start of the disproportionation reaction at the grain boundaries, and the fine distribution of Nd-H and Fe-B in an α-Fe matrix after the disproportionation reaction is completed [59 - 61].

Figure 7 – Schematic illustration of disproportionation in Nd-Fe-B grains

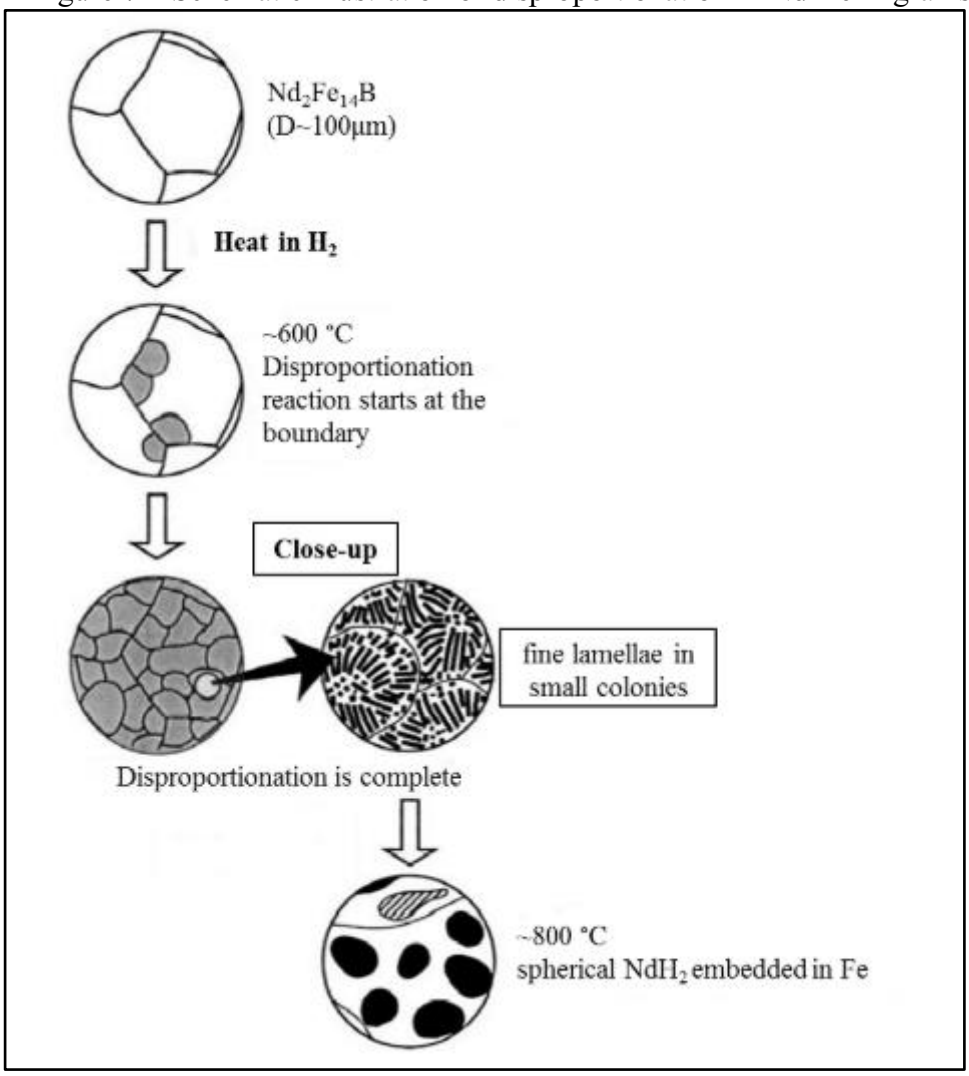

Source: [25].

Applying a vacuum at a suitable temperature (usually around 800°C) can desorb hydrogen. This process causes the neodymium hydride phase to become thermodynamically unstable and form elemental Nd. The Nd then recombines with the other constituents to produce the more stable and original $Nd_2Fe_{14}B$ phase, but with a submicron grain size (around 0.3 μm), similar in size to the critical single domain size for the $Nd_2Fe_{14}B$ phase (0.24 μm) [59 – 61, 63, 64]. Figure 8 illustrates the evacuation process of the system and the resultant formation of a refined grain structure in the $Nd_2Fe_{14}B$ phase. This figure highlights the contrast between the grain size of the original microstructure and following HDDR processing. As shown in Figure 9, the HDDR treatment of an End-of-Life Nd-Fe-B magnet results in a significantly refined microstructure, with submicron grain sizes ranging from 0.5 to 0.2 μm.

Figure 8 – Formation of a refined grain structure after the recombination step in HDDR processing

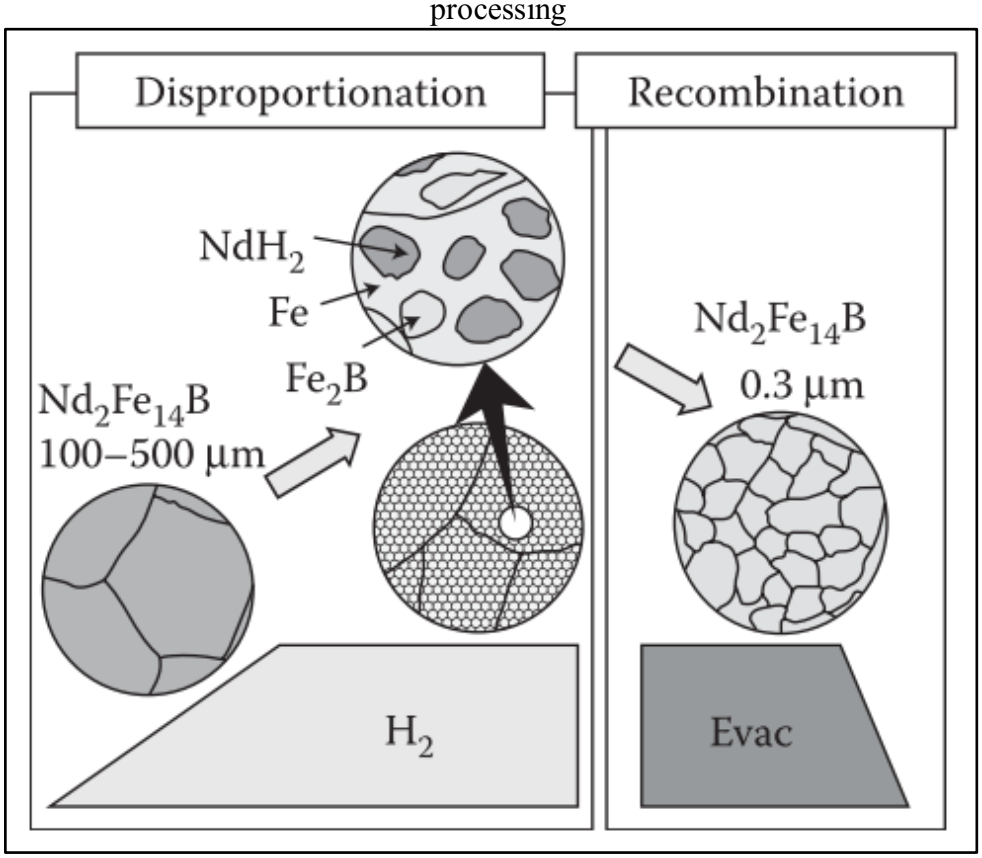

Source: [32].

Figure 9 – Submicron grain sizes in Nd-Fe-B magnet after HDDR processing (fracture surface)

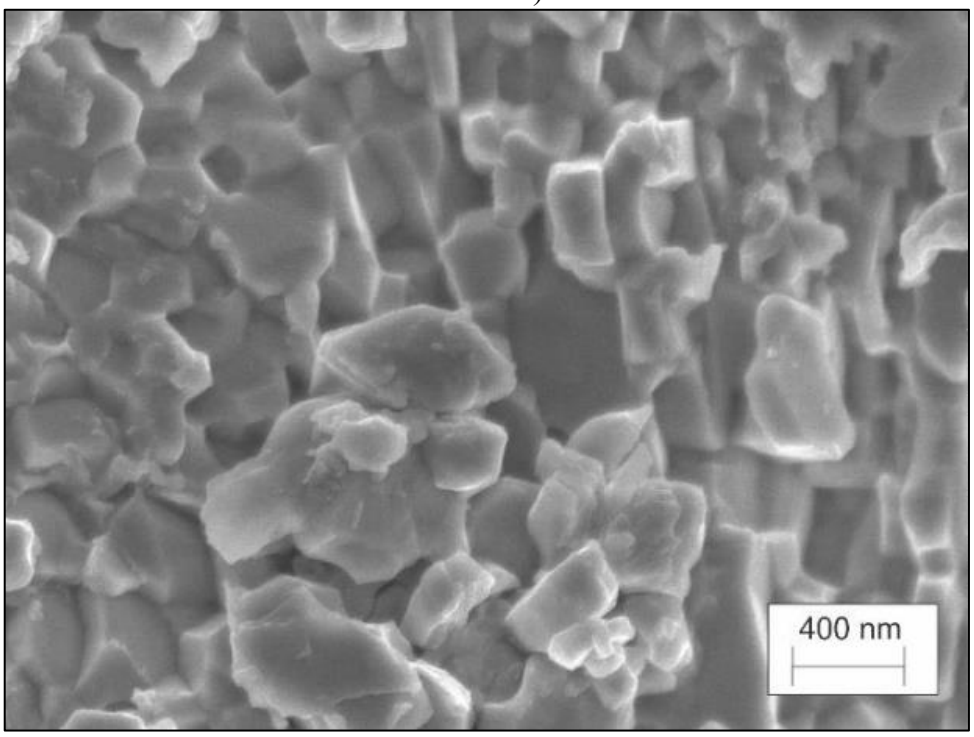

Source: [26].

Takeshita *et al*. [57] created a magnetically coercive powder by exposing Nd-Fe-B alloys to hydrogen, followed by a vacuum treatment within a temperature range of 750°C-900°C. Subsequent studies have shown that the recombined material exhibits a grain size of ~0.3 μm, compared to the initial ingot material of around 50 μm. It has also been demonstrated that the final grain size of the treated material is highly dependent on the processing temperature. This, in turn, becomes a critical factor in determining coercivity [64].

The coercivity of HDDR magnets is influenced by the nature and size of the recombined grains, which is dependent on the processing temperature. At low temperatures, the presence of soft ferromagnetic α-Fe leads to a decrease in coercivity. On the other hand, when the processing temperature exceeds the optimum value, the coercivities are limited by the presence of large faceted grains that are easily demagnetized. Faceted grains are observed at the center of the original $Nd_2Fe_{14}B$ grains, indicating that recombination starts from this point. To prevent grain growth, tight control of temperature and hydrogen evacuation is crucial. Nakayama *et al*. [65] studied the microstructure of recombined materials and found that the grain size of recombined grains was about 0.3 μm for optimum processing, and no boundary phase was found between the newly formed grains [62].

Refocusing the discussion from the coercivity of HDDR particles to the coercivity mechanisms in HDDR powder and sintered magnets reveals the critical importance of understanding how different magnets resist demagnetization. These mechanisms are broadly classified into two categories: pinning type and nucleation type.

In pinning type magnets, the movement of domain walls is hindered by pinning centers. These pinning centers can be chemical inhomogeneities or defects that create a favorable energy environment for a domain wall to form. To overcome a pinning center, a higher magnetic field is required to unpin the domain wall. One way to enhance pinning is by reducing the grain size. These regions, characterized by a highly refined grain structure, provide a strong pinning force that effectively anchors the magnetic domains. As a result, demagnetization only occurs under higher applied magnetic fields. Li *et al*. [66] demonstrated the importance of magnetic domain pinning at grain boundaries for coercivity in HDDR magnets. Their findings, based on Lorentz TEM observations of magnetic domain walls, emphasize the significance of having a refined grain structure [45].

On the other hand, in nucleation type magnets, domain walls can easily move until all domain walls are driven out of a specific grain. This mechanism is responsible for coercivity in sintered magnets. Managing grain boundaries is crucial in preventing the formation of reversed domains, resulting in magnets that have high resistance to demagnetization. This approach

involves regulating the interfacial microstructure between the $Nd_2Fe_{14}B$ phase and the Nd-rich phase. This coercivity mechanism, also known as interfacial control, focuses on magnetic reversal caused by defects on the surface of $Nd_2Fe_{14}B$ grains. The coercivity of sintered magnets primarily arises from the magnetic isolation of individual $Nd_2Fe_{14}B$ grains. This is achieved by the formation of a thin, continuous, non-ferromagnetic Nd-rich layer surrounding the $Nd_2Fe_{14}B$ grains [67]. Reversed magnetic domains are observed to nucleate at localized regions with lower anisotropy or defects, or in proximity to non-ferromagnetic grains that exhibit a higher stray field [45].

2.2.3 Recycling Nd-Fe-B Magnets

The instability regarding the prices of rare-earth metals, notably Nd and Dy, is also attributed to the global surge in environmental legislation and the increasing emphasis on resource protection and sustainable development. This escalation in prices has, in turn, significantly elevated the production costs of Nd-Fe-B sintered magnets. As a consequence, there is a growing recognition of the pressing need for the recycling of waste Nd-Fe-B materials. This initiative is strongly advocated by the Organization for Economic Co-operation and Development (OECD) countries as a strategic response to the prevailing global crisis concerning the supply of rare-earth elements [68, 69].

Over the past decade, considerable efforts have been made on a global scale to recycle bulk Nd-Fe-B sintered magnet waste materials. These waste materials possess substantial secondary rare-earth resources for two compelling reasons. Firstly, they contain a total rare-earth content exceeding 30 wt. %, surpassing the concentration found in most natural rare-earth mines. Secondly, despite deterioration of the magnet from corrosion and contamination, the waste remarkably retain the essential intrinsic properties of the original magnets.

Various techniques have been developed for recycling bulk Nd-Fe-B sintered magnet waste, allowing for the preservation or even enhancement of the overall properties of the recycled magnets [9 – 12, 70 – 79]. This offers a significant opportunity for large-scale production of recycled magnets, reintroducing their high intrinsic value back into the supply chain [80, 81].

Nd-Fe-B sintered magnet waste originates from two primary sources: industrial waste and End-of-Life waste. Industrial waste is generated during the production process of these magnets and encompasses furnace slags, ultrafine powders, defective blocks, scraps, and sludges. Machining processes are the primary contributors to industrial waste, with scraps retaining the magnetic

properties of the magnets, while sludges are characterized by heavy oxidation and impurity content [82].

On the other hand, End-of-Life waste emanates from devices that incorporate Nd-Fe-B sintered magnets, such as hard disk drives in computers, which annually contribute to the disposal of these magnets. Extensive work has been undertaken to identify End-of-Life magnets and explore recycling opportunities, thereby significantly contributing to the realization of a more circular economy [82].

There are various techniques described in the literature for reprocessing waste magnets generated during the fabrication process or at the end of their life cycle. One example is recycling indirectly through a conventional oxidation roasting and acid leaching flowsheet. This involves several steps for the forced oxidation of elements, and the resulting material can be reused as new raw material for rare earth alloys [74]. Another method is reprocessing the magnet sludge through reduction diffusion, which allows for the collection of rare earth elements that can be reprocessed in different ways [9, 10, 70, 71].

Moreover, a commonly used technique involves using hydrogen processing to transform the bulk magnet into pulverized raw material [11, 12]. This powder can be directly recycled into new sintered magnets using a technique known as Magnet-to-Magnet processing [72]. In this approach, the HD process fragilizes the material, which is then finely milled to produce new recycled sintered magnets. This magnet-to-magnet recycling technique has been thoroughly tested and appears to be suitable for large-scale production. The resulting magnetic performance demonstrates the practicality of using recycled Nd-Fe-B magnets in real-world applications [13, 73 – 76].

In addition to previously mentioned magnet recycling techniques, hydrogen processing has been extensively explored in the field of nanocrystalline magnets. Beyond the simple use of HD, the Hydrogenation, Disproportionation, Desorption, and Recombination (HDDR) process has also been employed [21]. This method facilitates the production of a refined grain structure, resulting in enhanced magnetic properties [79]. Significant progress has been made in creating new bonded magnets from these recycled materials, including densification through the spark plasma sintering process [78]. However, further exploration is needed regarding the application of HDDR-processed recycled magnets as raw materials for AM.

2.2.3.1 Detrimental effect of oxygen and carbon uptake in Nd-Fe-B magnets

Evaluating the corrosion status of raw materials is crucial when reprocessing End-of-Life Nd-Fe-B magnets. These magnets, comprising approximately 30% rare earth constituents [5], are notably vulnerable to corrosion, particularly in humid environments. This susceptibility is attributed to their complex multi-phase structure. This structure comprises three main phases: the ferromagnetic phase of $Nd_2Fe_{14}B$ (φ-phase), which constitutes 85% of the volume, the boron phase of $NdFe_4B_4$ (also known as phase K) at 3%, and the neodymium rich phase (Nd-rich) at 12% [83]. The absorption of oxygen and carbon during both manufacturing and magnet operation in corrosive environments can significantly compromise the performance of reprocessed magnets.

The presence of oxygen in Nd-Fe-B magnets primarily occurs during processing stages such as fine powder handling after milling and during sintering. Oxygen is highly reactive and easily introduced into the Nd-Fe-B alloy, while carbon can infiltrate through various sources such as lubricants and protective coatings. Once incorporated, oxygen tends to form paramagnetic oxides, such as Nd_2O_3, which disrupt the magnetic properties by hindering remanence and coercivity. On the other hand, carbon tends to segregate at grain boundaries, forming complex compounds with Nd, thereby affecting the microstructure and coercivity values of the magnets [83].

The presence of oxygen and carbon alters the microstructure of sintered Nd-Fe-B magnets, leading to the formation of undesirable phases and grain boundary segregation. Oxygen-rich regions inhibit the development of continuous Nd-rich layers, crucial for ferromagnetic isolation and coercivity development. Additionally, carbon accumulation exacerbates grain boundary effects, further reducing coercivity. As a result, the nucleation coercivity mechanism type is compromised, leading to decreased magnetic properties [13].

Controlling the uptake of oxygen and carbon is important in ensuring the high property values and quality for reprocessed Nd-Fe-B magnets, especially in the context of recycling. Recycled magnets often exhibit elevated levels of oxygen and carbon, which can significantly impair magnetic properties. Therefore, strategies for minimizing oxygen and carbon uptake during reprocessing must be prioritized to maintain the integrity and sustainability of recycled Nd-Fe-B magnet applications.

2.3 ADDITIVE MANUFACTURING

Additive Manufacturing (AM) has emerged as a transformative technology in the processing of Nd-Fe-B based magnets. This advanced manufacturing technique enables the creation of components with complex geometries and near-net shapes, significantly enhancing processing flexibility while circumventing the need for costly tooling. The near-net shape capability of AM not only minimizes post-processing expenses associated with achieving precise dimensional and shape tolerances for magnetic components but also reduces the wastage of valuable raw materials. As such, AM presents a cost-effective and resource-efficient solution for the production of high-performance magnetic parts, aligning with the industry's goals of sustainability and economic viability [52].

The initial step in the AM process involves generating a specific format document, typically in Standard Tessellation Language (STL), derived from a computer-aided design (CAD) file used for material deposition programming. The operator must define various process parameters, such as scan speed, laser power, and scanning strategy, to ensure the successful production of 3D objects. These crucial parameters significantly influence the quality and accuracy of the final product [16]. Once the programming and processing parameters are established, the machine deposits material layer by layer, culminating in the fabrication of 3D objects [84]. Figure 10 illustrates the main steps in additive manufacturing, from modeling the 3D part and programming the layer-by-layer path to the final printed part.

Figure 10 - Main steps in additive manufacturing: From CAD modeling to final 3D printed part

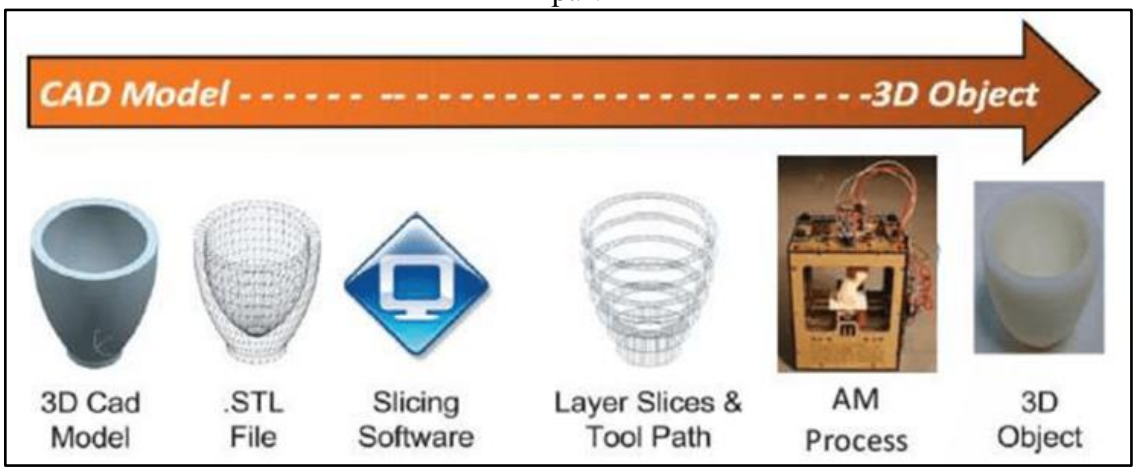

Source: [85]

Additive manufacturing technologies offer significant advantages over traditional injection molding by enabling the rapid and efficient creation of new shapes using computational models. Unlike injection molding, which involves a lengthy and costly process to produce tooling and prototypes, AM streamlines the entire production chain [86]. Traditional manufacturing requires multiple stages, including design with drawing preparation, process delimitation, tool availability, and meeting dimensional accuracy requirements. Any modifications necessitate changes across various aspects of the production chain, resulting in considerable time and resource investments. Conversely, AM reduces preparation and prototype manufacturing times, thereby enhancing overall efficiency and adaptability in product development [84].

This technology offers significant advantages in achieving dimensional tolerances by building objects layer by layer, which eliminates the need for post-processing. This layer-by-layer approach allows for precise control over the shape and dimensions of the final product, reducing the reliance on traditional subtractive methods that remove material to achieve the desired form. Consequently, AM can lead to substantial reductions in production costs and material waste, making it an efficient and sustainable alternative for producing complex and high-precision components [86].

2.3.1 Technologies

Several technologies are available for producing Nd-Fe-B magnets through AM. The most promising methods include Binder Jet Technology, Direct Energy Deposition, Fused Filament Fabrication, and Powder Bed Fusion. However, all of these techniques are experimental, and the manufacturing of Nd-Fe-B-based magnets through AM is still in its early stages.

Binder Jet Technology works by selectively depositing melted binder to join magnetic material particles. The 3D printer head moves over the platform, depositing binder drops onto the previously spread powder. When one layer is complete, the manufacturing base moves downwards, and a new layer of powder is spread on that platform. The process is repeated layer by layer until all the parts are manufactured. After printing, the parts are in a green state and require post-processing before use [86].

Direct Energy Deposition (DED) is a manufacturing method that uses focused thermal energy to bond magnetic particles by melting them during deposition. During the process, powder is expelled from a nozzle into a melting pool on the substrate where the deposition takes

place. The system generates the melting pool with its focused thermal energy. However, this technology is often large in size and requires a closed and controlled environment for operation [86].

Fused Filament Fabrication (FFF) is a widely used AM technology for producing magnets. The process involves passing a continuous filament, mixed with a thermoplastic binder and magnetic material, through an extrusion chamber where the binder is melted by heating. The resulting composite material is then forced out of the nozzle of the extruder and selectively deposited layer by layer onto a manufacturing platform until the final piece is formed [84].

Laser Powder Bed Fusion (LPBF) is an advanced AM technique pertinent to the production of permanent magnets. This method encompasses two primary technologies: Selective Laser Sintering (SLS) and Selective Laser Melting (SLM). The process initiates by heating the raw particulate material to a temperature just below its melting point to minimize distortion and enhance layer adhesion. A laser beam, manipulated through a series of mirrors and lenses, follows a pre-programmed path to selectively fuse the powder. Subsequently, the manufacturing platform descends by a layer thickness, and another layer of powder is spread. This iterative process continues until the entire component is fabricated. Figure 11 illustrates the principal components of a PBF-based machine. During the procedure, any unused powder is collected in a container for reuse in future production cycles [84].

Figure 11 - Principal components of a Laser Powder Bed Fusion (LPBF) machine

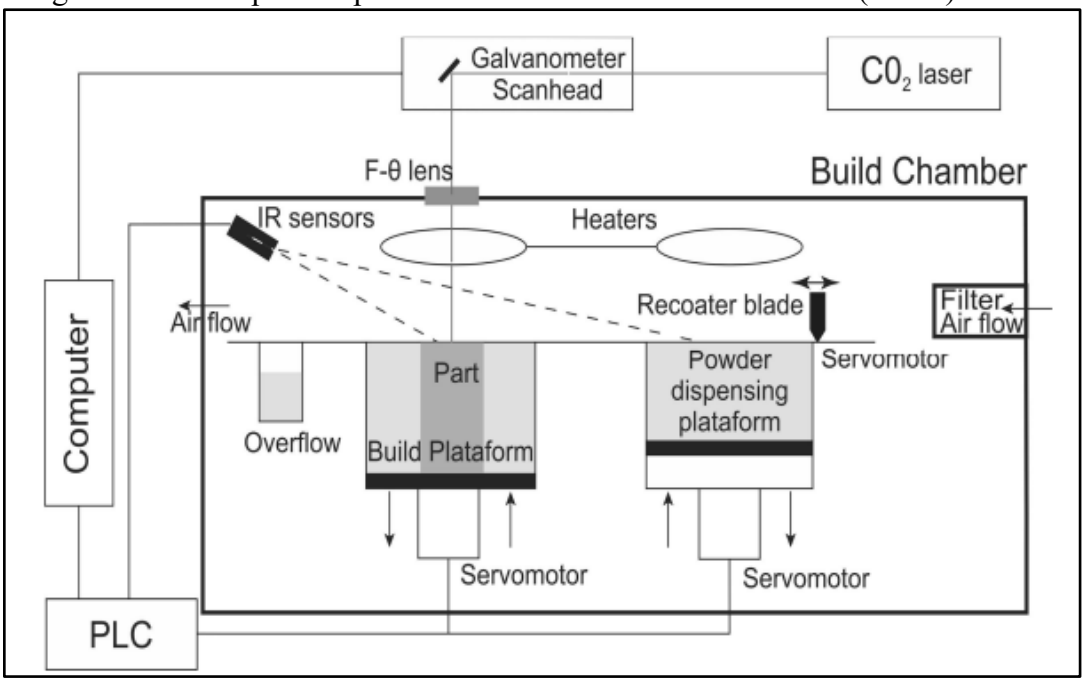

Source: [87]

Selective Laser Sintering (SLS) and Selective Laser Melting (SLM) both utilize a laser beam as a thermal energy source for material processing, with the wavelength of the laser being dependent on the specific material being processed. The primary distinction between these two additive manufacturing technologies lies in the degree of particle fusion achieved. SLM facilitates complete fusion of the particles, leading to full densification of the material. In contrast, SLS is typically used for composite or fully polymeric feedstock and involves only the sintering of the polymer. Specifically, when processing a feedstock composed of ferromagnetic particles and a polymeric binder, the laser interacts solely with the binder, embedding the ferromagnetic particles within the polymeric matrix. This fundamental difference in processing methods results in varying material properties and applications for each technology.

The densification of parts produced by the LPBF technique involves several mechanisms, primarily solid-state sintering, which is the main sintering mechanism in SLS processing. Solid-state sintering facilitates the joining of particles without surpassing the material's melting temperature. This process minimizes the total free energy of the particles, similar to traditional powder metallurgy methods. The surface energy is proportional to the particle's surface area and is dependent on its size. Sintering mechanisms are directly related to the surface area-to-volume ratio of a set of particles. Smaller particle sizes enhance the number of contact points, leading to improved consolidation and densification of the material [88].

Defects in components produced by LPBF are associated to the processing methods employed. Among these, porosity stands out as the predominant defect, exerting a considerable impact on the mechanical and magnetic properties of the final manufactured part. The origins of porosity can be traced to various factors, including the quality of the particulate raw material, the specific processing parameters used, and the inherent characteristics of the sintering or solidification processes [16]. The quality of the raw materials is paramount in determining the ultimate properties of the produced components. Key attributes such as the shape, size, internal porosity, surface morphology, and composition of the particulate raw material all significantly influence these properties [23, 23].

In powder bed processing, certain conditions must be meticulously prepared and maintained. The process must continue uninterrupted with a sufficient powder reserve, reaching at least the maximum programmed building height. An adequate volume of powder must be transported from the feeding platform to the manufacturing platform to cover the previous layer [88]. The powder should be uniformly spread to form a smooth, thin, and homogeneous layer without generating excessive tensions that could deform earlier layers. Therefore, factors such

as powder flowability significantly influence the final characteristics of the manufactured component. Powder Bed Fusion systems typically utilize particles sized between 20 and 50 µm to meet flowability requirements [16, 24]. As particle size decreases, friction between particles and electrostatic forces increase, potentially compromising the powder's flowability [88].

2.3.2 Processing additively manufactured Nd-Fe-B based magnets

The current study investigates the use of hydrogen processing to produce high coercive powders from recycled Nd-Fe-B magnets. This innovative method addresses the significant issue of waste generated by End-of-Life Nd-Fe-B magnets and explores the feasibility of utilizing recycled raw materials in AM processing.

Zakotnik *et al*. [89] pioneered the exploration of recycling scrap sintered magnets using the HD process, specifically targeting Nd-Fe-B sintered magnets recovered from voice coil motors in hard disk drives. The HD process was conducted at a hydrogen pressure of 1 bar, resulting in the generation of particulated materials. However, the authors encountered significant challenges in achieving full density in the recycled materials. Consequently, the recycled sintered magnets exhibited a maximum energy product that was 15% lower than that of the original magnets.

To provide further context, Zakotnik *et al*. [90] previously proposed two potential approaches for recycling Nd-Fe-B sintered magnets: the HD and HDDR processes. The HDDR process, conducted at a hydrogen pressure of 0.4 bar and a temperature of 800°C, produces isotropic high coercive powders. This method offers the potential for an efficient recycling of Nd-Fe-B End-of- Life magnets, contributing to the sustainable management of critical raw materials.

Périgo *et al*. [91] investigated later the recycling of sintered Nd-Fe-B magnets using the HDDR process. They optimized the values of magnetic properties from recycled powders by adjusting the processing parameters, specifically varying the recombination plateau temperature from 800°C to 920°C and the hydrogen pressure from 60 kPa to 150 kPa. Their study resulted in the production of isotropic powders with a remanence of 0.58 T and a coercivity around 900 kA/m, achieved at an optimal recombination temperature of 860°C and a hydrogen pressure of 135 kPa.

These unique powders exhibit significant potential as feedstock materials for LPBF technology, offering a sustainable approach to recycling. By integrating these powders into AM processes, a more environmentally friendly method is established. This not only reduces waste

but also promotes a circular economy, emphasizing the reutilization of materials and enhancing the sustainability of manufacturing practices.

Recent advancements in the AM of Nd-Fe-B bonded magnets primarily target the production of commercial powders and the optimization of processing techniques. Pioneering work by Baldissera *et al*. [92] delved into the development of polymeric matrix composite magnets utilizing LPBF. Their study assessed the influence of laser parameters on the magnetic properties of isotropic Nd-Fe-B composite magnets.

Fim *et al*. [93] advanced the research on Nd-Fe-B composite magnets by investigating the influence of laser parameters and printing feedstock composition on the final porosity of magnets produced via LPBF. Their study emphasized the critical role of sintering kinetics and binder volume in minimizing porosity and enhancing the magnetic properties of the resulting bonded magnets.

In the current research context, a novel proposal is under investigation to utilize hydrogen processing for the production of additively manufactured recycled bonded magnets. This research focuses on evaluating the feasibility of applying Hydrogen Decrepitation (HD) and Hydrogenation, Disproportionation, Desorption, Recombination (HDDR) processes to End-of-Life magnets. The objective is to generate a feedstock with tailored magnetic properties, adequate for LPBF-based AM techniques.

3 METHODOLOGY

3.1 RAW MATERIALS

In this study, ferromagnetic powders based on Nd-Fe-B and a binder system consisting of polyamide 12 (PA-12) were used. These ferromagnetic powders were obtained from End-of-Life magnets (class N42) that were previously utilized in wind turbines. Figure 12 illustrates the End-of-Life magnet that was used for the purpose of this study. The magnet has a weight of 1.5 kg and is coated with epoxy.

Figure 12 - The End-of-Life magnet (class N42) that was previously used in wind turbines

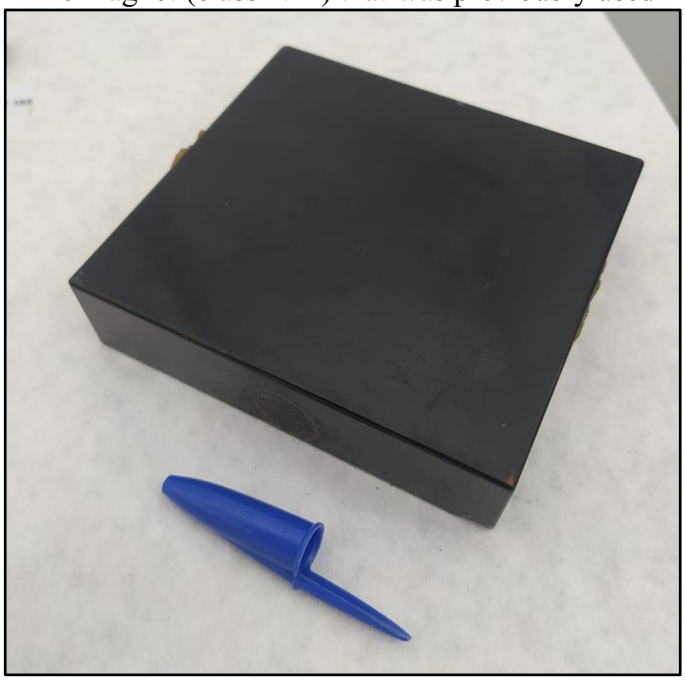

Source: Author

The magnetic characterization of the End-of-Life magnet is presented in Figure 13, which shows the demagnetization curve. The x-axis represents the applied field, measured in kilo Amperes per meter (kA/m). The y-axis represents the polarization of the sample, measured in Tesla (T), indicating the magnet's ability to retain magnetization when the applied field is zero. For the End-of-Life magnet used in this work, the remanence value is 1.2 T and the coercivity is approximately 1500 kA/m.

Figure 13 - Demagnetization curve of the End-of-Life magnet used for the investigations of this study

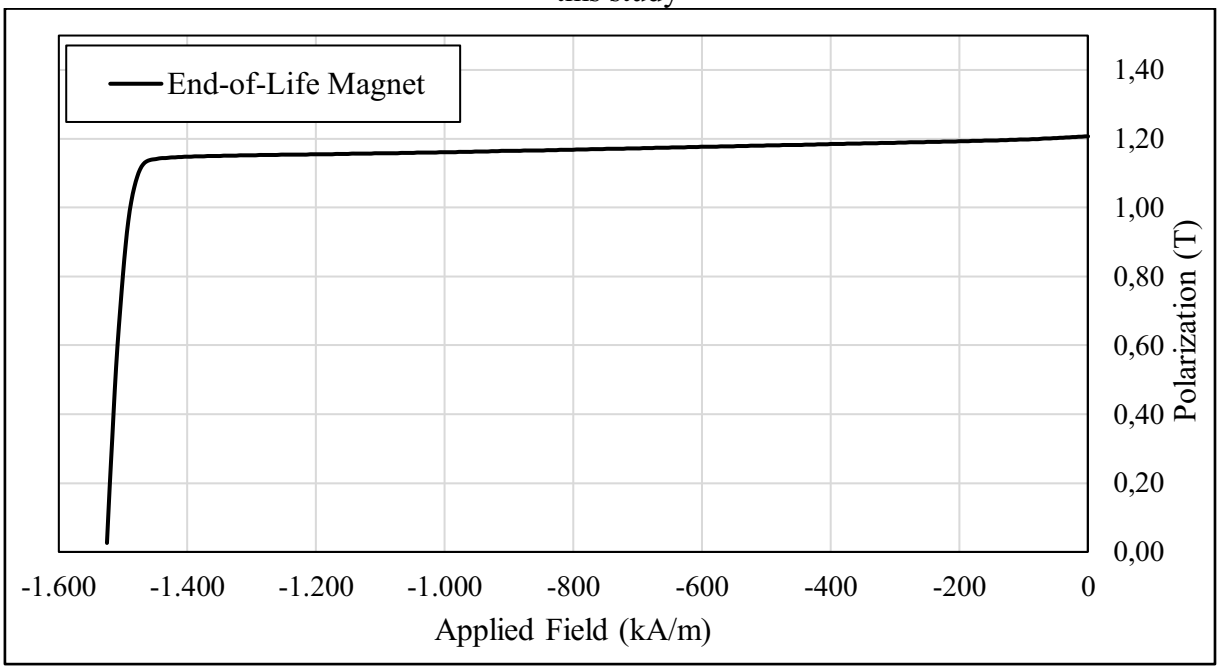

Source: Author

The PA-12 binder system used in this study was sourced from the DuraForm PA2200 class, which is manufactured by 3Dsystems, a well-known provider of 3D printing raw materials. The choice of PA-12 was based on its technological and thermal properties, which make it suitable for laser processing. Table 1 provides more information regarding this polymeric binder. PA-12 is commonly employed as a binder for producing composite magnets using LPBF.

Table 1 - Technological and thermal properties of Polyamide-12 used in this study as the polymeric binder

Powder Properties	PA-12	Test Method	Units
Tap Density	0.59	ASTM D4164	g/cm³
Particle Size Average	58	Laser Diffraction	µm
Melting Point: T_m	184	DSC	°C

Source: [94]

3.2 PROCESSING

A flowchart of the methodology for the processing used in this work is presented in Figure 14. This methodology involves three main steps, namely powder production, feedstock production and printing magnets.

Figure 14 - Flowchart of the processing methodology used in this study, detailing the three main steps: powder production, feedstock production, and printing magnets.

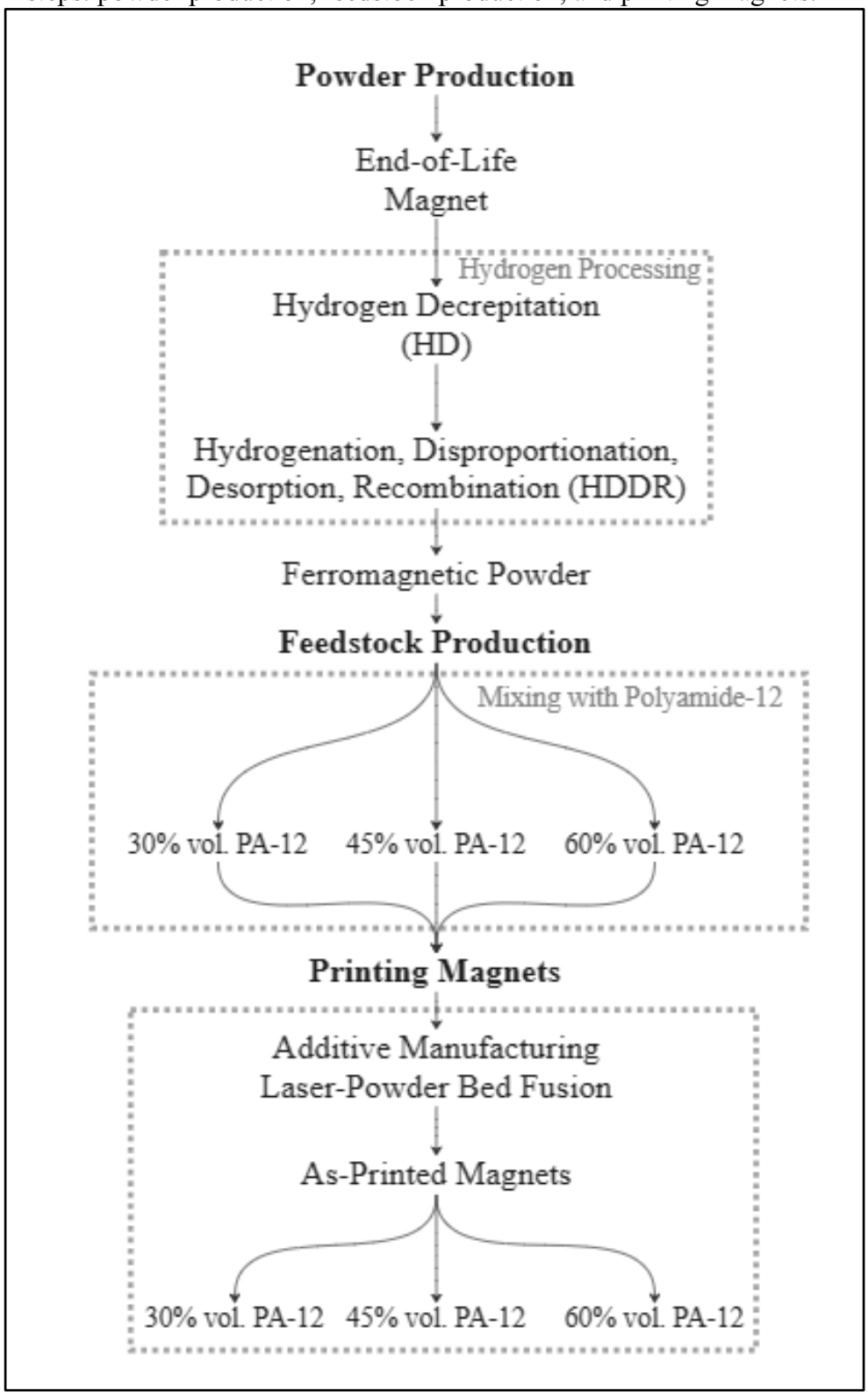

Source: Author

The initial step involves disintegrating the End-of-Life bulk magnet into a friable powder with the suitable technological properties for utilization in LPBF. The resultant powder must exhibit high coercivity values, rendering it adequate for the production of bonded magnets. This transformation process employs two hydrogen-based techniques: Hydrogen Decrepitation (HD) and Hydrogenation, Disproportionation, Desorption, Recombination (HDDR). These methods are instrumental in both the pulverization and magnetic hardening of the powder.

During the feedstock production step, the ferromagnetic powder derived from the preceding process is combined with Polyamide 12 (PA-12). This combination is utilized to investigate and analyze various feedstock compositions and their influence in the final properties of printed bonded magnets.

In the final stage, bonded magnets are produced using a prototype additive manufacturing LPBF machine. Following production, the recycled Nd-Fe-B bonded magnets are subjected to microstructure analysis and evaluation of their magnetic properties. The subsequent subsections of this chapter will provide a detailed description of the processing route utilized in this study, which includes Powder Production (Section 3.2.1), Feedstock Production (3.2.2), and Printing Magnets (3.2.3).

3.2.1 Powder Production

3.2.1.1 Hydrogen Decrepitation (HD) Methodology

This study employs the HD process, initially developed by Harris *et al*. [35] and subsequently utilized by McGuiness *et al*. [95] among others, who have significantly advanced the understanding and application of this process. The HD process implemented in this research is based on fundamental principles extensively documented in the literature and is routinely applied in the activities of the Magnetic Materials Laboratory (MAGMA). The HD procedure, as illustrated in Figure 15, is detailed as follows:

Figure 15 - Simplified procedure for the HD employed in this work, including crushing the End-of-Life magnet into fragments and placing them into the decrepitation chamber under a hydrogen atmosphere.

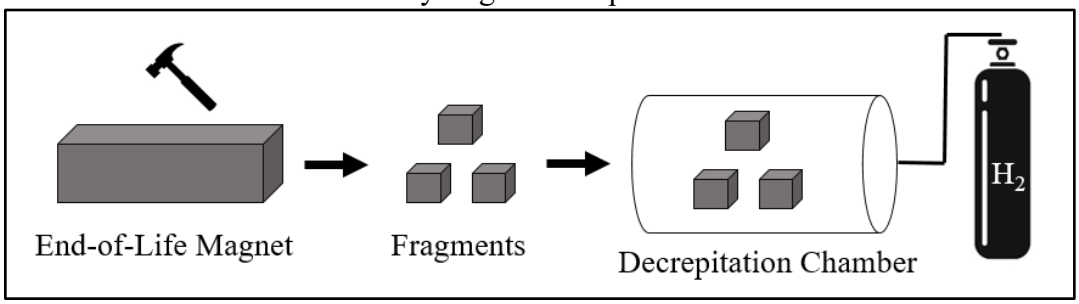

Source: Author

1. The fragmented sintered magnet block, weighing 1.5 kg, was placed within the decrepitation chamber of the HD rig and sealed.

2. Subsequently, the system underwent evacuation, reducing the internal pressure to approximately 10^{-2} mbar.

3. To initiate the decrepitation reaction, the chamber was then filled with hydrogen until a pressure of 1.5 bar was attained. The pressure level was continuously monitored until it displayed a decrease, indicating the commencement of the decrepitation process.

4. In response to pressure reduction, additional hydrogen was introduced into the system as needed to maintain a stable pressure of 1.5 bar.

5. Once the pressure remained constant for a period of 1 hour, marking the completion of the reaction, the system was evacuated once more.

6. Following evacuation, the sealed decrepitation chamber was transferred to an argon-filled glovebox, providing an inert and controlled environment.

7. Within the glovebox, the resulting HD powder was managed and stored, ensuring its exposure to an atmosphere containing less than 50 ppm oxygen

The system utilized in this study for the HD process is depicted in Figure 16. It comprises a hydrogen cylinder serving as the H_2 source for the HD process. The fragmented End-of-Life magnet is placed in the decrepitation chamber. Pressure during processing is monitored by a manometer, while a rotary vacuum pump evacuates the system to minimize atmospheric contamination. Additionally, a Pirani gauge is employed to monitor low pressure during the evacuation process.

Figure 16 - Principal components of the HD process system used in this study

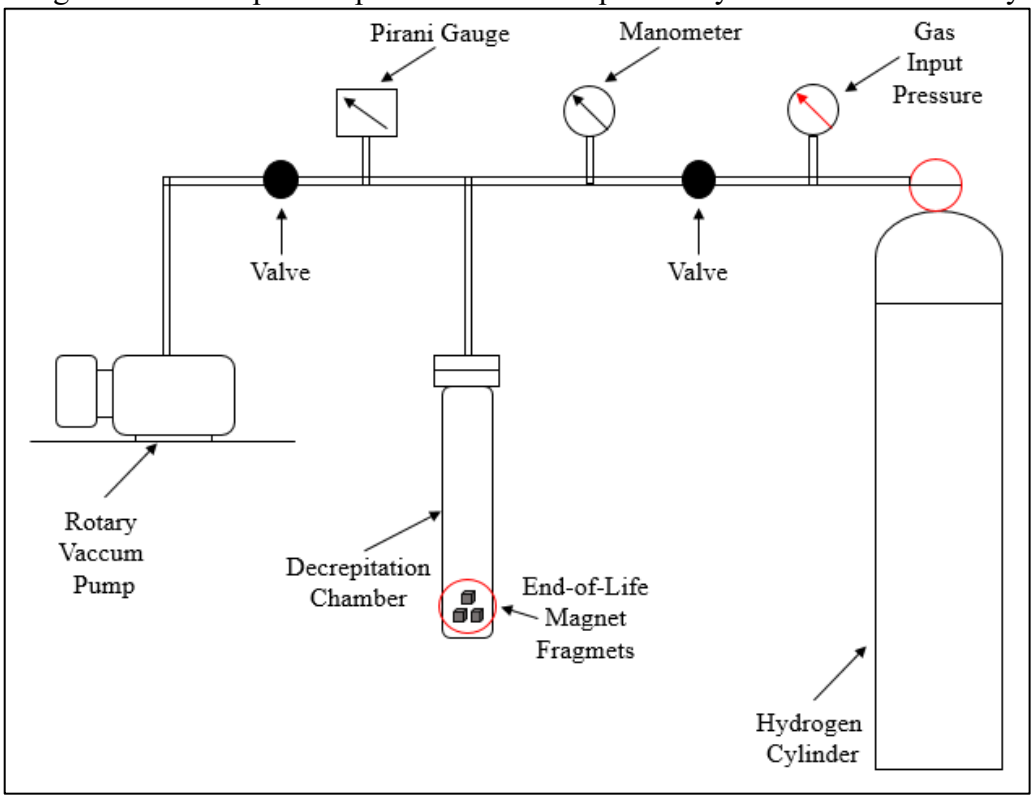

Source: Author

To verify the suitability of HD powder as a feedstock for LPBF, a comminution process was performed. The HD powder underwent size reduction using a porcelain mortar and pestle, followed by sieving through a 106 µm sieve. This procedure, illustrated in Figure 17, was selected based on literature insights [22 – 24], thereby ensuring adherence to recommended particle size distribution standards.

Figure 17 - Comminution process for HD recycled powder preparation that involves milling using a porcelain mortar and pestle, followed by sieving through a 106 µm sieve.

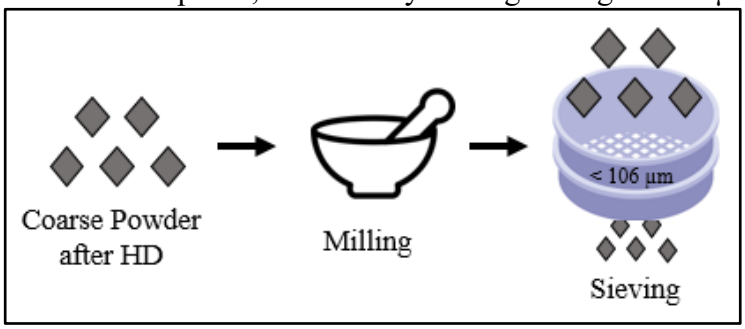

Source: Author

Following HD processing, the resulting powder underwent characterization to assess its properties. A scanning electron microscope (SEM) operating in secondary electron mode was employed to examine the microstructure and evaluate the morphology of particles after HD treatment and sieving. The size and morphology of the powder particles were found to significantly influence the quality of magnets produced by LPBF technique [16, 24]. Detailed information on the characterization methods, including the specific models of the equipment used, can be found in Subchapter 3.3.

Magnetic characterizations of the HD product were conducted using a hystograph to measure coercivity, remanence, and maximum energy product. These measurements are essential for evaluating the need for further enhancement of the magnetic properties of the powder, ensuring its suitability as a raw material for bonded magnets. Literature indicates that powder produced via the HD process exhibits significantly diminished magnetic properties compared to the original End-of-Life magnet [17]. This reduction in magnetic properties, critical for material performance, is primarily attributed to microstructural defects induced by the HD processing method.

3.2.1.2 Hydrogenation, Disproportionation, Desorption, Recombination (HDDR) Methodology

Several advanced technological methods can produce particles with submicrometric grain sizes. These methods include surfactant-assisted high-energy ball milling, gas atomization, chemical reduction from oxides, rapid quenching, recrystallization from the amorphous state, and the Hydrogenation, Disproportionation, Desorption, Recombination (HDDR) process [96]. In this study, the HDDR process was selected to promote hard magnetic properties to recycled HD powder due to its relatively straightforward processing involving hydrogen.

The HDDR process, a well-established method for refining the grain microstructure of rare-earth-based alloys, was initially developed by Takeshita and Nakayama [57] and later refined by McGuinness *et al*. [58]. The parameters utilized in this study integrate principles from these and other references [25, 26, 53, 59 – 61, 97, 98]. The procedure was executed using a furnace tube and the system similar to the one illustrated in Figure 16. Figure 18 offers a simplified illustration of the HDDR process, with the specific parameters detailed below:

Figure 18 - Simplified illustration of the HDDR process, showing the HD powder inside the retort under a hydrogen atmosphere and the furnace tube.

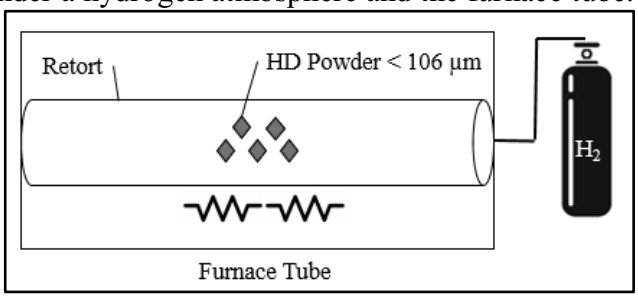

Source: Author

1. Sample Preparation:
    - A 10 g mass of HD powder was retrieved from the glove box.
    - The HD powder was transferred into a sealed retort.
2. Transfer to HDDR Rig
    - The retort, containing the HD powder in the sample tube, was positioned within the HDDR furnace tube.
3. Evacuation and Heating
    - The HDDR rig system was subjected to a complete evacuation using a rotary vacuum pump, reaching a pressure of approximately 10^{-2} mbar.
    - Then the chamber was filled with hydrogen until a pressure of 1.5 bar was attained. The pressure level was continuously monitored and maintained from 1.4 to 1.6 bar of hydrogen.
    - The system was then heated to the desired processing temperature within the range of 800-940°C.
    - After reaching the processing temperature, a hold time of 15 minutes was maintained.
4. Recombination Reaction
    - The recombination reaction was initiated by reducing the hydrogen pressure within the system using the rotary vacuum pump
    - After 20 minutes, hydrogen was completely removed from the system, achieving a pressure of approximately 10^{-2} mbar.
5. Cooling
    - With the furnace tube under full vacuum, the recombination reaction was allowed to conclude.

- To accelerate the cooling process, the furnace tube was rapidly cooled by immersing it in a water bath, enhancing the cooling rate.

In step three, the optimization of the plateau temperature (ranging from 800 to 940 ºC) was conducted to maximize the magnetic properties of the recycled powder. Previous research from the Magnetic Materials Laboratory (MAGMA) [26] and other consulted source [25] indicated that other process parameters, such as hold time for disproportionation, recombination, and hydrogen pressure, had minimal or no influence on the magnetic properties. Consequently, these factors were not further investigated in this study.

Figure 19 illustrates the temperature versus time profile for the HDDR process. The graph provides detailed information on the hydrogen pressure, set at 1.5 bar, and outlines the specific steps involved in the disproportionation and recombination phases. The disproportionation phase is maintained for a dwelling time of 15 minutes, followed by the recombination phase, which lasts for 20 minutes.

Figure 19 - Temperature versus time profile for the HDDR process used in this study, showcasing the hydrogen pressure, temperature range tested and dwelling time for both disproportionation and recombination

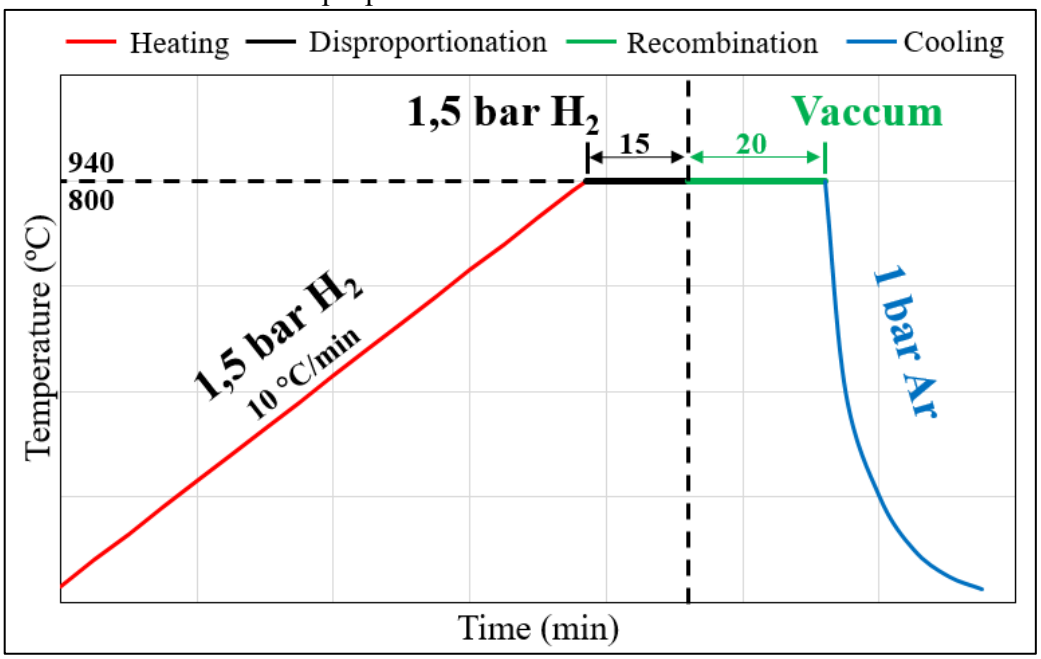

Source: Author

Following the HDDR process conducted at temperatures between 800 and 940 ºC, the resulting powders were analyzed using a hystograph to evaluate their magnetic properties. The ferromagnetic powder obtained was then combined with a polymeric binder (PA-12) to

fabricate compressed bonded samples, which served solely to measure the magnetic properties of the HDDR particles and provide a reference for the printed bonded samples detailed in section 3.2.3 of this study. The fabrication process involved creating a mixture with a specific volume ratio of 55% HDDR powder and 45% PA-12, which was subjected to Cold Isostatic Pressing (CIP) at a pressure of 150 MPa for 10 seconds. The resulting samples were cylindrical, with an approximate diameter of 9 mm and a height of 6 mm.

In addition to measuring the magnetic properties of HDDR, a scanning electron microscope (SEM) operating in secondary electrons (SE) mode was used to evaluate the morphology and grain size of the recycled particles.

3.2.2 Feedstock Production

Following the flowchart in Figure 14, the next step is feedstock preparation. This process involves forming a mixture with varying volume fractions of PA-12 and HDDR. To evaluate the binder fraction's impact on the feedstock and its resulting effect on the final properties of the produced bonded magnets, feedstock compositions of 30%, 45%, and 60% vol. PA-12 were selected.

The volume fraction of the polymeric binder in printed bonded magnets, as highlighted in the literature [92, 93, 99, 100], has a significant influence on the part's consolidation and directly impacts the integrity and quality of the printed magnet. To embed ferromagnetic particles effectively, a continuous polymeric matrix is essential [93]. Furthermore, having a high density to eliminate the existence of pores is desired, as it contributes to the magnetic properties of the printed magnet.

Previous study by Fim *et al*. [93] investigated the density optimization of 3D printed Nd-Fe-B magnets with different feedstock compositions (36, 40, and 45% volume of binder). Similarly, Röhrig *et al*. [101] performed density optimization investigations on printed magnets, but using Sm-Fe-N ferromagnetic particles. With these studies as a basis, three distinct volume fractions (30, 45, and 60% vol.) of the polymeric binder (PA-12) were chosen to fabricate printed bonded magnets. This was carried out to investigate the impact of different feedstock compositions and the characteristics of bonded magnets when recycled HDDR powder is used as raw material.

Figure 20 illustrates the feedstock preparation process, which involves the incorporation of HDDR particles into PA-12 using a Y mixer. The HDDR particles, produced in the preceding stages of this study, are combined with PA-12 to create three distinct feedstock

compositions: 30%, 45%, and 60% by volume of PA-12. The mixing process is conducted at a rotational speed of 30 rpm for a duration of 15 minutes, ensuring homogeneity in the resulting feedstock.

Figure 20 - Feedstock preparation process, detailing the incorporation of recycled ferromagnetic particles into the polymeric binder and the resulting three feedstock compositions.

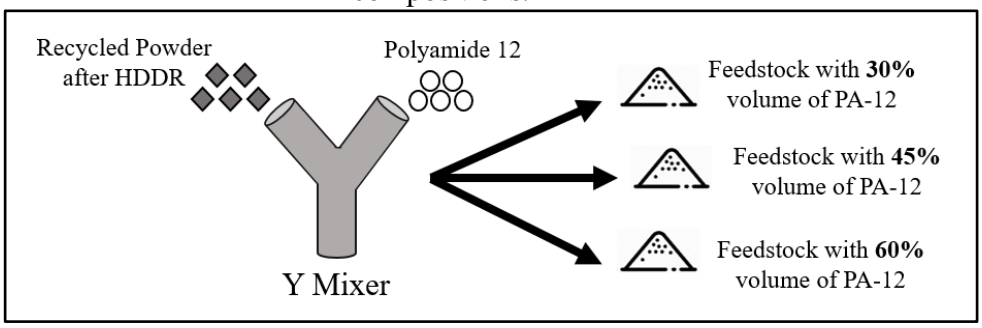

Source: Author

3.2.3 Printing Magnets

The final stage of the processing methodology in this study involved the fabrication of printed bonded magnets via additive manufacturing (AM). A prototype Selective Laser Sintering (SLS) machine, LaserFunde, produced by Alkimat, was employed to generate the samples. This equipment includes a feeding platform, a building platform, and a dispenser, as depicted in Figure 21. It operates using a gas-based carbon dioxide (CO_2) laser with a power output of 100 W. Each platform is equipped with dual internal heaters located at the top. The design of each component was facilitated through STL file reading software, enabling precise component design and customization of construction parameters for each sample batch.

Figure 21 - Main components of the LPBF machine used in this work

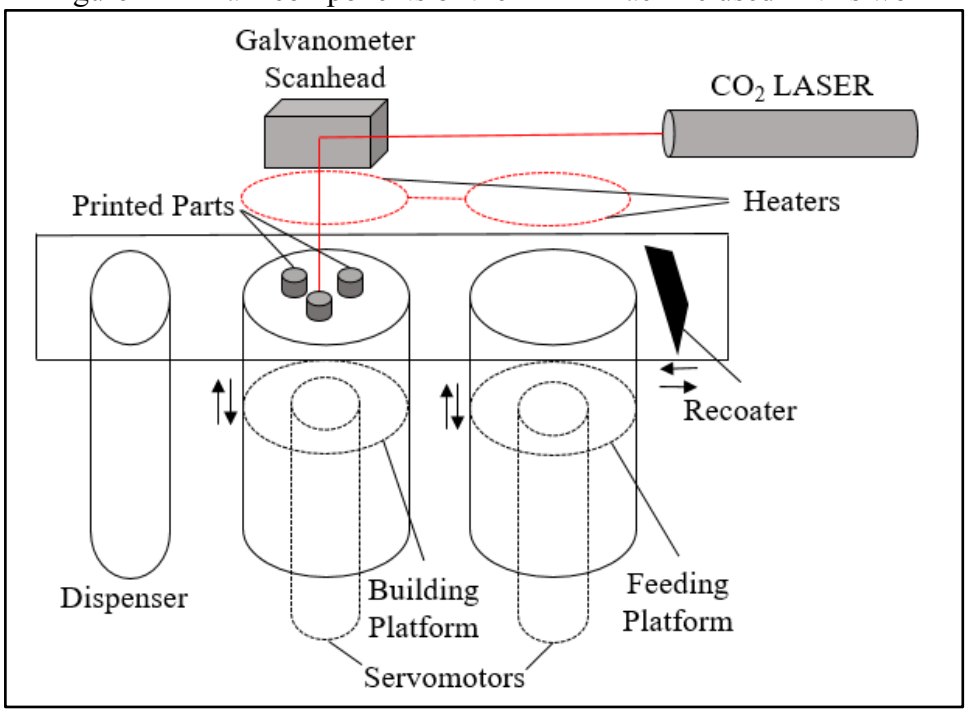

Source: Author

The samples used in this research were obtained from the prepared feedstock, which combined HDDR and PA-12, utilizing the LaserFunde equipment. The selected parameters are presented in the Table 2. These parameters were chosen based on the investigations of Fim *et al*. [93], who optimized the additive manufacturing process for Nd-Fe-B bonded magnets by exploring the interplay of polyamide-12 volumetric fraction and laser speed values.

Table 2 - Parameters of the LPBF to obtain Nd-Fe-B recycled bonded magnets of this study

Laser	CO_2 (λ = 10600 nm)
Laser beam power	40 W
Scan speed	600 mm/s
Hatch spacing	0.2 mm
Layer thickness	0.1 mm
Powder bed temperature	130 °C

Source: [93]

This equipment is available at the Innovation Center for Molding and Additive Manufacturing (NIMMA), located at the UFSC Technological Center (CTC). A simplified scheme showing the production of the printed bonded samples is illustrated in Figure 22 and each LPBF cycle consisted of the following steps:

Figure 22 - Scheme to produce bonded magnets from different feedstock compositions

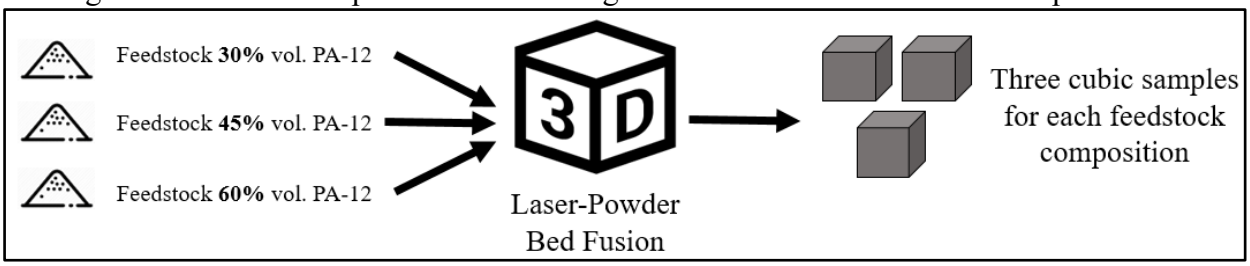

Source: Author

1. Each print batch was allocated in the equipment's feeding system and preheated to 160 °C for 20 minutes using infrared lamps.

2. Then, the composition of each studied print batch was processed using laser, following the parameters described in Table 2.

3. After completing the printing cycle, each batch of samples was slowly cooled down to room temperature while still inside the LPBF equipment.

4. Each fabricated batch consisted of printing three cubic samples measuring 10 mm in dimensions.

After the printing process was completed, the samples underwent a series of characterizations to evaluate their properties. The first characterization method employed was the evaluation of geometrical density. This method is useful for determining the porosity and magnetic load of the printed magnets.

Following the geometrical density characterization, the printed magnets were subjected to microstructural characterization using scanning electron microscopy. This technique allowed to observe the HDDR recycled powder embedded within the polymeric matrix.

A hystograph was used to measure the magnetic properties of the magnets, providing their coercivity and remanence. These measurements are important for assessing the effectiveness of the printing process and determining whether the recycled HDDR powder is suitable for use in LPBF.

3.3 CHARACTERIZATION TECHNIQUES

This subsection describes the characterization techniques used in this work. It is divided into three main categories: 3.3.1 Magnetic Characterization, 3.3.2 Microstructural Characterization, and 3.3.3 Other Techniques.

3.3.1 Magnetic Characterization

The aim of magnetic characterization is to obtain the main figures of merit of a magnet. The hystograph subjects the sample to a magnetic field of sufficient intensity to demagnetize the sample. Additionally, the measuring equipment detects the field induced by the sample. In this way, the equipment plots the B-H cycle of the magnet and calculates the main properties of these materials, such as remanence, coercivity, and maximum energy product.

A Brockhaus hystograph (model HG 200) was used in this study. This equipment allows measurements at temperatures ranging from 25 to 180 ºC, with a maximum applied field of approximately 1700 kA/m. The software MAG-Expert was utilized for constructing the B-H cycle. Prior to hystograph characterization, the samples underwent magnetization using a GlobalMag CP2000 pulse magnetizer that applies a magnetic field of up to 4 T. The magnetic characterization analyses were conducted at the Magnetic Materials Laboratory (MAGMA) on the UFSC campus in Florianópolis.

3.3.2 Microstructural Characterization

The microstructural characterization was conducted using a Scanning Electron Microscope (SEM) - JEOL JSM-6390 LM model with a maximum resolution of 1 nm (15 kV). Images were captured in Secondary Electrons (SE) mode for topography and in Backscattered Electrons (BSE) mode for chemical composition contrast of the phases. This process is useful for identifying the phases present in the magnet. The analysis was conducted at the Central Laboratory of Electron Microscopy (LCME) situated on the UFSC campus in Florianópolis/SC.

For the BSE mode characterization, the preparation of samples was carried out using the following steps: embedding the sample in resin, followed by sanding using sandpapers (from 80 to 2000) and finally the sample was polished using diamond paste (1 μm). It is important to note that no kind of etching was utilized.

Additionally, Magneto-Optic Kerr Effect (MOKE) analysis (using Zeiss Axio Imager. D2m evico magnetics GmbH) was performed to analyse the domain structure of the end-of-life magnet. The preparation of samples was the same as described for microstructural analysis using SEM. A scheme of the surface analysis is shown in Figure 23, where the images were captured on the surface perpendicular to the sample's c-axis (easy magnetization). This analysis was carried out in the Functional Materials Laboratory of the Technical University of Darmstadt, Germany (*Funktionale Materialien – Technische Universität Darmstadt*).

Figure 23 - Scheme of the surface analysis for Magneto-Optic Kerr Effect (MOKE)

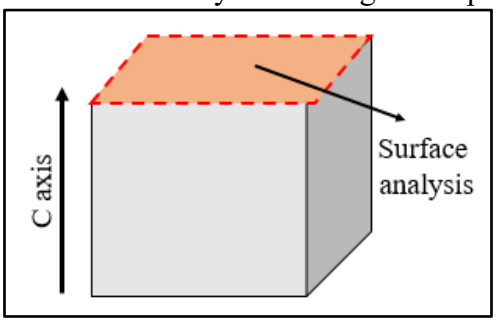

Source: Author

3.3.3 Other Techniques

3.3.3.1 Geometric Density

The analysis of geometric density (ρ) was conducted by measuring the volume and mass of the samples. A digital caliper with two decimal place readings was used to determine the volume. The mass was determined using a precision balance of the XS204 model from Mettler Toledo. Based on the collected data, it is possible to estimate the porosity level of the magnets by comparing the obtained values with maximum theoretical references. These references are calculated using the Law of Mixtures, as shown in Equation 5 [24],

$$\rho_{theo} = (\rho\ PA12 \times f\ PA12) + (\rho\ Nd_2Fe_{14}B \times f\ Nd_2Fe_{14}B) \qquad \text{(Eq. 5)}$$

where f and ρ represent the volumetric fraction and density of each component used in the feedstock, respectively. By comparing ρ_{geo} (geometric density) and ρ_{theo} (theoretical density), it is possible to determine the porosity of the produced magnets based on the volumetric fraction of PA-12 and the processing parameters used, according to the Equation 6:

$$\text{Porosity} = 100 - (\rho_{geo}/\rho_{theo}) \quad \text{(Eq. 6)}$$

3.3.3.2 Elemental Analysis of Carbon, Oxygen and Hydrogen

The quantification of carbon and oxygen impurities was conducted at various stages of the recycling process, including the bulk End-of-Life magnet, post Hydrogen Decrepitation (HD), and post Hydrogenation, Disproportionation, Desorption, Recombination (HDDR). This characterization aims to evaluate impurity uptake during each recycling phase. Additionally, hydrogen quantification was performed to monitor hydrogen levels in samples fo llowing HD and HDDR treatments.

Carbon content was determined using the EMIA Carbon/Sulfur Analyzer, which employs infrared technology. The device combusts the sample within an induction furnace, producing gases such as carbon dioxide and sulfur dioxide. These gases are then quantified using HORIBA's Non-Dispersive Infrared (NDIR) technology, which identifies specific gas molecules based on their infrared light absorption.

Elemental analysis of oxygen and hydrogen was carried out using inert gas fusion on the Leco ONH836 instrument. Each analysis utilized 0.2 g of the material, with three measurements taken per sample to ensure accuracy.

4 RESULTS AND DISCUSSION

This chapter details the results obtained throughout the research, segmented into three primary subsections:

- End-of-Life Magnet Characterization: This subsection elaborates on the characterization of the recycled raw material utilized in this study.
- Hydrogen Processing: This subsection presents an in-depth analysis of the results and discussions regarding Hydrogen Decrepitation (HD) (4.2.1) and the Optimization of the Hydrogenation, Disproportionation, Desorption, Recombination (HDDR) treatment (4.2.2).
- Additive Manufacturing of Bonded Magnets from Recycled Powders: This section presents the findings on the processing of HDDR in Laser Powder Bed Fusion (LPBF) for the fabrication of recycled bonded magnets, focusing on microstructural (4.3.1), geometrical (4.3.2), and magnetic characterization (4.3.3).

4.1 END-OF-LIFE MAGNET CHARACTERIZATION

To characterize the End-of-Life magnet, a detailed microstructural analysis was conducted using a scanning electron microscope (SEM) in Backscattered Electrons (BSE) mode. This technique revealed the distinct phases present within the magnet. Figure 24 illustrates two discernible phases: Figure 24(a) presents an overview of the magnet, while Figure 24(b) shows it at a higher magnification. The $Nd_2Fe_{14}B$ phase is identified by its darker appearance, whereas the Nd-rich phase is brighter. This contrast arises from the differing chemical compositions of these phases, as observed in the BSE mode. The Nd-rich phase appears lighter due to the higher atomic weight of Nd and its greater concentration in this phase compared to the main $Nd_2Fe_{14}B$ phase.

Figure 24 - Microstructural analysis of the End-of-Life magnet using SEM in BSE mode. Figure (a) provides a comprehensive overview of the magnet, while (b) offers a higher magnification view

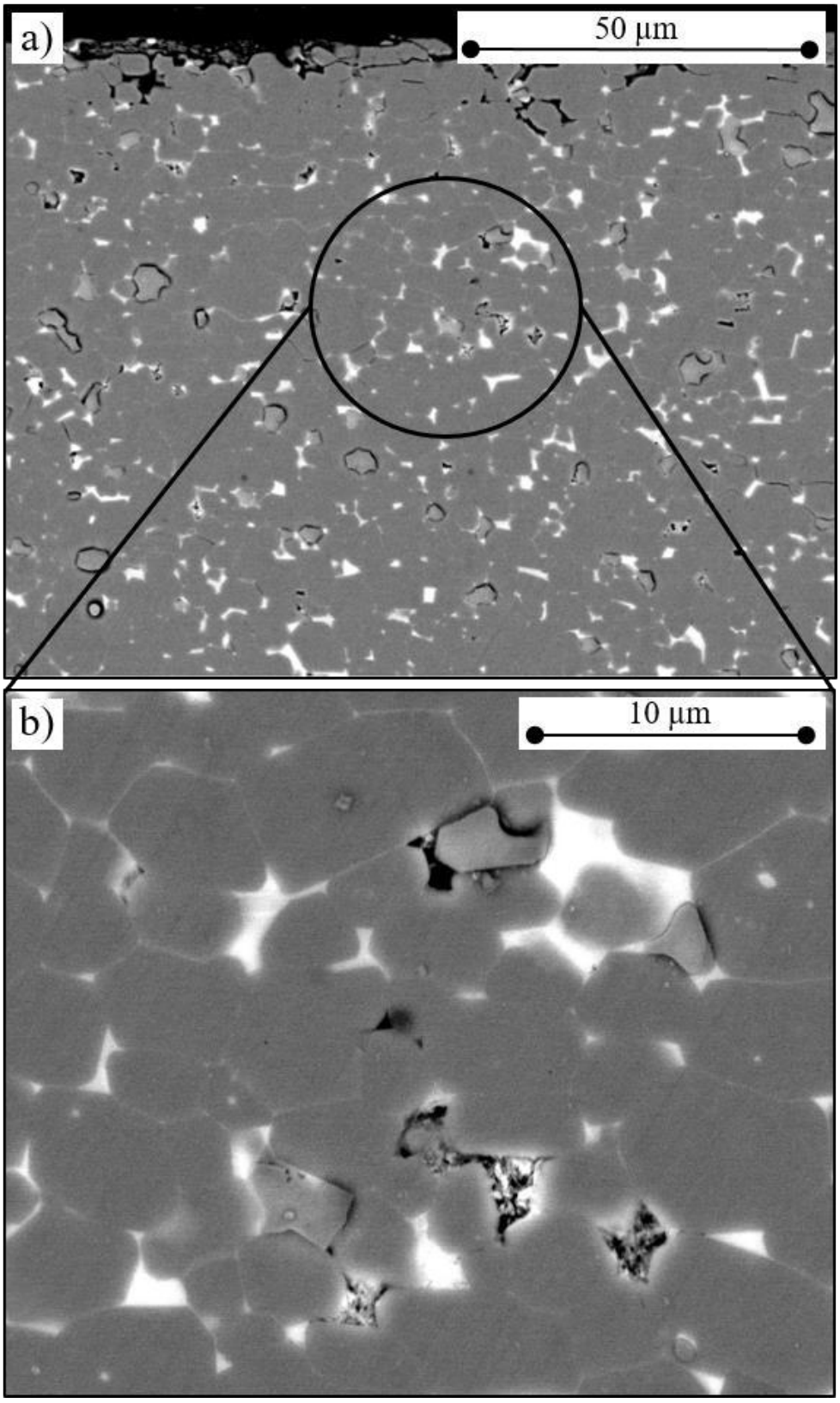

Source: Author

The $Nd_2Fe_{14}B$ phase, also referred to as the φ-phase, exhibits high intrinsic magnetic properties, including high saturation polarization (J_s) and significant magnetocrystalline anisotropy (H_A). By optimizing processing conditions and achieving desirable microstructural characteristics, it is possible to produce high extrinsic magnetic properties values for a Nd-Fe-B magnet. Notable extrinsic properties include remanence (B_r), coercivity (H_{cj}), and the maximum energy product ($(BH)_{max}$).

In terms of recycling, it is crucial to maintain the integrity of the φ-phase and prevent oxidation. This is because direct reprocessing of these magnets is not possible without their composition and intrinsic properties. If the characteristics of the φ-phase are not preserved, additional processing (such as reduction-diffusion) is required to recover the Nd-Fe-B hard magnetic phase. For the End-of-Life magnet used in this study, the initial condition of the φ-phase is satisfactory, and the magnet's corrosion status is not advanced.

Another important aspect to note is the grain size of the φ-phase. As illustrated in Fig. 24 (b), the grain size is around 10 μm. Such a size is typical for sintered magnets produced using powder metallurgy techniques. Magnets with smaller grain sizes are known to exhibit higher coercivity values, which accounts for the H_{cj} observed in Fig. 13.

The brighter phase in Fig 24 refers to the Nd-rich phase and it provides insights into the distribution of Nd in the microstructure of the magnet. A microstructure containing a thin layer of the Nd-rich phase on the boundaries of each grain improves the magnetic properties, particularly the coercive force. This improvement is attributed to the decoupling of the ferromagnetic phase, which influences the interactions between Nd-Fe-B grains and prevents the formation of reverse domains [32].

Additionally, the presence of at least two contrasts in the Nd-rich phase triple junction grains suggests multiple phases, such as Nd oxide. This provides insight into the initial condition of the raw material used for recycling in this study. Nd oxide could result from the powder metallurgy processing, as it involves fine powder in a condition where Nd is highly reactive with the air present in the atmosphere. Furthermore, the working conditions of the magnet might affect the absorption of oxygen.

In Figure 25 and 26, the magnetic domain structures of the End-of-Life magnet and a commercial magnet are presented, respectively. The images reveal a maze-like pattern of bright and dark domains. These domains are characterized by their magnetizations directed perpendicular to the observation surface, creating a visually interplay of contrasting regions. This maze domain pattern is specifically observed at the c-plane [102, 103].

Figure 25 - Magneto-optic Kerr effect (MOKE) image of the End-of-Life Magnet

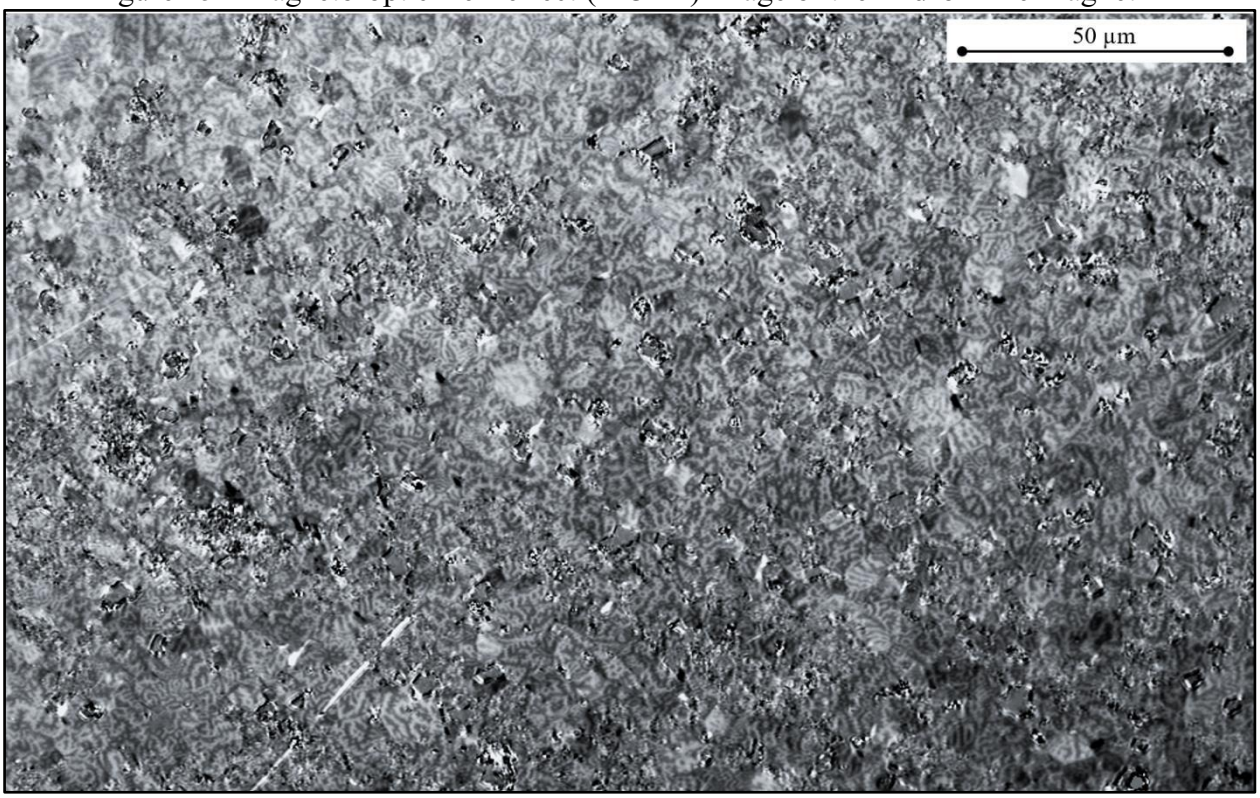

Source: Author

Figure 26 - Magneto-optic Kerr effect (MOKE) image of a Commercial Magnet

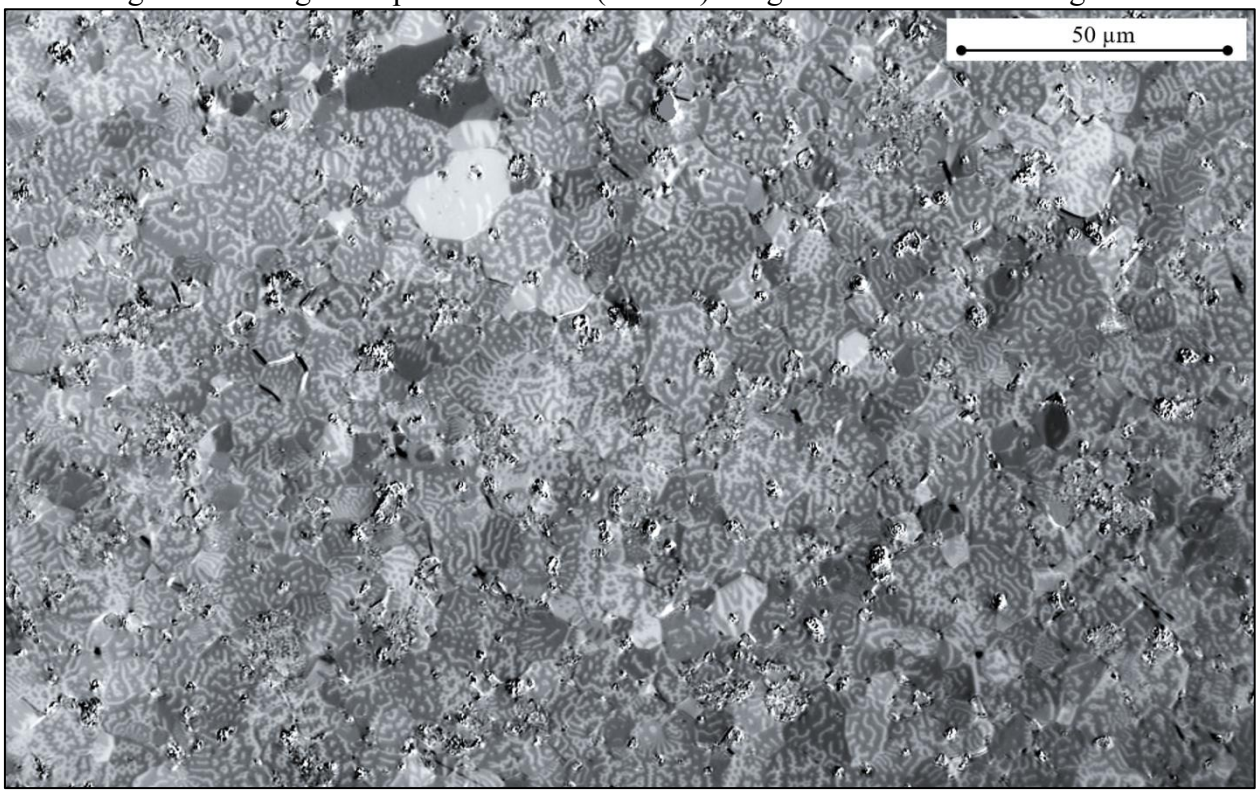

Source: Author

The comparative analysis of Magneto-optic Kerr effect (MOKE) images reveals that both the End-of-Life magnet utilized in this study and a commercially available magnet exhibit identical maze-like patterns in their magnetic domain structures. This observation suggests that the critical characteristics of the φ-phase have been preserved in the End-of-Life magnet. The preservation of these characteristics is crucial for maintaining the high property values and quality of reprocessed Nd-Fe-B magnets.

In addition to the microstructural characterizations presented, an elemental analysis was conducted to assess the carbon and oxygen content in the raw material used in this study. Table 3 provides the measured values of the carbon and oxygen content in parts per million (ppm). The raw material derived from End-of-Life magnets exhibited a carbon content of 1200 ppm, an oxygen content of 2500 ppm, and a hydrogen content of 60 ppm. It is important to note that these values represent the mean of three measurements conducted on the same sample.

Table 3 - Carbon, Oxygen and Hydrogen content in the End-of-Life magnet and in a commercial alloy

Sample	C (ppm)	O (ppm)	H (ppm)
End-of-Life Magnet used in this work	1200	2500	58
Commercial Alloy	160	450	-

Source: Author

In the context of recycling magnetic components, a critical consideration is the uptake of carbon and oxygen in End-of-Life magnets, which serve as raw materials for new magnet production. Existing literature [104, 105] has extensively studied the impact of these elements on magnetic properties. High oxygen content, in particular, can detrimentally affect the magnetic properties, especially in sintered Nd-Fe-B magnets. Significant oxygen uptake is primarily observed in the Nd-rich phase, a crucial component for maintaining optimal magnetic properties. This phase is essential for the decoupling of hard magnetic grains [106, 107].

A significant reference point is the typical oxygen content in a commercial alloy, which is approximately 450 ppm, as detailed in Table 3. This value is considerably lower compared to the oxygen content in the End-of-Life magnet used in this study, which measures 2500 ppm. The elevated oxygen levels in the sintered magnet can be attributed to its prior processing via powder metallurgy techniques. During this process, the bulk alloy undergoes hydrogen decrepitation (HD) and fine milling, resulting in a powder form. Due to the reactive

susceptibility of Nd-Fe-B, its interaction with the environment is more pronounced when in powder form.

The recycling of End-of-Life magnets for the production of new magnets via reprocessing necessitates careful consideration of the potential impacts on magnetic properties. Utilizing recycled magnets as raw materials introduces elevated initial levels of oxygen and carbon. Further increases in these levels during the reprocessing phase could adversely affect the magnetic characteristics of the resultant magnet. Hence, the rise in carbon and oxygen content in the final magnet's chemical composition, as influenced by the recycling process, must be meticulously managed to preserve and optimize its magnetic properties [105 – 107].

4.2 HYDROGEN PROCESSING

This subsection presents the results derived from the application of two hydrogen processing techniques aimed at producing suitable raw materials for Laser Powder Bed Fusion (LPBF). The methods under investigation are Hydrogen Decrepitation (HD) and Hydrogenation, Disproportionation, Desorption, Recombination (HDDR). Section 4.2.1 details the outcomes of the HD process, while Section 4.2.2 elaborates on the results from the HDDR method.

4.2.1 Hydrogen Decrepitation (HD)

The initial step in the recycling process examined in this study involved the application of Hydrogen Decrepitation (HD) to the End-of-Life magnet. The HD process was conducted in a hydrogen atmosphere at ambient temperature, as delineated in subsection 3.2.1.1.

4.2.1.1 Magnetic Characterization of the Decrepitated Powder

Figure 27 illustrates the demagnetization curves of the End-of-Life magnet (depicted in black) and the decrepitated powder (depicted in orange). The HD product in this instance is in particle form. Bonded samples were created by embedding HD particles in a polymeric binder to secure these metallic particles. Magnetometry was then employed to measure these samples. The graph (Fig. 27) displays a normalized demagnetization curve for the bonded sample, indicating that only the ferromagnetic volume was taken into account. For this case,

the remanence value is normalized, facilitating a direct comparison with the bulk properties of the End-of-Life magnet.

The decrepitated powder has suboptimal magnetic properties, as shown in Fig. 27. This is evidenced by its remanence of 0.18 T and a coercivity of 70 kA/m. The H_{cj} indicate a 95% reduction compared to the bulk properties of the End-of-Life magnet.

Figure 27 - Demagnetization curves of End-of-Life magnet (black) and decrepitated powder (orange)

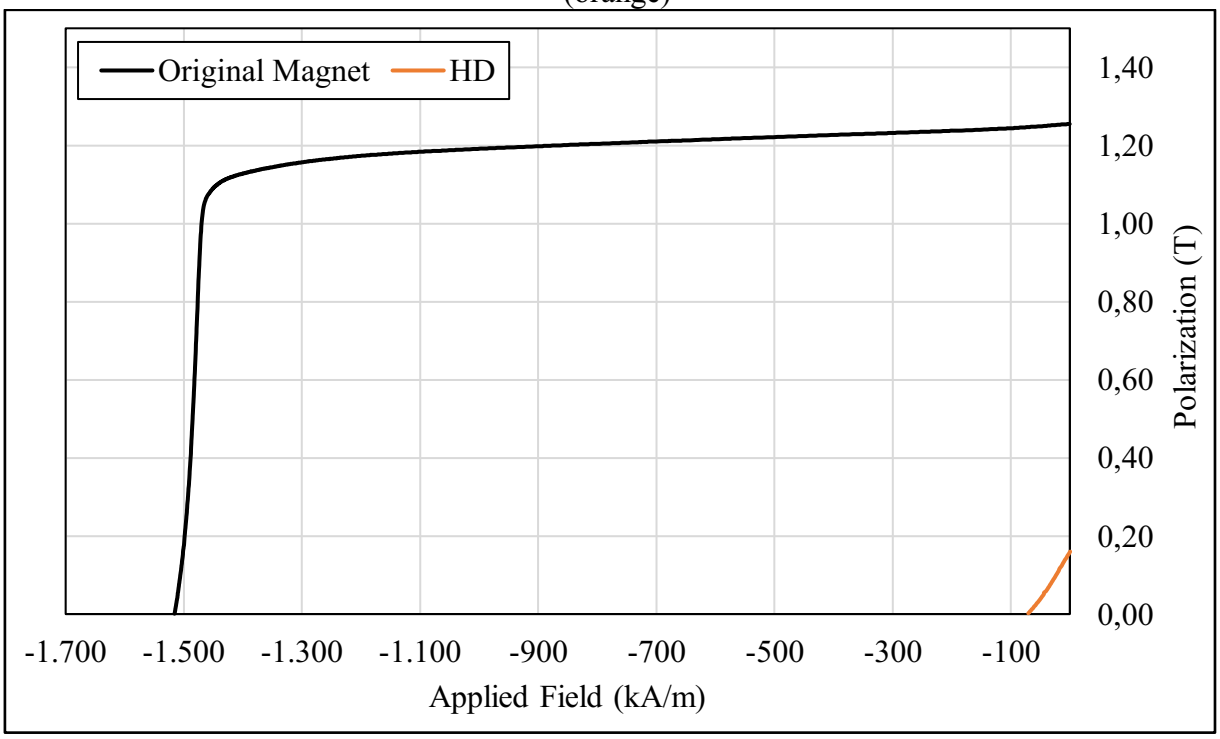

Source: Author

The low coercivity value observed in the case of HD can be attributed to some factors. The presence of hydrogen in solid solution reduces the anisotropy field of the $Nd_2Fe_{14}B$ phase, and consequently, the coercivity [108].

In addition, the strong exothermic reaction during the HD involved in the formation of Nd-H leads to the localized disproportionation of the material, thereby producing free iron in the grain boundary material [108]. This subsequently results in a soft magnetic phase (α-Fe) which is thought to be one factor that decreases the coercivity value of the powder.

In a study conducted by Zakotnik *et al*. [90] it was suggested that it is possible to nearly fully recover the coercivity value of the initial magnet following a degassing heat treatment, in which the hydrogen is removed from φ-phase and Nd-rich phase.

For further evaluation, a sample of the HD product derived from the End-of-Life magnet was subjected to a degassing process. This process involved heating the sample under vacuum conditions at a controlled rate of 10 °C/min until reaching a plateau, which was maintained for 1 hour at a temperature of 900 °C. Post-degassing, the resulting powder was sieved to classify particles into distinct size fractions: less than 63 µm, between 63-125 µm, between 125-500 µm, and greater than 500 µm. The coercivity values corresponding to each particle size range are presented in Figure 28.

Figure 28 - Coercivity values for different particle size ranges before and after the degassing process.

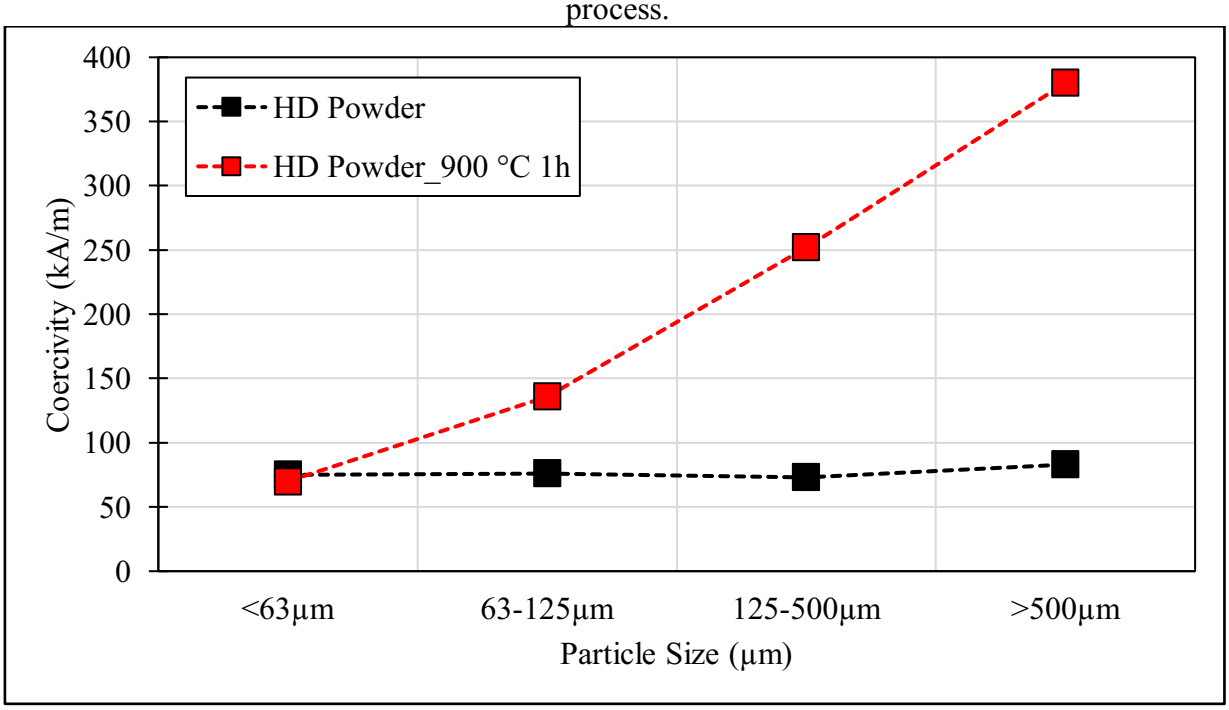

Source: Author

In the referenced study [90], the authors successfully recovered approximately 90% of the initial magnet's coercivity. However, their analysis focused on particles with an approximate diameter of 1 mm. As illustrated in Figure 28, the enhancement of coercivity post-degassing is significantly influenced by the particle size. Initial measurements indicated coercivity values around 70 kA/m. Notably, as the particle size increased, H_{cj} values correspondingly rose, with particles larger than 500 µm achieving a coercivity of approximately 370 kA/m.

Based on the model by Kobayashi *et al.* [109], smaller particles are assumed to have a higher defect concentration, which eases the formation of reverse domains during demagnetization, thus reducing the coercivity. Reversed magnetic domains are observed to nucleate at localized regions with lower anisotropy or defects, or in proximity to non-

ferromagnetic grains that exhibit a higher stray field. The cracks and defects induced by HD processing, as well as smaller particle sizes, can increase the number of these localized regions. Thus, leading to an increase in the nucleation of reversed magnetic domains and a decrease in coercivity [45, 67].

4.2.1.2 Microstructural Characterization of the Decrepitated Powder

Figure 29 presents a detailed examination of the powder in image (a), together with a higher magnification view of the particle grain structure in image (b). The observed polyhedral geometries have an average size of approximately 10 μm. These geometries are derived from the grains of the φ-phase, which were identified prior to the HD process, as illustrated in Figure 29(b).

Hydrogen absorption induces different volume expansions in phases such as $Nd_2Fe_{14}BH_{2.7}$ (4.8% vol.) and NdH_3 (16.4% vol.) [47], leading to decrepitation. The HD process causes most cracks to manifest at the interfaces between $Nd_2Fe_{14}B$ and Nd-rich phases in Nd-Fe-B alloys. As depicted in Fig. 29 (a), a broad distribution of particle sizes is observed, ranging from 10 μm to over 100 μm. Notably, larger particles exhibit grain agglomeration, which did not fully separate post-HD, despite the particles being fragile by the processing.

Figure 29 - Detailed examination of powder after HD process, where (a) provides an overview of the powder and (b) particle grain structure

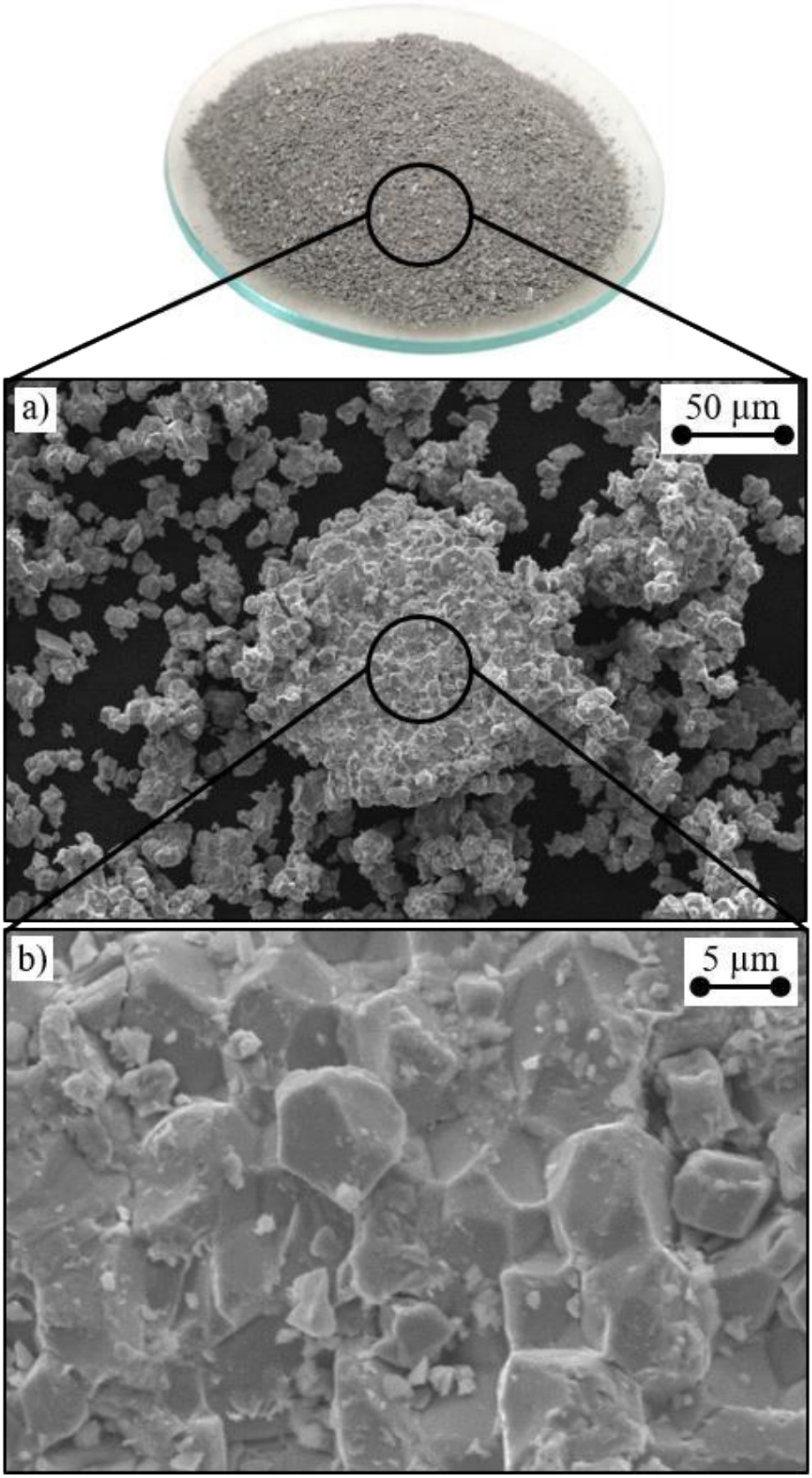

Source: Author

The powder subjected to decrepitation exhibits an irregular particle morphology, characterized by angular particles of varying sizes. This heterogeneity in particle size contributes to the powder's complex morphology, which significantly impacts its techno logical properties. Notably, the flowability of the powder, critical for powder spreading during LPBF processing, is directly influenced by this particle size distribution. Additionally, the packing density, another critical technological property, is affected. The packing density, which determines the volume of powder that can be compacted into a given space, has a direct impact on the densification of the printed parts, influencing their final structural integrity and performance [22 – 24].

To ensure compliance with the recommended powder size requirements for LPBF technologies, as indicated in the literature [22 – 24], a sieving process was conducted. The procedure involved sieving all particles to achieve a size below 106 µm, in alignment with the suggested parameters. This approach is consistent with methodologies employed in similar studies, as referenced in the provided literature [99, 101, 110, 111].

Figure 27 illustrates that the HD powder, post-degassing, displays minimal coercivity within the specified size range (< 106 µm). Consequently, coercivity adjustments are imperative before utilizing this powder as feedstock. To address this, the Hydrogenation, Disproportionation, Desorption, Recombination (HDDR) process is employed to pro duce nanocrystalline particles.

The present study details the utilization of End-of-Life magnets as raw materials and the application of HD to produce powder. This method uses the friability of the material under HD conditions, optimizing particle size for specific AM process through milling and sieving. Following this, the coercivity of the powder can be fine-tuned using the HDDR process. This approach introduces a novel pathway for incorporating recycled raw materials into powder-based AM technologies.

4.2.2 Optimization of the Hydrogenation Disproportionation Desorption Recombination (HDDR) Treatment

As detailed in subsection 4.2.1, the recycled powder exhibited suboptimal magnetic properties, necessitating the implementation of an alternative strategy to enhance these properties. One viable approach involves the development of a nanocrystalline grain structure within the recycled powder. The HDDR process is a recognized method for achieving refined grain structures in Nd-Fe-B alloys. This technique induces hydrogen-induced phase

transformations to produce highly coercive Nd-Fe-B powders. This subsection focuses on the optimization of the HDDR treatment performed in this study, with the objective of generating high-coercivity powders suitable for use in LPBF applications.

4.2.2.1 Magnetic Characterization of the HDDR Powder

According to the methodology outlined in section 3.2.1, a series of plateau temperature experiments were conducted, ranging from 800 to 940 ºC, to maximize the magnetic properties of the recycled powder. Other variables, including hold time for disproportionation, recombination, and hydrogen pressure, were not examined. Prior research conducted at the Magnetic Materials Laboratory (MAGMA) [26], as well as studies by other authors [25], suggest that these parameters have a negligible impact on the magnetic properties values of treated powders.

The experimental results reported by Engerrof [26] indicate that variations in the disproportionation time, ranging from 60 to 240 minutes, do not significantly impact the magnetic properties of the material. Furthermore, the recombination plateau time was found to stabilize after 15 minutes, suggesting that this duration is adequate for the completion of the recombination reaction. Notably, the plateau temperature emerged as the most critical factor influencing the coercivity value. This finding is corroborated by Lixandru [25], who also observed that temperature plays a pivotal role in determining the final coercivity value of HDDR powder.

Therefore in this study, the disproportionation and recombination plateau times were not further investigated. Instead, the plateau temperature was varied and the properties of the product were measured.

The demagnetization curves depicted in Figure 30 illustrate the magnetic properties of samples subjected to varying HDDR plateau temperatures. The ferromagnetic powder obtained from these distinct HDDR processing temperatures was combined with a polymeric binder (PA-12) to fabricate compressed bonded samples. The samples were prepared with a volumetric ratio of 55% HDDR powder to 45% PA-12, specifically to assess their magnetic properties. Importantly, the polarization values presented in Figure 30 are normalized. This normalization assumes that the samples are composed entirely of ferromagnetic particles, thereby excluding the volume contribution of the polymeric binder.

Figure 30 - Demagnetization curves of samples produced with various HDDR plateau temperatures

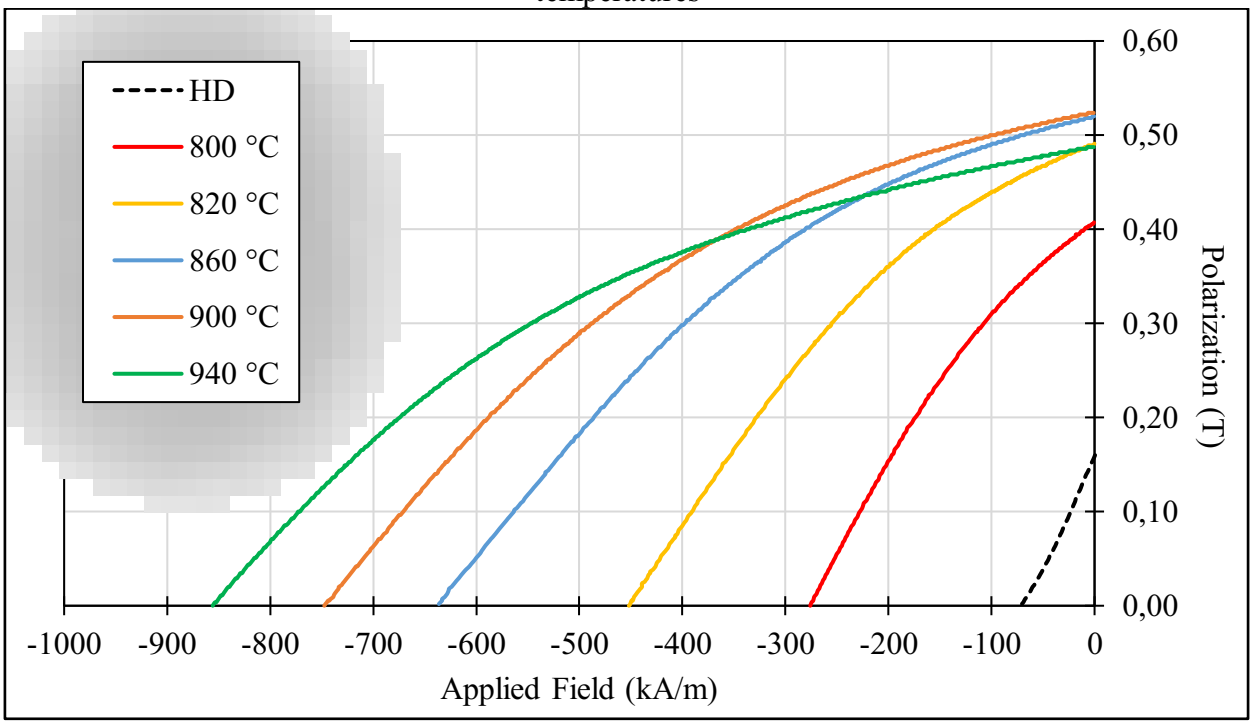

Source: Author

The initial processing carried out under 800 ºC (red line) yielded a HDDR product with a coercivity value of 270 kA/m and remanence of 0.40 T. A gradual increase in the HDDR temperature plateau to 860 ºC resulted in a product with H_{cj} around 640 kA/m and B_r of 0.51 T. The processing conducted at 940 °C produced the highest coercivity value of 850 kA/m, which signifies a 600% increase when compared to the HD powder. These findings confirm that higher temperature plateaus correspond to increased coercivity values, reinforcing the strong relationship between thermal processing conditions and magnetic properties.

The primary criterion employed in this study to determine the optimal set of processing parameters is the resultant coercivity value of the powder. Based on findings from prior optimizations in other studies [25, 26], coercivity values approximating 800 kA/m were judged adequate for the ongoing investigation. These values are also indicative of the feasibility of using the produced recycled in LPBF processes.

Additionally, the HDDR powder demonstrated coercivity values comparable to those of commercially available powders. This is shown in Figure 31, which presents three demagnetization curves for reference. These curves include the HD powder produced in this study (depicted by the black dashed line), a spherical commercial powder (Magnequench MQP -

S) shown by the red full line, and the optimized HDDR powder produced under the best conditions (940 °C) shown by the green full line.

Figure 31 - Comparison of demagnetization curves for HD powder produced in this study, a spherical commercial powder (Magnequench MQP-S), and optimized HDDR powder produced at 940 °C

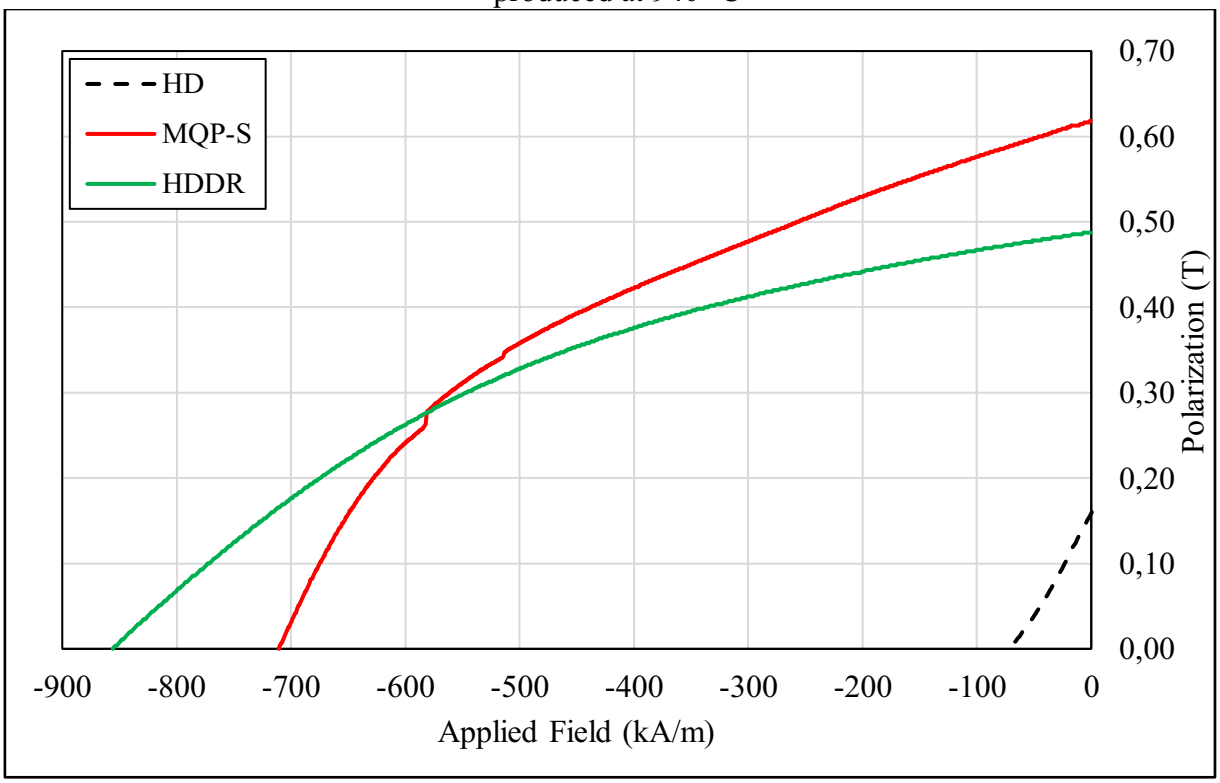

Source: Author

The HD powder exhibited mean coercivity and remanence values of 70 kA/m and 0.18 T, respectively. Following HDDR processing, these values significantly increased to 850 kA/m and 0.50 T. The magnetic properties of the HDDR powder are comparable to those of the MQP-S powder, which has H_{cj} = 710 kA/m and B_r = 0.60 T. Notably, the produced HDDR powder demonstrates a higher coercivity value than the referenced commercial powder, indicating the potential for utilizing recycled raw materials in the production of additively manufactured bonded magnets.

4.2.2.2 Microstructural Characterization of the HDDR Powder

Figure 32 presents a comparative analysis of the powder following the HDDR (a) and HD (b) processes. Post-HDDR, the general characteristics of the powder are preserved, as depicted in Figure 32 (a) and (b). The particle size exhibits significant variability, ranging from approximately 100 μm to as small as 10 μm. Additionally, the HDDR process results in a visually noticeable irregular morphology of the particles. The morphology, which refers to the overall shape and surface of the particles, plays a critical role in various aspects of LPBF processing. The irregular morphology impacts packing density, flowability, and heat transfer properties during the LPBF process [22, 23].

Figure 33 illustrates scanning electron microscopy (SEM) images of HDDR-processed particles. Panel (a) shows a detailed view of a single particle, while panel (b) presents the same particle at a higher magnification. The polyhedral structures of the original grains from the End-of-Life magnet are preserved post-HDDR processing. The particle surface exhibits increased roughness, likely resulting from the refined grain structure within the particles. As shown in Fig. 33(b), the average grain size is approximately 300 nm. The high coercivity value of 850 kA/m observed in the HDDR sample is attributed to this refined 300 nm grain structure. This observation aligns with studies by Lixandru [25] and Engerrof [26], who reported sub-micrometric grains ranging from 200 nm to 500 nm while optimizing HDDR parameters.

Figure 32 - Comparative analysis of powder morphology post-HDDR (a) and post-HD (b) processes

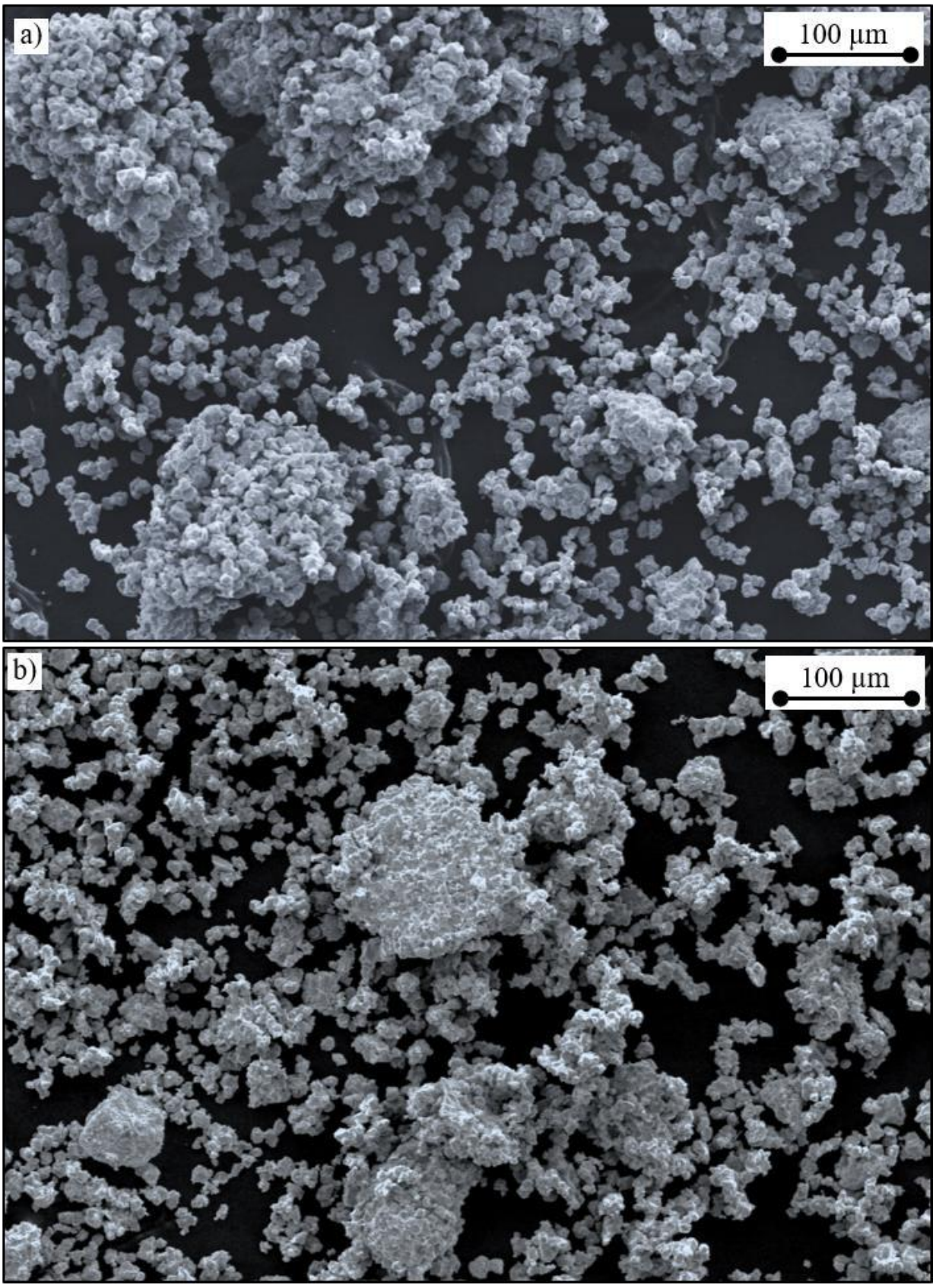

Source: Author

Figure 33 - SEM images of HDDR powder: a) a single HDDR particle, and b) the same area viewed at a higher magnification

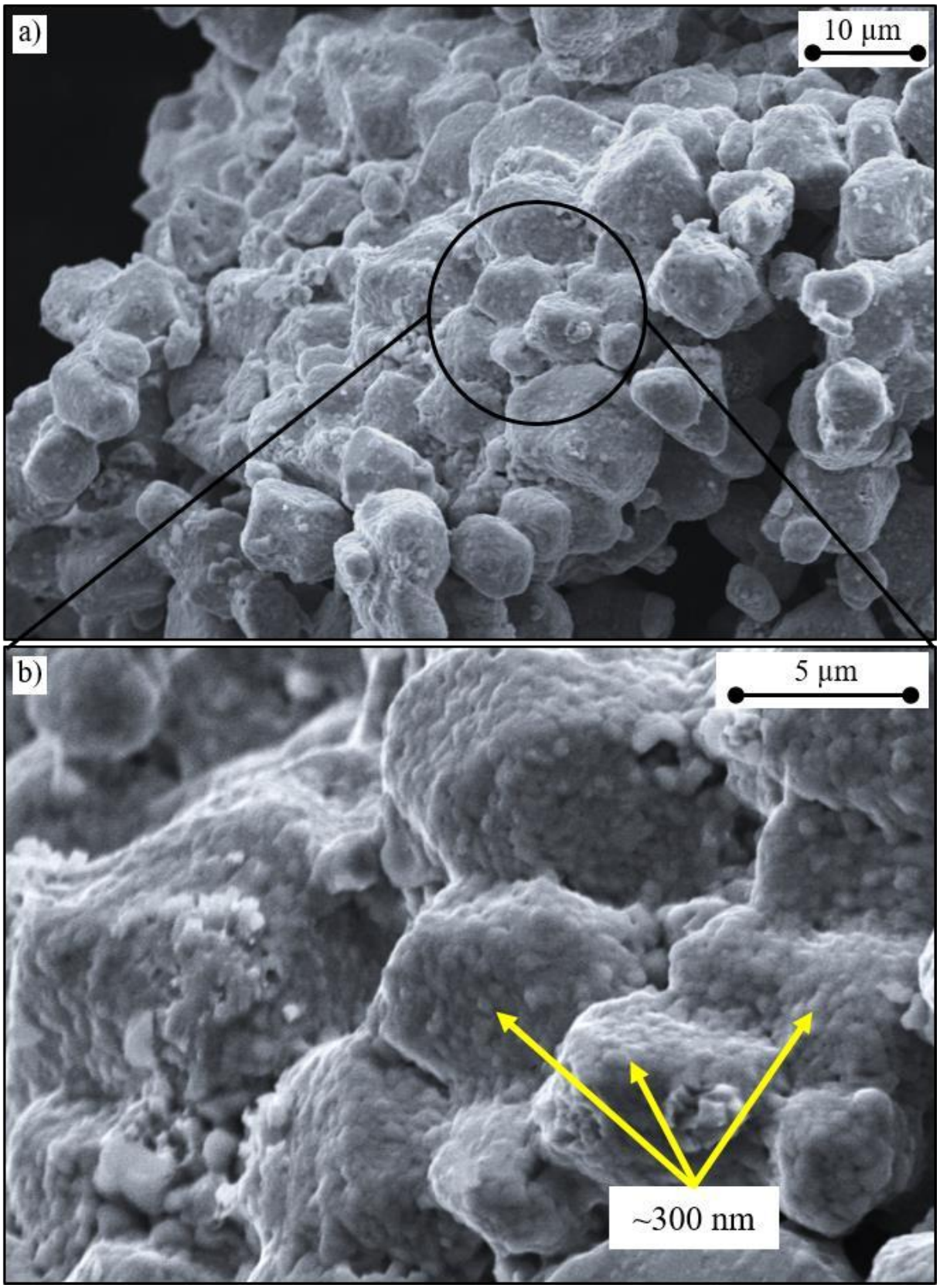

Source: Author

As outlined and noted in various research findings [57 – 62], the HDDR processing leads to the disproportionation of Nd-Fe-B into a finely dispersed mixture of Fe-B and Nd-H into an α-Fe matrix. This phenomenon arises due to the higher stability of Nd-H in contrast to Nd-Fe-B-H. The disproportionation becomes evident at higher temperatures due to the increased atomic diffusion within the solid-state structure [58].

Initially documented by [57] and subsequently corroborated by subsequent researchers [58 – 61], the removal of hydrogen from Nd-H can be achieved through heating under vacuum conditions at temperatures exceeding 800 °C. Consequently, the use of vacuum during processing removes hydrogen, causing the recombination of α-Fe, Fe_2B, and Nd-H components, and ultimately restoring the original Nd-Fe-B phase. This process would be expected to proceed from many nucleation sites and result in very fine, spherical-type grains [58]. Thus, the initial microstructure of the end-of-life magnet, characterized by grains approximately 10 μm in size, undergoes a transition to a significantly finer grain size after the HDDR treatment.

The peak coercivity recorded at 940 °C (as shown in Fig. 30) can be ascribed to the establishment of an optimum grain size and the elimination of free iron, factors critical for the development of high values of coercivity. Lower temperatures in the HDDR yield residual free iron, while excessively high temperatures lead to undesirable grain enlargement, both of which are detrimental to coercivity development [11].

In the diffraction analysis conducted by Engerrof [26], the presence of Nd-H and α-Fe phases was noted in samples subjected to a plateau temperature of 730 °C. This occurrence was attributed to the incomplete recombination of disproportionated phases back into Nd-Fe-B. Similarly, comparable observations can be made in the samples examined in the current study, treated within the temperature range of 800 ºC to 900 ºC. It is assumed that the inadequate energy availability in the system at lower temperatures may account for this partial reaction.

Higher temperatures used in the HDDR process lead to excessive grain growth, a phenomenon also observed by Engerrof [26]. In Figure 34, the micrograph obtained from scanning electron microscopy analysis illustrates the powder sample treated at 850 °C [26]. A comparison with the microstructure of the sample produced in the present study (Fig. 32) reveals heterogeneities. The sample from [26] displays grains with an average diameter exceeding 4 μm alongside others measuring approximately 600 nm. Correspondingly, low coercivity values are measured for the powder obtained by the HDDR, as this magnetic property is influenced by grain size and microstructural irregularities. Considering the hardening

mechanism characteristic of nanocrystalline materials, it is expected that coercivity values would be low.

Figure 34 - SEM image (fracture surface) of HDDR powder with excessive grain growth.

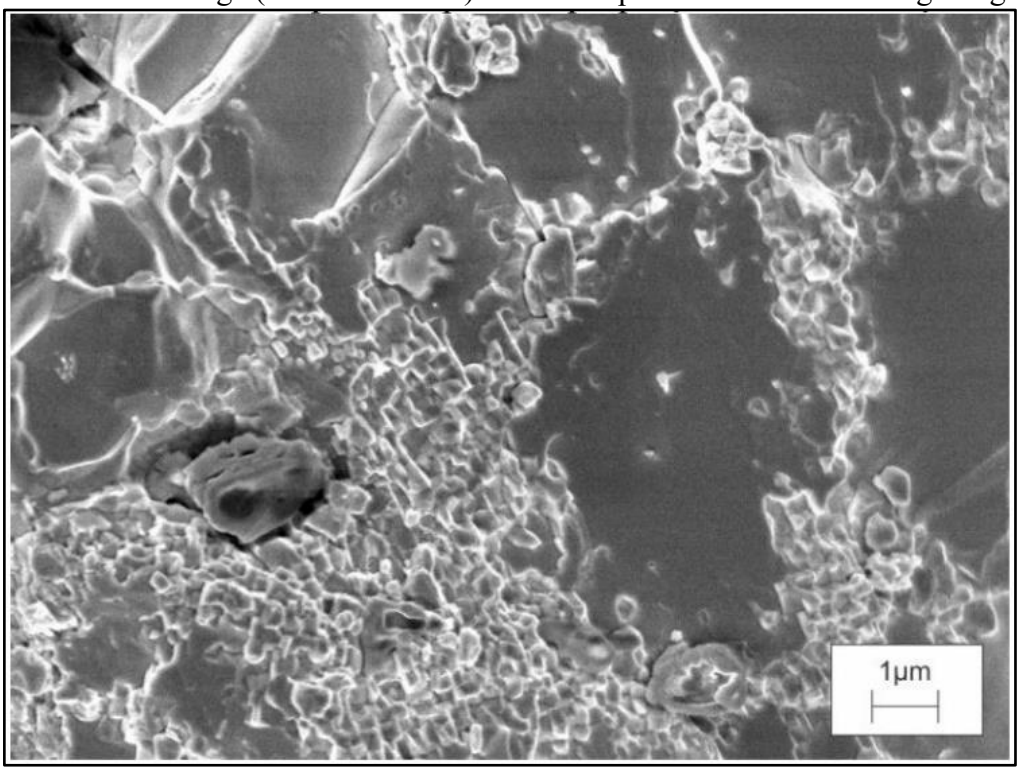

Source: [26]

It is well known that the coercivity mechanism plays a significant role in the strategy to enhance the magnetic properties. In pinning type magnets, as described in subsection 2.2.2.2 of this work, the movement of domain walls is hindered by pinning centers. These centers can be chemical inhomogeneities or defects that create a favorable energy environment for a domain wall to form. Unpinning the domain wall from these centers requires a higher magnetic field. One effective way to enhance pinning is by reducing the grain size. Regions with a highly refined grain structure provide a strong pinning force that effectively anchors the magnetic domains. As a result, demagnetization only occurs under higher applied magnetic fields [45].

This study investigated the application of HDDR processing to fabricate isotropic particles. Future research could explore the utilization of dynamic-HDDR (d-HDDR) to generate anisotropic particles. This technique has the potential to enhance the texture of individual particles, enabling the production of anisotropic bonded samples through LPBF with high remanence values. Such advancements could significantly progress the state-of-the-art in textured bonded magnets manufactured by Additive Manufacturing.

Despite the nascent stage and challenges associated with producing anisotropic magnets via AM, preliminary studies have demonstrated its potential [110]. However, due to the intricate nature of this method and the current lack of requisite infrastructure, this study does not further delve into the application of HDDR for creating anisotropic particles for LPBF processing.

4.2.2.3 Elemental Analysis of the HD and HDDR Powder

Table 4 presents a comparative analysis of the oxygen, carbon, and hydrogen content between the HD and HDDR products. Post-HD processing, the powder displayed a carbon content of 1400 ppm, an oxygen content of 4900 ppm, and a hydrogen content of 1120 ppm. Subsequent to the HDDR process, the carbon content was approximately 1290 ppm, the oxygen content increased to 5100 ppm, and the hydrogen content significantly decreased to 110 ppm.

Table 4 - Carbon, Oxygen and Hydrogen content in the HD powder and after HDDR

Sample	C (ppm)	O (ppm)	H (ppm)
End-of-Life Magnet after HD	1400	4900	1120
End-of-Life Magnet after HD and HDDR	1290	5100	110

Source: Author

Comparing the values obtained from the End-of-Life magnet in its bulk state and after HD processing (refer to tables 3 and 4), a significant increase in oxygen content was noted (from 2500 ppm to 4900 ppm). This suggests potential contamination during or after the process. The rise in hydrogen content (from 60 ppm to 1120 ppm) can be attributed to the HD process itself, which introduces nascent hydrogen and causes the material to pulverize. This phenomenon, however, increases the surface area of the particulated material in comparison to the bulk state, making it more susceptible to environmental interaction and potentially leading to oxygen uptake. Therefore, the higher oxygen content can be explained by moisture adsorption into the surface of HD particles due to handling this powder under atmospheric conditions.

Chun-Lin *et al*. [112] investigated the impact of hydrogen on the oxidation of coarse decrepitated Nd-Fe-B powder using a weight change method. Their findings revealed that HD

powder exhibited a higher oxidation rate and greater water absorption compared to the dehydrogenated powder. According to the authors, hydrogen significantly influences the oxidation process of decrepitated powder. Hydrogen bonds formed between hydrides in the powder and water molecules in the surrounding air facilitate the rapid absorption of water. This, in turn, accelerates the electrochemical reaction within the powder. Moreover, defects induced by hydrogen in the powder induces oxygen diffusion.

Following the HDDR process, a notable decrease in hydrogen content was observed from 1120 ppm to 110 ppm. This suggests successful recombination during processing. The reduced pressure in the evacuated system destabilizes the Nd-H phase, prompting the recombination of the three phases formed from disproportionation (Nd-H, Fe, and Fe-B) to reform the $Nd_2Fe_{14}B$ phase. Nearly complete removal of hydrogen is essential for HDDR to restore the φ-phase and eliminate any leftover soft magnetic phases. This process is significant in achieving the desired coercivity value in the final particulate material produced by HDDR.

Although the carbon content after HDDR is slightly lower compared to the HD powder, this discrepancy is not considered significant enough to draw definitive conclusions. It is likely that this minor difference can be attributed to the measurement process. For the purposes of this work, the values are considered comparable.

The observed increase in oxygen content after HDDR, although not as significant as the earlier uptake from the bulk End-of-Life magnet to the HD stage (from 2500 ppm to 4900 ppm of oxygen, as shown in table 3), raises attention to potential sources of contamination. One possible source could be inadequate degassing of the chamber with HD powder during the preparation prior to HDDR processing, leading to the initiation of the treatment with some contamination inside the retort. However, oxygen is probably being absorbed by the Nd-rich phase, thus preserving the Nd-Fe-B phase and resulting in the high magnetic properties observed after optimizing the HDDR process.

In nanocrystalline powders, the rich phase does contribute to the development of high magnetic properties. However, the lack of a rich phase is even more problematic in sintered magnets, as it directly affects the coercivity mechanism and the densification of the Nd-Fe-B magnet. In sintered magnets, the coercivity mechanism, known as the nucleation type, involves the Nd-rich phase preventing the nucleation of reversed domains by smoothing defects along the grain boundaries and creating “magnetic isolation” of Nd-Fe-B grains [67].

In contrast, the situation in HDDR powder is different. Here, the coercivity mechanism is directly related to the grain size of the φ-phase. These grains, being smaller than the critical domain size (~300 nm), act as barriers to the propagation of reversed magnetic domains [45].

Therefore, while the rich phase does play a role in enhancing magnetic properties in nanocrystalline powders, its absence in sintered magnets poses a greater challenge due to its critical role in the coercivity mechanism and densification process.

Furthermore, the substantial absorption of oxygen subsequent to HD and HDDR processing does not impede the reprocessing through the selected hydrogen-based method. End-of-Life magnets can be effectively repurposed as raw material sources, generating powder via the discussed process for application in powder-based AM technologies.

4.3 ADDITIVE MANUFACTURING OF BONDED MAGNETS FROM RECYCLED POWDERS

This section provides a comprehensive explanation LPBF process applied to recycled powder derived from End-of-Life magnets. The primary objective is the conversion of recycled powder into additively manufactured bonded magnets. The initial phase involves the preparation of feedstock, which includes selecting high coercive HDDR particles and a polymer binder, specifically polyamide 12 (PA-12). These components are mechanically mixed in varying volume fractions of PA-12, ranging from 30% to 60%. Subsequently, the prepared feedstock is loaded into a prototype Selective Laser Sintering machine, with detailed processing parameters outlined in Section 3.2.3 of this work.

4.3.1 Microstructural Characterization of As-Printed Magnets

The feedstock tested with a 30% vol. PA-12 concentration was unable to produce a sample with mechanical integrity. This is likely due to the low binder fraction and high porosity after printing, which is insufficient to form a continuous matrix that holds all the HDDR particles together. Fim [111] observed that a bonded magnet obtained by LPBF needs a minimum binder fraction in the feedstock to have less porosity and form a continuous polymeric matrix. Therefore, in the case of the tested feedstock with a 30% vol. PA-12, it was not possible to form this matrix.

Figure 35 shows SEM images obtained from the surface of printed magnets with a volume fraction of 45% PA-12. In image a), an overview of the bonded magnet is provided, while image b) shows a higher magnification of a specific area. These images visually depict two solid phases and the presence of pores. The gray regions in the images represent HDDR

particles, while the black regions represent the PA-12 binder. Thus, the microstructure is characterized by the embedded HDDR particles within a polymeric matrix.

SEM images of the surface of the printed magnets, with a 60% volume fraction of PA-12, are shown in Figure 36. Figure a) provides an overall view of the bonded magnet, while Figure b) offers a closer look at a specific area. The same characteristics observed in the magnet with 45% volume fraction of PA-12 are present in this case. There are two solid phases present, with gray regions corresponding to HDDR particles and black regions corresponding to PA-12 binder. However, the magnet with a higher volume fraction of PA-12 exhibits a greater presence of the polymeric phase.

Figure 35 - SEM images of as-printed magnets with 45% vol PA-12

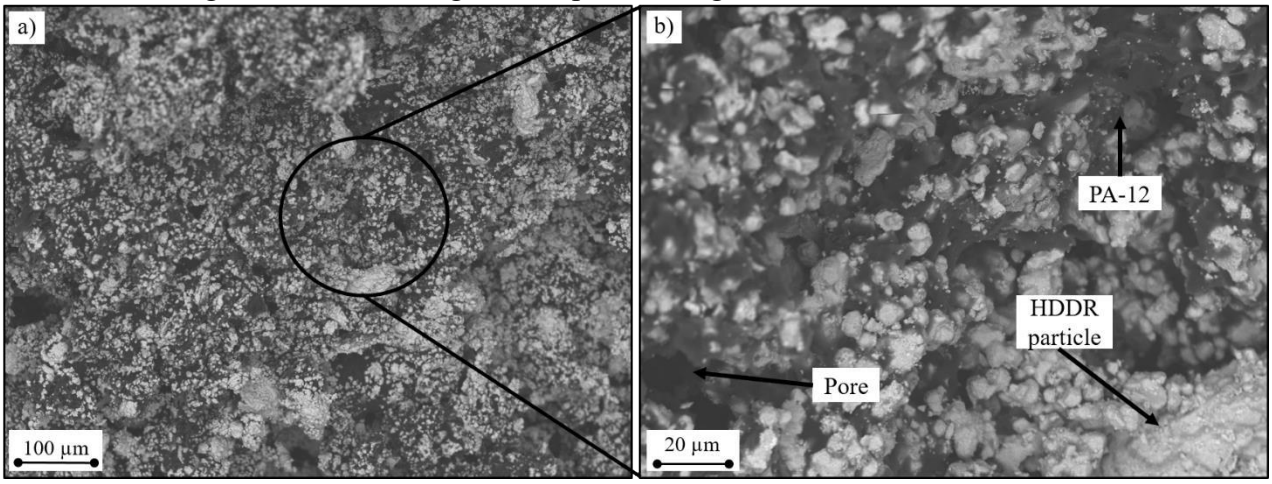

Source: Author

Figure 36 - SEM images of as-printed magnets with 60% vol PA-12

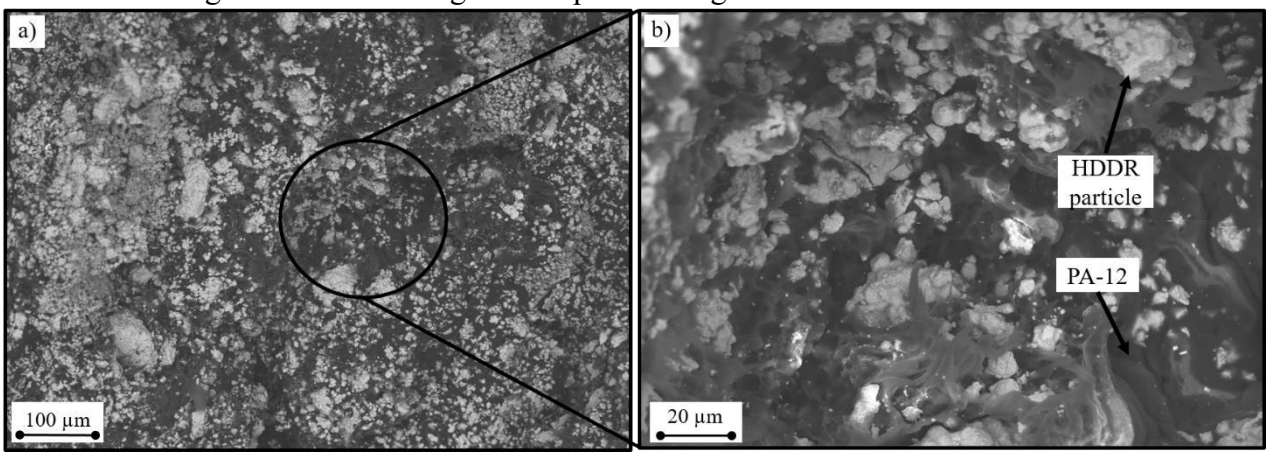

Source: Author

4.3.2 Geometrical Characterization of As-Printed Magnets

Table 5 presents a comprehensive analysis of the as-printed samples, focusing on their density and porosity values. For the samples incorporating 45% vol. PA-12, the density remained stable at approximately 2.10 g/cm³, corresponding to a porosity fraction of around 52%. This consistency in density suggests a relatively homogeneous polymeric matrix when compared to the feedstock containing 30% vol. PA-12. Nonetheless, as illustrated in Figure 35(b), Scanning Electron Microscopy (SEM) analysis identified the presence of pores within the polymeric matrix and the HDDR particles.

Table 5 - Density and porosity analysis of as-printed samples with different PA-12 volume fractions

Sample	ρ (g/cm³)	ρ_{theo} (g/cm³)	Porosity (%)	Magnetic Load (%)
45 % vol. PA-12	2.10	4.63	55	24
	2.26		51	27
	2.06		56	24
60 % vol. PA-12	2.73	3.65	25	30
	2.55		30	28
	2.61		28	29

Source: Author

For samples with 60% volume of PA-12, the density was approximately 2.60 g/cm³, indicating a porosity fraction of about 28%. In contrast with samples containing 45% volume of PA-12, the ones with 60% vol. PA-12 exhibited a more continuous polymeric matrix. This is demonstrated by the absence of porosity in Figure 36(b), where SEM analysis reveals that the polymeric phase more effectively encapsulates the HDDR particles.

The reduction of porosity in the LPBF process of Nd-Fe-B composite magnets is also affected by the composition of the feedstock. Some authors have investigated the improvement of densification through this AM processings.

Baldissera [113] and Engerroff [114] employed a volume fraction of 34% polyamide-12 in the feedstock for LPBF. Baldissera [113] achieved the highest geometric density of ρ = 3.60 g/cm³ (30% porosity), while Engerroff [114] obtained a maximum density of ρ = 2.48 g/cm³ (52% porosity). However, in both cases, the formation of a continuous matrix was suboptimal.

According to the optimal processing conditions described by Fim [111], the densification process improved with an increased volumetric fraction of PA-12. Produced bonded magnets using 36% volume of PA12 achieved a maximum density of $\rho = 3.91$ g/cm³, with a corresponding porosity of 24%. Increasing the fraction of PA12 to 40% volume resulted in a higher density of $\rho = 4.57$ g/cm³ (5% porosity), representing a significant reduction in porosity compared to the bonded magnets obtained. Further increasing the fraction of PA-12 to 45% volume resulted in magnets with a density of $\rho = 4.33$ g/cm³ and a porosity of 4%.

The significant increase in the values of geometric density of composite magnets obtained via LPBF observed in the study of Fim [111] can be explained by some factors. One important consideration is the requirement for a minimum amount of binder in order to create a continuous polymeric matrix. This is essential in LPBF, as it involves consolidating loose layers of powder. As a result, it is necessary to adjust the volume fraction of polymeric binder in order to ensure full consolidation.

As stated by Kruth *et al.* [115], liquid phase assisted sintering in LPBF not only eliminates porosity but also causes the rearrangement of Nd-Fe-B particles. This rearrangement is driven by capillary forces exerted by the liquid phase on the solid particles. LPBF utilizes the polymeric binder as the liquid phase during laser melting, making it a form of liquid phase assisted sintering.

In addition to controlling the binder fraction in the feedstock, other factors can significantly influence the densification of additively manufactured bonded magnets. Fim [111] conducted a study to investigate the optimization of printing parameters and its impact on the geometrical density of a 45% vol. PA-12 bonded magnet. The findings showed that by using a laser speed of 600mm/s, the density achieved was 4.30 g/cm³ with only 4% porosity. On the other hand, when the laser speed was increased to 1400 mm/s, the density decreased to 3.06 g/cm³ with a higher porosity of 32%.

The crucial aspect of optimizing processing parameters during printing is managing the energy density while the laser beam interacts with the powder bed. The appropriate energy density facilitates the fusion and complete coalescence of the polymeric particles, as well as the bonding of the Nd-Fe-B particles to the matrix. When the energy density is reduced (by increasing the laser speed parameter), the laser energy becomes insufficient for the complete fusion of the binder, resulting in the formation of porous bonded magnets.

Thus, the high porosity observed in this study (refer to Table 5) might be due to the inappropriate parameters used to produce bonded magnets. Therefore, additional investigations

into processing parameters could be conducted to optimize the energy density during laser processing, which could help maximize the densification of printed parts.

The morphology of the ferromagnetic particles used in the feedstock can also influence the densification of the printed bonded magnet. Röhrig [101] conducted a study investigating a wide range of PA-12 volumetric proportions in composite materials containing Sm-Fe-N particles with a "plate" morphology. It was observed that when the volume of the binder exceeds 60%, a cohesive polymeric matrix is formed. The study resulted in composite magnets with a peak geometric density of $\rho = 3.35$ g/cm³ (11% porosity) when using this feedstock composition.

Röhrig *et al.* in another work [99] also discovered that altering the Sm-Fe-N particles from a “plate” shape to an “irregular” form reduced the necessary volume of binder for creating a continuous matrix. With 40% PA-12 by volume, they were able to produce composite magnets with a density of $\rho = 4.20$ g/cm³, equating to 16% porosity. For comparison, magnets made with “plate” type particles had a density of $\rho = 2.68$ g/cm³, or roughly 48% porosity.

Mapley *et al*. [116] produced magnets from Nd-Fe-B powders with both flake and spherical particle morphologies. Their findings indicated that the printed bonded magnets made with spherical powder had a higher density than those made with flaked powder. The authors explained that this was expected due to the better packing density of spherical particles, which is attributed to their smooth and regular shape.

Therefore, the irregular morphology of the HDDR recycled particles utilized in this study can impact in the density of the printed magnet. The findings presented in Table 5 can be attributed to this morphological irregularity. Additionally, the polymeric fraction in the feedstock and the specific parameters used during the printing process further contribute to the observed results.

Figure 37 visually illustrates the levels of magnetic load, polymer, and porosity in the produced bonded magnets. These values were derived from the data presented in Table 5, which averages the results of three printed samples. The percentages of these components were determined using theoretical densities to calculate the porosity. The remaining volume was then proportionally calculated from the original feedstock mixture, considering the remaining magnetic load and the polymeric binder.

Figure 37 - Illustration of magnetic load, polymer content, and porosity levels in fabricated bonded magnets

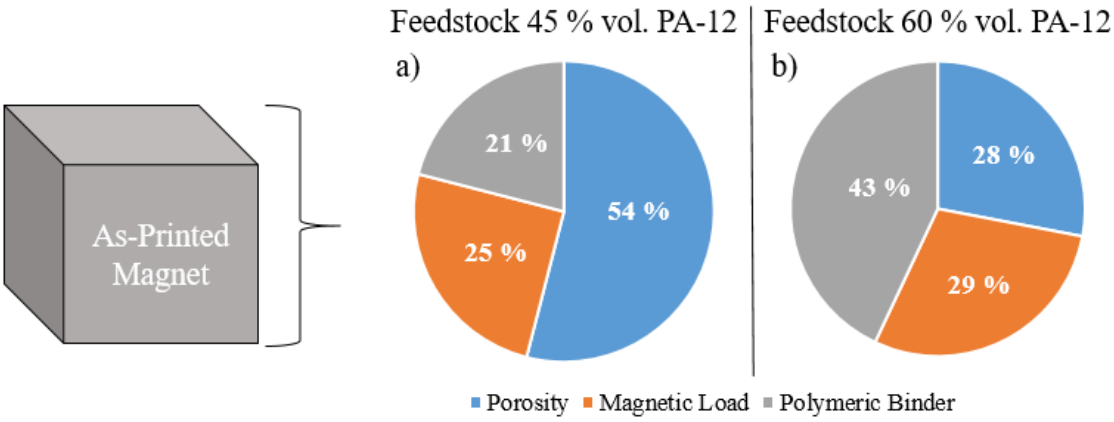

Source: Author

Figure 37(a) illustrates that magnets fabricated from a feedstock containing 45% vol. PA-12 exhibited an average magnetic loading of 25% and a porosity of 54%. In contrast, the feedstock with 60% vol. PA-12 (Fig. 37 b) achieved a magnetic loading of 29%. Despite the higher concentration of ferromagnetic particles in the 45% vol. PA-12 feedstock, a decrease in density was observed following laser processing. Consequently, the magnetic properties of the 45% vol. PA-12 feedstock were inferior to those of the 60% vol. PA-12 feedstock, which maintained a magnetic loading of 29%.

With a composition of 45% vol. PA-12, the presence of pores is more pronounced due to the partial adherence of the ferromagnetic particles to the polymer matrix. When the binder volume is increased to 60%, there is a marked improvement in the adherence of these particles, leading to a higher material density. This increased density is achieved as the polymer matrix fills the spaces previously occupied by pores, thereby incorporating more HDDR particles.

Understanding the significance of the magnetic load volume in a bonded magnet is important for maximizing its magnetic properties. The volumetric fraction of the magnetic phase within the composite material directly influences the magnet's overall magnetic performance. A higher volume of the magnetic phase correlates with enhanced magnetic properties, such as increased energy product. Consequently, the volumetric fraction of ferromagnetic material is a critical determinant of the bonded magnet's properties and its potential applications [117]. Future investigations should focus on maximizing the magnetic load in printed bonded magnets made from HDDR recycled powder.

4.3.3 Magnetic Characterization of As-Printed Magnets

The demagnetization curves of the printed magnets are illustrated in Figure 38, while the magnetic characterization values, specifically remanence and coercivity as a function of binder fraction, are detailed in Table 6. The samples containing 45% volume of PA-12, represented by the solid yellow line, exhibited a remanence of approximately 180 mT and coercivity values around 600 kA/m. In contrast, the samples with 60% volume of polymeric binder, depicted by the solid red line, demonstrated a remanence of approximately 190 mT and coercivity values of around 668 kA/m. Additionally, Figure 38 includes a black dashed line representing the HDDR powder before printing as a reference.

Figure 38 - Demagnetization curves of printed magnets with varying binder fractions (45% and 60% volume of PA-12) compared to HDDR powder before printing

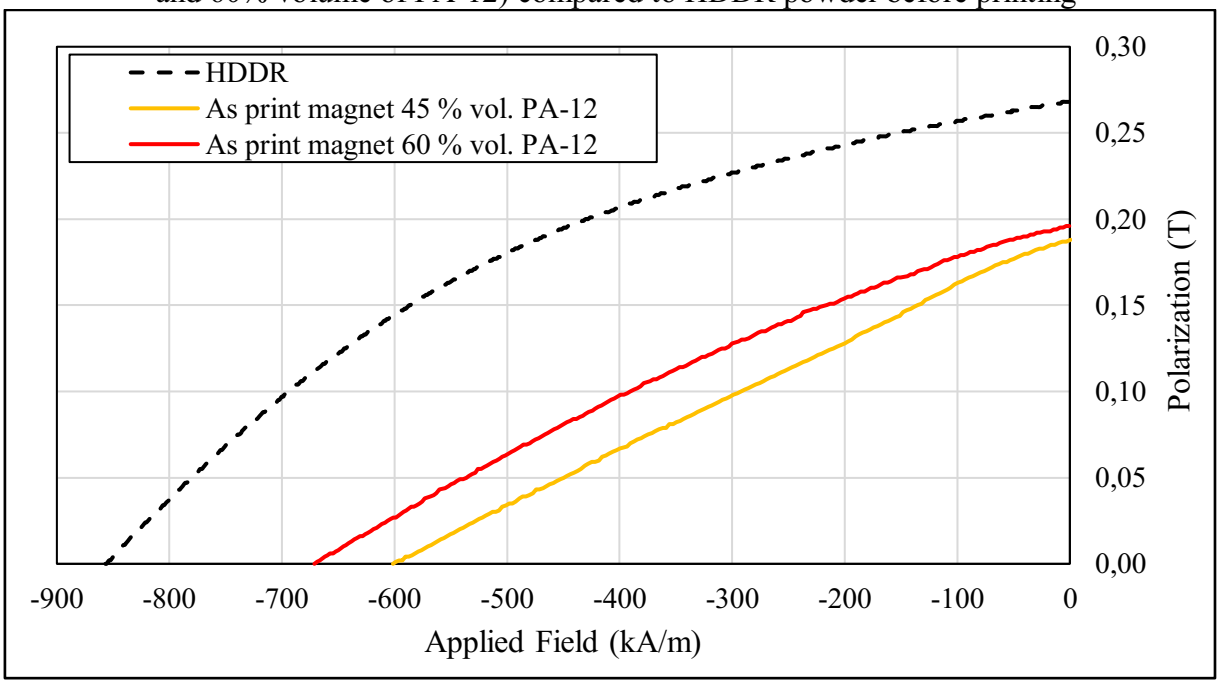

Source: Author

Table 6 - Magnetic characterization values of printed magnets showing remanence and coercivity as a function of binder fraction (45% and 60% volume of PA-12)

Sample	B_r (mT)	H_{cj} (kA/m)
45 % vol. PA-12	170	610
	190	600
	170	596
60 % vol. PA-12	200	672
	190	667
	190	665

Source: Author

The comparison of coercivity values between the starting HDDR material and the bonded magnets reveals a loss of approximately 30% for samples with 45% volume of binder and a loss of 21% for those with 60% volume of PA-12. This divergence in measured values can be attributed to the significantly increased porosity observed in the as-printed samples. Specifically, the porosity was measured to be around 50% for samples with 45% volumetric fraction of PA-12 and 30% for those with 60% volumetric fraction of PA-12.

The observed decrease in coercivity values can be attributed to the enhanced capacity of the magnetic particles to undergo rotation during magnetometry. This rotation is facilitated by an incomplete bond between the magnetic particles and the PA-12 matrix, which occurs as a result of inadequate melting in the printing process. When the polymer matrix volume fraction is lower, it can lead to the formation of more porous regions within the sample. These porous regions offer limited points of contact for the ferromagnetic particles (specifically, the HDDR particles), enabling weaker bonds between particles to rotate under the influence of an external magnetic field.

Schäfer *et al*. [100] observed this behavior when the volume fraction of polymeric binder is approximately 10%, more MQP-S particles undergo rotation. This rotation leads to a significant decrease in coercivity values compared to samples with a higher volume fraction of polymeric binder. This finding is consistent with the research conducted by Engerroff *et al*. [114], who also observed a reduction in H_{cj} during the LPBF process of Sm-Fe-N.

Thus, it is apparent that the observed decrease in coercivity values in the printed bonded samples can be attributed to the rotation of HDDR particles during magnetometry measure ment. This phenomenon occurs when the magnetic particles within the sample undergo rotational movement, leading to a reduction in coercivity.

However, it is expected that the coercivity values will increase in a system with lower porosity, where the magnetic particles form stronger bonds with the polymeric matrix. This occurrence can be attributed to the more efficient attachment of magnetic particles in the polymeric matrix, leading to greater resistance against demagnetization forces. As a result, the magnetic particles exhibit increased resistance to rotation during measurement, ultimately favoring higher coercivity.

In order to obtain a sample with reduced porosity, a set of the samples was chosen for Cold Isostatic Pressing (CIP). This further investigation was implemented to study how the porosity evolves in correlation with the magnetic properties of the printed bonded magnets.

Figure 39 illustrates the demagnetization curves for various samples under two distinct conditions. The dashed lines represent the as-printed samples, with the yellow line corresponding to the sample containing 45% volume of PA-12 and the red line representing the sample with 60% volume of PA-12. In contrast, the solid lines depict the same samples following CIP at 150 MPa for 10 seconds. Here, the blue line denotes the sample with 45% volume of PA-12, while the green line represents the sample with 60% volume of PA-12.

Figure 39 - Demagnetization curves of as-printed and cold isostatic pressed samples with varying polyamide-12 volumes

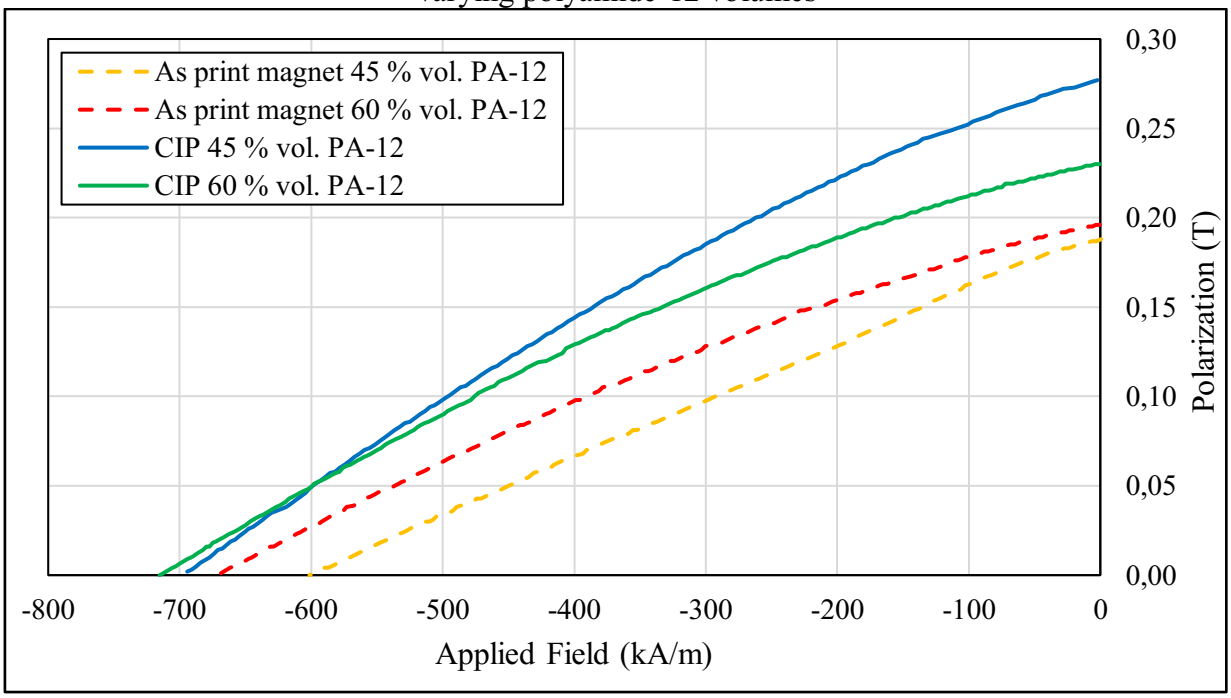

Source: Author

Table 7 provides an analysis of the geometric and magnetic characterization of printed magnets, both prior to and following CIP. For samples containing 45% vol. PA-12, there is a

notable enhancement in geometric density, rising from 2.10 to 3.18 g/cm³. This improvement corresponds to a significant reduction in porosity, decreasing from 55% to 31%. Similarly, samples with 60% vol. PA-12 exhibit an increase in densification, with geometric density values improving from 2.73 to 3.16 g/cm³, which translates to a decrease in porosity from 25% to 13%.

Table 7 - Geometric and magnetic characterization of printed magnets before and after cold isostatic pressing (CIP)

Sample	Density (g/cm³)	Porosity (%)	Br (mT)	Hcj (kA/m)
45 % vol. PA-12 (as-printed)	2.10	55	170	610
60 % vol. PA-12 (as-printed)	2.73	25	200	672
45 % vol. PA-12 (CIP)	3.18	31	280	698
60 % vol. PA-12 (CIP)	3.16	13	230	715

Source: Author

Table 7 also demonstrates the impact of pressing on the magnetic properties of printed samples. For samples containing 45% vol. PA-12, the remanence exhibited a notable increase from 170 mT to 280 mT, while the coercivity improved from 610 kA/m to 698 kA/m. Similarly, samples with 60% vol. PA-12 showed enhancements, with remanence rising from 200 mT to 230 mT and coercivity increasing from 672 kA/m to 715 kA/m.

A comparable enhancement in magnetic properties was documented in the research conducted by Baldissera [113]. In this study, a significant reduction in porosity was observed, diminishing from 25% to nearly zero for spherical Nd-Fe-B particles. The system incorporated a 34% volume fraction of PA-12. Following this densification improvement, the remanence of the samples notably increased from 300 mT to 450 mT.

As previously discussed, it was expected that coercivity values would increase with reduced sample porosity [100, 111]. This can be attributed to the decreased rotation of ferromagnetic particles during magnetometry measurement. The same phenomenon was observed in the samples produced in this study. Following CIP, the ferromagnetic particles exhibited stronger adherence to the polymeric matrix, thereby enhancing resistance to rotation during measurement.

However, it is observed that the coercivity value did not revert to its original benchmark of H_{cj} = 850 kA/m. This reduction in H_{cj} was evident when comparing values measured before

and after the laser processing. Despite the partial elimination of porosity, the coercivity value in the bonded magnets remained at approximately 700 kA/m.

A potential reason for the decrease in intrinsic coercivity following LPBF is particle degradation. This hypothesis, while unproven through experiments, is speculated for HDDR particles obtained from End-of-Life magnets. Nonetheless, this behavior is not observed in spherical MQP-S particles or other ferromagnetic powders published in literature [26, 101, 110, 111, 113].

Baldissera's study [113] did not conclusively establish the effect of the laser beam on coercivity of printed bonded samples. The author employed commercial spherical Nd-Fe-B particles (MQP-S) as the magnetic load in the feedstock. The coercivity values measured in the study fell within the expected range for this powder type, approximately 640 to 760 kA/m. However, the influence of various processing variables on the magnet's coercivity was not conclusively determined. Therefore, the relationship between processing variables and coercivity requires further investigation.

According to Röhrig *et al.* [99], similar observations were made in a HDDR developed based on Sm-Fe-N. After LPBF, the coercivity values did not degrade significantly and remained close to the original measured value even after laser processing (~770 kA/m).

The observed degradation in this study appears to be specific to the powder produced by HDDR from End-of-Life magnets. This suggests that a microstructural alteration occurred in the ferromagnetic particles when exposed to laser processing under specific LPBF conditions. Consequently, this microstructural change could account for the observed reduction in certain magnetic properties, notably coercivity, in the bonded magnet.

4.3.3.1 Final Observations

The bonded magnet developed in this research exhibits coercivity values comparable to those reported in the literature for commercial Nd-Fe-B spherical powder (MQP-S). Table 8 provides a comprehensive overview of relevant studies on bonded magnet production using LPBF. Remarkably, the as-printed magnets, even without optimization of processing parameters, achieve coercivity values that are consistent with those in other studies. Additionally, the as-printed samples, after undergoing cold isostatic pressing, demonstrate higher coercivity values than those documented in other works.

Table 8 - Comprehensive overview of coercivity values in bonded magnet production using LPBF: comparison with commercial Nd-Fe-B spherical powder (MQP-S) and the recycled HDDR powder developed in this study

Reference	Raw Material	Coercivity [kA/m]
Fim [93]	MQP-S	720
Schäfer [100]		675
Baldissera [113]		694
Mapley [116]		734
45 % vol. PA-12 (as-printed)	Recycled HDDR	610
60 % vol. PA-12 (as-printed)		672
45 % vol. PA-12 (CIP)		698
60 % vol. PA-12 (CIP)		715

Source: Author

This observation is particularly significant given that the raw material utilized in this study is derived from End-of-Life magnets. The results indicate that the feedstock produced from recycled materials, when processed according to the methodology outlined in this research, exhibits no substantial disadvantages compared to commercial powders used in prior investigations.

Furthermore, Figure 40 illustrates examples of complex-shaped bonded magnets that can be produced using LPBF technology. These magnets can be fabricated using either commercially available spherical Nd-Fe-B powder or the recycled HDDR powder developed in this study.

Figure 40 –Examples of complex-shaped bonded magnets fabricated using LPBF technology

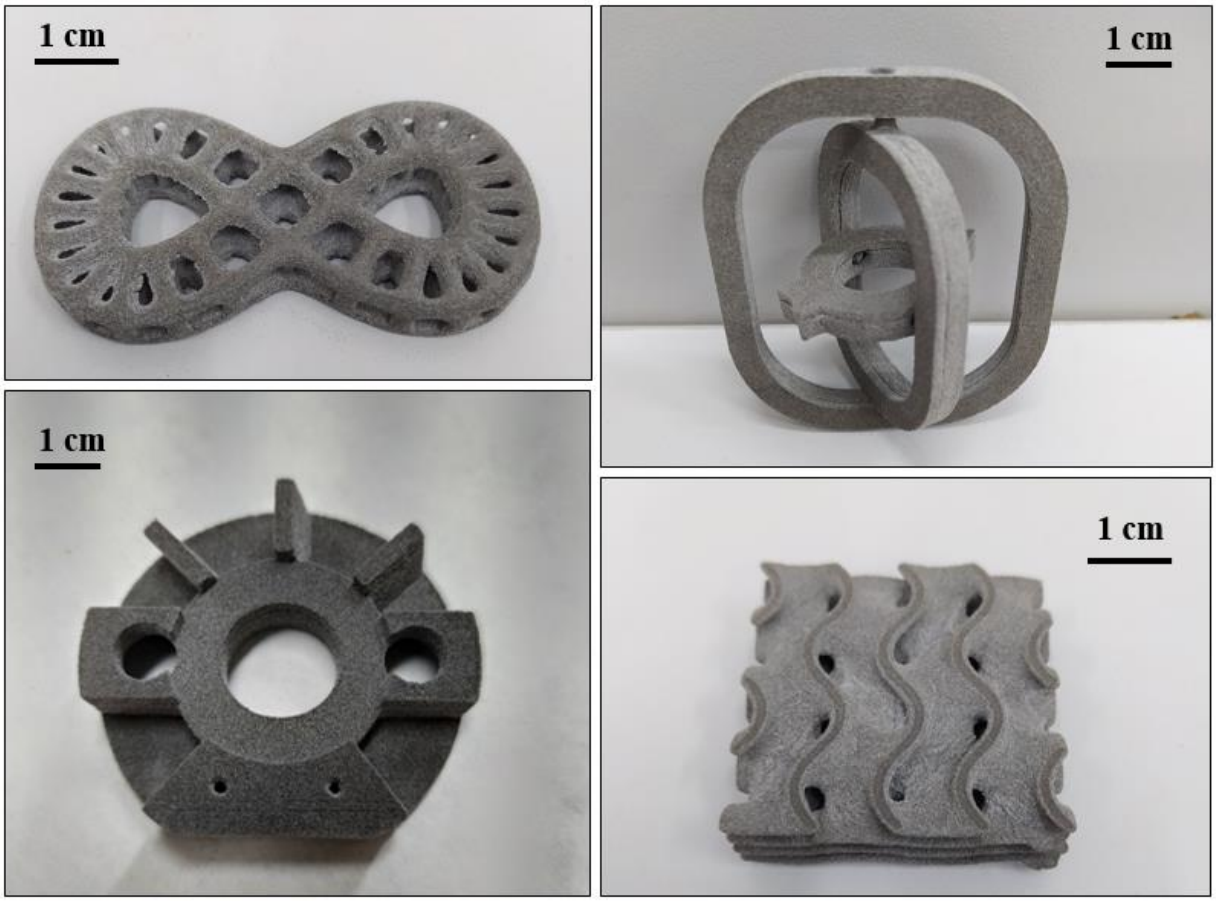

Source: Author

Another notable advantage of particulate material derived from recycling and reusing End-of-Life magnets is its capability to create powders that can be aligned through the HDDR process. Specifically, the d-HDDR process produces anisotropic powders that can be aligned during or after laser processing in AM. This alignment facilitates the potential optimization of the remanence values of recycled magnets produced by LPBF.

5 CONCLUSION

In this chapter, the main findings of the study will be outlined. The focus has been on reprocessing End-of-Life magnets using the hydrogen processing route. This involves Hydrogen Decrepitation (HD) and Hydrogen Disproportionation Desorption Recombination (HDDR). The primary goal was to create a feedstock suitable for Laser Powder Bed Fusion (LPBF) additive manufacturing, which enables the production of recycled bonded Nd-Fe-B magnets.

The microstructural analysis of the End-of-Life magnet revealed crucial insights into its constituents and integrity. Through scanning electron microscopy, distinct phases within the magnet were revealed, namely the $Nd_2Fe_{14}B$ phase and the Nd-rich phase. The former, also known as the φ-phase, is pivotal for high intrinsic magnetic properties, such as saturation polarization and magnetocrystalline anisotropy, which are essential for the performance of permanent magnets. Furthermore, the grain size of the φ-phase plays a significant role in determining the magnet's coercivity, with smaller grain sizes associated with higher coercivity values. The presence of a thin layer of the Nd-rich phase around each grain boundary enhances magnetic properties, particularly coercive force, by decoupling the ferromagnetic phase and preventing the formation of reverse domains.

The microstructural integrity of the End-of-Life magnet, including the preservation of the φ-phase, was confirmed through magnetic domain structure analysis. The maze-like patterns observed in the magnetic domain structures of both the End-of-Life magnet and a commercially available magnet indicate the retention of critical characteristics necessary for high-quality reprocessed Nd-Fe-B magnets. However, the recycling process introduces challenges related to the uptake of carbon and oxygen, which can negatively impact magnetic properties, especially in sintered Nd-Fe-B magnets. The higher initial levels of oxygen and carbon in End-of-Life magnets, compounded by potential increases during reprocessing, require careful consideration to maintain and optimize magnetic properties in recycled magnets.

The magnetic characterization of the decrepitated powder provides valuable insights into its properties and potential applications in AM processes. The suboptimal magnetic properties of the powder, indicated by its low remanence and coercivity values, underscore the importance of understanding the factors influencing these properties. The presence of hydrogen in solid solution and the formation of α-Fe during the HD process contribute to the reduced coercivity of the powder. However, through a degassing heat treatment, it is possible to recover

a significant portion of the initial magnet's coercivity, particularly for larger particle sizes. This highlights the importance of particle size and defect concentration in determining coercivity values.

Microstructural analysis reveals the presence of polyhedral grains originating from the φ-phase, as well as cracks and irregularities induced by the HD process. These features affect the powder's technological properties, such as flowability and packing density, which are critical for AM processes like LPBF. To ensure the suitability of the HD powder for AM applications, sieving processes are performed to achieve the recommended particle size distribution. Despite minimal coercivity within the desired size range, the powder can undergo further processing, such as HDDR, to adjust its coercivity as needed.

The optimization of the HDDR treatment focused primarily on varying the plateau temperature, as it was identified as the most influential factor in determining coercivity values. Other process parameters such as disproportionation and recombination plateau times were found to have minimal impact on magnetic properties. The demagnetization curves of samples processed at different HDDR temperatures revealed a significant increase in coercivity values with higher temperature plateaus. Processing at 940 °C resulted in a coercivity value of 850 kA/m, representing a substantial improvement over the initial HD powder. Comparison with commercially available powders demonstrated that the HDDR powder achieved coercivity values comparable to industry standards. This suggests the feasibility of using recycled raw materials to produce bonded magnets using LPBF.

Microstructural analysis revealed that the HDDR process maintained the general aspect of the powder while refining the grain structure. The irregular morphology of the particles post-HDDR processing can impact technological properties such as flowability and packing density, critical for LPBF.

The decrease in hydrogen content after HDDR processing indicates successful recombination and removal of hydrogen, essential for restoring the $Nd_2Fe_{14}B$ phase and achieving desired coercivity values. Although an increase in oxygen content was observed after HDDR processing, it did not significantly hinder the reprocessing route chosen in this study.

The final section of this study involved using the developed recycled powder in LPBF to create printed bonded magnets. Regarding the geometrical characterization of the obtained magnets, the density and porosity values varied significantly depending on the volume fraction of polyamide-12 (PA-12) binder in the feedstock, with higher concentrations resulting in denser magnets with lower porosity.

SEM imaging provided visual confirmation of the microstructural features, revealing the presence of pores and the distribution of HDDR particles within the polymeric matrix. Optimization of processing parameters, including laser speed, was identified as crucial for achieving desired density and minimizing porosity. Furthermore, the morphology of ferromagnetic particles and their packing density significantly influenced magnet density. Future research directions should prioritize maximizing the magnetic load in printed bonded magnets to enhance magnetic properties

Regarding the magnetic properties of printed magnets, the observed decrease in coercivity values was attributed to the enhanced rotation of HDDR particles during magnetometry, facilitated by incomplete bonding between the magnetic particles and the PA-12 matrix. However, post-processing techniques like Cold Isostatic Pressing (CIP) showed promise in reducing porosity and enhancing magnetic properties. Notably, CIP led to significant improvements in density, porosity reduction, and enhanced remanence and coercivity values.

The findings also suggest the possibility of microstructural changes in the ferromagnetic particles affected by the laser during the LPBF process, potentially explaining the observed decrease in coercivity. Further research is warranted to elucidate the relationship between processing variables and coercivity, particularly concerning the unique characteristics of HDDR powder derived from end-of-life magnets.

Furthermore, comparisons with existing literature underscored the competitiveness of the developed bonded magnets, particularly considering the use of recycled HDDR powder sourced from End-of-Life magnets. The study demonstrated that the printed magnets, even without optimization of processing parameters, exhibited comparable coercivity values to those achieved using commercial spherical Nd-Fe-B powder (MQP-S). Moreover, after CIP, the magnets showed higher coercivity values than reported in previous works, highlighting the potential of recycled materials in AM applications.

Suggestions for Further Research

Looking ahead to future prospects in activities related to the preparation of feedstock from End-of-Life magnets for utilization in LPBF for the production of bonded magnets, several promising possibilities can be explored:

- Optimizing Powder Bed Fusion Parameters: Future investigations should focus on fine-tuning powder bed fusion parameters to achieve higher density in the final bonded

magnet. The optimization of parameters such as laser power, scanning speed, and layer thickness is crucial for enhancing the overall structural integrity and magnetic performance of the bonded magnets. Investigating the interplay between these parameters will contribute to a more nuanced understanding and pave the way for improved manufacturing processes.

- Production of d-HDDR for Anisotropic Raw Material: Exploring the production of anisotropic raw material through dynamic-HDDR (d-HDDR) is a promising avenue. This involves utilizing recycled powder in powder bed fusion additive manufacturing to fabricate anisotropic bonded magnets. By aligning magnetic particles in a specific direction during or after the manufacturing process, the goal is to optimize remanence values, enhancing the magnetic properties of the final product. This approach aligns with the pursuit of tailoring magnetic properties for specific applications, offering a more versatile range of magnet functionalities.
- Grain Boundary Engineering for Improved Coercivity: The search for improved coercivity values can be advanced by exploring grain boundary engineering techniques. By modifying the composition of grain boundaries and surface properties of the particles through the addition of rare earth elements or non-rare earth elements to the recycled powder, future studies can investigate new methods to enhance coercivity values. Understanding the complex interactions at grain boundaries and implementing innovative engineering approaches will play a crucial role in achieving higher coercivity, ultimately resulting in magnets with superior magnetic performance.

Future explorations in the field of recycled Nd-Fe-B bonded magnets are pivotal for advancing the technology. Emphasizing optimization strategies, the production of anisotropic materials, and innovative techniques for enhancing coercivity will contribute significantly to the evolution of sustainable and high-performance magnet manufacturing. These efforts are aligned with the broader objectives of minimizing environmental impact, reducing reliance on expensive rare earth metals, and unlocking new possibilities for the application of magnets in various high-tech industries.

REFERENCES

[1] GUTFLEISCH, O.; WILLARD, M. A.; BRÜCK, E.; CHEN, C. H.; SANKAR, S. G.; LIU, J. P.. Magnetic Materials and Devices for the 21st Century: stronger, lighter, and more energy efficient. Advanced Materials, v. 23, n. 7, p. 821-842, Wiley (2010)

[2] BOBBA, S.; CARRARA, S.; HUISMAN, J.; MATHIEUX, F.; and PAVEL, C. "Critical Raw Materials for Strategic Technologies and Sectors in the EU - A Foresight Study." (2020). Avaliable in: https://www.mybib.com/pt/ferramentas/gerador-referencias-abnt. Accessed in November 2023.

[3] SMITH, B. J.; RIDDLE, M. E.; EARLAM, M. R.; ILOEJE, C.; and DIAMOND, D. "Rare Earth Permanent Magnets: Supply Chain Deep Dive Assessment." (2022). Available at: https://www.osti.gov/biblio/1871577 . Accessed in November 2023

[4] GAUß, R.; BURKHARDT, C.; CARENCOTTE, F.; GASPARON, M.; GUTFLEISCH, O.; HIGGINS, I.; KARAJIĆ, M.; KLOSSEK, A.; MÄKINEN, M.; SCHÄFER, B.; SCHINDLER, R.; VELURI, B. "Rare Earth Magnets and Motors: A European Call for Action." (2021). Available at: https://eit.europa.eu/library/rare-earth-magnets-and-motors-european-call-action . Accessed in November 2023

[5] YANG, Y.; WALTON, A.; SHERIDAN, R.; GÜTH, K.; GAUß, R.; GUTFLEISCH, O.; BUCHERT, M.; STEENARI, B.; VAN GERVEN, T.; JONES, P.. REE Recovery from End-of-Life NdFeB Permanent Magnet Scrap: a critical review. Journal Of Sustainable Metallurgy, v. 3, n. 1, p. 122-149, Springer Science and Business Media LLC. (2016)

[6] EUROPEAN COMMISSION, report on: "Critical raw materials for the EU", (2014). Available in: https://op.europa.eu/en/publication-detail/-/publication/57318397-fdd4-11ed-a05c-01aa75ed71a1. Acessed in August 2023

[7] WALTON, A.; YI, Han; ROWSON, N.A.; SPEIGHT, J.D.; MANN, V.s.J.; SHERIDAN, R.s.; BRADSHAW, A.; HARRIS, I.R.; WILLIAMS, A.J.. The use of hydrogen to separate and recycle neodymium–iron–boron-type magnets from electronic waste. Journal Of Cleaner Production, v. 104, p. 236-241. Elsevier BV. (2015)

[8] HOGBERG, S.; HOLBOLL, J.; MIJATOVIC, N.; JENSEN, B.; BENDIXEN, F. B.. Direct Reuse of Rare Earth Permanent Magnets—Coating Integrity. Ieee Transactions On Magnetics, v. 53, n. 4, p. 1-9, Institute of Electrical and Electronics Engineers (IEEE). (2017)

[9] CONG, L.; YU, L.; ZHOU, Q.; LU, Q.; YUE, M.. Short-process recycling of Nd-Fe-B sintered magnet sludge wastes: challenges and approaches. Journal Of Rare Earths, v. 41, n. 10, p. 1467-1477, Elsevier BV. (2023)

[10] YIN, X.; LIU, M.; WAN, B.; ZHANG, Y.; LIU, W.; WU, Y.; ZHANG, D.; YUE, M.. Recycled Nd-Fe-B sintered magnets prepared from sludges by calcium reduction-diffusion process. Journal Of Rare Earths, v. 36, n. 12, p. 1284-1291 Elsevier BV. (2018)

[11] LI, C.; YUE, M.; LIU, W.; ZUO, T.; YI, X.; CHEN, J.; ZHOU, Z.; WU, Y.. Recycling of scrap sintered Nd–Fe–B magnets as anisotropic bonded magnets via hydrogen decrepitation process. Journal Of Material Cycles And Waste Management, v. 17, n. 3, p. 547-552, Springer Science and Business Media LLC. (2014)

[12] LI, X.; YUE, M.; ZAKOTNIK, M.; LIU, W.; ZHANG, D.; ZUO, T.. Regeneration of waste sintered Nd-Fe-B magnets to fabricate anisotropic bonded magnets. Journal Of Rare Earths, v. 33, n. 7, p. 736-739, Elsevier BV. (2015)

[13] PROSPERI, D.; TUDOR, C.O.; BEVAN, A.I.; QUIROZ, E. de Leon; PEH, H.; FURLAN, G.; SKOMSKI, R.; SUVOROV, D.; ZAKOTNIK, M.. Thermal-stability and microstructure comparison between recycled M2M and conventionally produced sintered neodymium-iron-boron magnets. Journal Of Cleaner Production, v. 239, p. 118091, Elsevier BV. (2019)

[14] DEBROY, T.; WEI, H. L.; ZUBACK, J. S.; MUKHERJEE, T.; ELMER, J. W.; MILEWSKI, J. O.; BEESE, A. M.; WILSON-HEID, A.; DE, A.; and ZHANG, W. Additive manufacturing of metallic components: process, structure, and properties. Progress in Materials Science, 92, 112-224 (2018)

[15] SAMES, W. J.; LIST, F. A.; PANNALA, S.; DEHOFF, R. R.; BABU, S. S. The metallurgy and processing science of metal additive manufacturing. International Materials Reviews, 61(5), 315–360 (2016)

[16] CHAUDHARY, V.; MANTRI, S. A.; RAMANUJAN, R. V.; BANERJEE, R. Additive manufacturing of magnetic materials. Progress in Materials Science, 114, 100688 Elsevier BV (2020)

[17] LI, X.; YUE, M.; ZAKOTNIK, M.; LIU, W.; ZHANG, D.; ZUO, T.. Regeneration of waste sintered Nd-Fe-B magnets to fabricate anisotropic bonded magnets. Journal Of Rare Earths, v. 33, n. 7, p. 736-739 Elsevier BV (2015)

[18] POENARU, I.; PATROI, E.; PATROI, D.; IORGA, A.; MANTA, E.. HDDR as advanced processing method and recycling technology to address the rare-earth resource criticality in high performance Nd2Fe14B magnets production. Journal Of Magnetism And Magnetic Materials, v. 577, p. 170777, Elsevier BV. (2023)

[19] SHERIDAN, R.; WILLIAMS, A.J.; HARRIS, I.R.; WALTON, A. Improved HDDR processing route for production of anisotropic powder from sintered NdFeB type magnets. Journal Of Magnetism And Magnetic Materials, v. 350, p. 114-118, Elsevier BV. (2014)

[20] GUTFLEISCH, O.; GÜTH, K.; WOODCOCK, T.; SCHULTZ, L.. Recycling Used Nd-Fe-B Sintered Magnets via a Hydrogen-Based Route to Produce Anisotropic, Resin Bonded Magnets. Advanced Energy Materials, v. 3, n. 2, p. 151-155, Wiley. (2012)

[21] LIXANDRU, A.; POENARU, I.; GÜTH, K.; GAUß, R.; GUTFLEISCH, O.. A systematic study of HDDR processing conditions for the recycling of end-of-life Nd-Fe-B magnets. Journal Of Alloys And Compounds, v. 724, p. 51-61,. Elsevier BV. (2017)

[22] HAFERKAMP, L.; HAUDENSCHILD, L.; SPIERINGS, A.; WEGENER, K.; RIENER, K.; ZIEGELMEIER, S.; LEICHTFRIED, G. J.. The Influence of Particle Shape, Powder Flowability, and Powder Layer Density on Part Density in Laser Powder Bed Fusion. Metals, v. 11, n. 3, p. 418, MDPI AG. (2021)

[23] SPIERINGS, A. B.; VOEGTLIN, M.; BAUER, T.; WEGENER, K.. Powder flowability characterisation methodology for powder-bed-based metal additive manufacturing. Progress In Additive Manufacturing, v. 1, n. 1-2, p. 9-20, Springer Science and Business Media LLC. (2015)

[24] DEBROY, T.; WEI, H. L.; ZUBACK, J. S.; MUKHERJEE, T.; ELMER, J. W.; MILEWSKI, J. O.; BEESE, A. M.; WILSON-HEID, A.; DE, A.; ZHANG, W. Additive manufacturing of metallic components – Process, structure, and properties. Progress in Materials Science, 92, 112-224 (2018)

[25] LIXANDRU, A. Recycling of Nd-Fe-B permanent magnets by hydrogen processes. 2018. 166 f. Tese (Doutorado) - Curso de Material- Und Geowissenschaften, Technische Universität Darmstadt, Darmstadt, (2018)

[26] ENGERROF, J. A. B. Obtenção via hddr de pós nanocristalinos anisotrópicos à base de Nd-Fe-B. 2015. 100 f. Dissertação (Mestrado) - Universidade Federal de Santa Catarina, Florianópolis, (2015)

[27] CULLITY, B. D.; GRAHAM, C. D. Introduction to Magnetic Materials. 2. ed. New Jersey: Ieee, (2009)

[28] COEY, J.M.D.; PARKIN, S. S. P. Handbook of Magnetism and Magnetic Materials. Springer (2021)

[29] COEY, J. M. D. Magnetism and magnetic materials. Cambridge: Cambridge University Press, (2001)

[30] SHACKELFORD, J. F. Introduction to materials science for engineers. 9th ed. Pearson, (2021)

[31] CROAT, J. J.; ORMEROD, J.. Modern Permanent Magnets. Elsevier (2022)

[32] SUGIMOTO, S. Current status and recent topics of rare-earth permanent magnets. Journal Of Physics D: Applied Physics, v. 44, n. 6, p. 064001, IOP Publishing. (2011)

[33] JILES, D. Introduction to Magnetism and Magnetic Materials. 3. ed. Boca Raton: Crc, (2016)

[34] GUTFLEISCH, O.; WILLARD, M. A.; BRÜCK, E.; CHEN, C. H.; SANKAR, S. G.; LIU, J. P. Magnetic Materials and Devices for the 21st Century: Stronger, Lighter, and More Energy Efficient. Advanced Materials, 23(7), 821–842 (2010)

[35] HARRIS, I.R. The potential of hydrogen in permanent magnet production. Journal Of The Less Common Metals, v. 131, n. 1-2, p. 245-262, Elsevier BV. (1987)

[36] PANCHANATHAN, V.; SPARWASSER, K. Recent developmentsin bonded Nd-Fe-B magnets and applications. In: RARE-EARTH MAGNETS AND THEIR APPLICATIONS, 15., 1998, Dresden. Proceedings of the fifteenth international workshop on rare-earth magnets. Dresden: Werkstoff-Informationsgeselschaft, p. 671-679. (1998)

[37] CROAT, J. J.; HERBST, J. F.; LEE, R. W.; PINKERTON, F. E. Relationships between crystal structure and magnetic properties in Nd2Fe14. Phys. Rev. B 29, 4176 (1984)

[38] CROAT, J. J.; HERBST, J. F.; LEE, R. W.; PINKERTON, F. E.. High-energy product Nd-Fe-B permanent magnets. Applied Physics Letters, v. 44, n. 1, p. 148-149. AIP Publishing. (1984)

[39] SAGAWA, M.; FUJIMURA, S.; TOGAWA, N.; YAMAMOTO, H.; MATSUURA, Y. New material for permanent magnets based on Nd and Fe (invited). Journal of Applied Physics, vol. 55, no. 6, pp. 2083-2087 (1984)

[40] SAGAWA, M.; FUJIMURA, S.; YAMAMOTO, H.; MATSUURA, Y.; HIRAGA, K. Permanent magnet materials based on rare earth-iron-boron tetragonal compounds. IEEE Transactions on Magnetics, 20(5), 1584-1589 (1984)

[41] ONODERA, H.; YAMAGUCHI, Y.; YAMAMOTO, H.; SAGAWA, M.; MATSUURA, Y.; YAMAMOTO, H. Magnetic properties of a new permanent magnet based on a Nd-Fe-B compound (neomax). Journal of Magnetism and Magnetic Materials, 46(1-2), 151-156 (1984)

[42] ZHANG, S.; ZHAO, D.. Advances in Magnetic Materials: Processing, Properties, and Performance. 1ª edição. Boca Raton: CRC Press, (2017)

[43] WIRTH, S. Determination of intrinsic magnetic properties of hard magnetic materials from demagnetization curves of polycrystalline samples. In: MAGNETIC ANISOTROPY AND COERCIVITY IN RARE-EARTH TRANSITION METAL ALLOYS, 10. 1998, Dresden. Proceedings of the fifteenth international symposium on magnetic anisotropy and coercivity in rare-earth transition metal alloys. Dresden: Werkstoff-Informationsgeselschaft, p. 139-157 (1998)

[44] WOODCOCK, T.G.; ZHANG, Y.; HRKAC, G.; CIUTA, G.; DEMPSEY, N.M.; SCHREFL, T.; GUTFLEISCH, O.; GIVORD, D.. Understanding the microstructure and coercivity of high performance NdFeB-based magnets. Scripta Materialia, v. 67, n. 6, p. 536-541. Elsevier BV. (2012)

[45] HONO, K.; SEPEHRI-AMIN, H. Strategy for high-coercivity Nd–Fe–B magnets. Scripta Materialia, v. 67, n. 6, p. 530-535. Elsevier BV (2012)

[46] CUI, J.; ORMEROD, J.; PARKER, D.; and other authors. Manufacturing Processes for Permanent Magnets: Part I—Sintering and Casting. JOM, 74, 1279–1295 (2022)

[47] OESTERREICHER, K.; OESTERREICHER, H. On the phase NdFe4B4 and its implication in the magnetic hardening of Nd2Fe14B permanent magnets. Journal Of The Less Common Metals, v. 104, n. 2, p. 19-21, Elsevier BV (1984)

[48] HARRIS, I. R.; RAGG, O. M.; KEEGAN, G.; NAGEL, H. Proc. 3rd Int. Symp. on Physics of Magnetic Materials (Seoul, Korea), vol. 2, ed. CS Kim et al. (Seoul: The Korean Magnetics Society), pp. 638–45. (1995)

[49] GRUPO SETORIAL DE METALURGIA DO PÓ. A Metalurgia do Pó: alternativa econômica com menor impacto ambiental. São Paulo: Metallum Eventos Técnicos, (2009)

[50] THÜMMLER, F.; OBERACKER, R. Introduction to Powder Metallurgy. London: The University Press, (1993)

[51] SEPEHRI-AMIN, H.; OHKUBO, T.; SHIMA, T.; HONO, K.. Grain boundary and interface chemistry of an Nd–Fe–B-based sintered magnet. Acta Materialia, v. 60, n. 3, p. 819-830. Elsevier BV. (2012)

[52] CUI, J.; ORMEROD, J.; PARKER, D.; OTT, R.; PALASYUK, A.; MCCALL, S.; PARANS PARANTHAMAN, M.; KESLER, M. S.; MCGUIRE, M. A.; NLEBEDIM, C.; PAN, C.; LOGRASSO, T. "Manufacturing Processes for Permanent Magnets: Part II—Bonding and Emerging Methods." JOM, vol. 74, no. 6, pp. 2492-2506 (2022)

[53] GUTFLEISCH, O.; BOLLERO, A.; HANDSTEIN, A.; HINZ, D.; KIRCHNER, A.; YAN, A.; MÜLLER, K.-H.; SCHULTZ, L.. Nanocrystalline high performance permanent magnets. Journal Of Magnetism And Magnetic Materials, v. 242-245, p. 1277-1283, Elsevier BV. (2002)

[54] LEE, R. W.. Hot-pressed neodymium-iron-boron magnets. Applied Physics Letters, v. 46, n. 8, p. 790-791. AIP Publishing. (1985)

[55] KHLOPKOV, K.; GUTFLEISCH, O.; HINZ, D.; MÜLLER, K.-H.; and SCHULTZ, L. Evolution of Interaction Domains in Textured Fine-Grained Nd₂Fe₁₄B Magnets. Journal of Applied Physics, vol. 102, no. 2, pp. 12-23 (2007)

[56] BROWN, D.; MA, B.; CHEN, Z.. Developments in the processing and properties of NdFeb-type permanent magnets. Journal Of Magnetism And Magnetic Materials, v. 248, n. 3, p. 432-440. Elsevier BV. (2002)

[57] TAKESHITA, T.; NAKAYAMA, R. Magnetic properties and microstructures of the NdFeB magnet powder produced by hydrogen treatment. In: Proceedings of the 10th International Workshop on Rare-Earth Magnets and Their Applications, Vol. 1. Kyoto, Japan, pp. 551–557 (1989)

[58] MCGUINESS, P.J.; ZHANG, X.J.; YIN, X.J.; HARRIS, I.R.. Hydrogenation, disproportionation and desorption (HDD): an effective processing route for Nd-Fe-B-type magnets. Journal Of The Less Common Metals, v. 158, n. 2, p. 359-365,Elsevier BV (1990)

[59] GUTFLEISCH, O.; MARTINEZ, N.; VERDIER, M.; HARRIS, I.R.. Development of microstructure of the disproportionated material during HDDR processes in a Nd16Fe76B8 alloy. Journal Of Alloys And Compounds, v. 204, n. 1-2, p. 21-23, Elsevier BV. (1994)

[60] GUTFLEISCH, O.; MARTINEZ, N.; VERDIER, M.; HARRIS, I.R.. Phase transformations during the disproportionation stage in the solid HDDR process in a Nd16Fe76B8 alloy. Journal Of Alloys And Compounds, v. 215, n. 1-2, p. 227-233, Elsevier BV. (1994)

[61] YARTYS, V.A; GUTFLEISCH, O; HARRIS, I.R. Further studies of hydrogenation, disproportionation, desorption and recombination processes in a Nd5Fe2B6 boride. Journal Of Alloys And Compounds, v. 253-254, p. 134-139, Elsevier BV. (1997)

[62] CANNESAN, N., HARRIS, I.R. Aspects of NdFeB HDDR Powders: Fundamentals and Processing. In: Hadjipanayis, G.C. (eds) Bonded Magnets. NATO Science Series, vol 118. Springer, Dordrecht. (2003)

[63] NAKAYAMA, R.; TAKESHITA, T.; ITAKURA, M.; KUWANO, N.; OKI, K.. Microstructures and crystallographic orientation of crystalline grains in anisotropic Nd-Fe-Co-B-(Ga or Zr) magnet powders produced by the hydrogenation-decomposition-desorption-recombination process. Journal Of Applied Physics, v. 76, n. 1, p. 412-417, AIP Publishing. (1994)

[64] HARRIS, I.R. The Use of Hydrogen in the Production of Nd-Fe-B-Type Magnets and in the Assessment of Nd-Fe-B-Type Alloys and Permanent Magnets. Proceedings of 12th International Workshop on RE Magnets and their Applications, Camberra, 347. (1992)

[65] NAKAYAMA, R.; TAKESHITA, T. Nd-Fe-B anisotropic magnet powders produced by the HDDR process. Journal Of Alloys And Compounds, v. 193, n. 1-2, p. 259-261. Elsevier BV. (1993)

[66] LI, W.F.; OHKUBO, T.; HONO, K.; SAGAWA, M.. The origin of coercivity decrease in fine grained Nd–Fe–B sintered magnets. Journal Of Magnetism And Magnetic Materials, v. 321, n. 8, p. 1100-1105. Elsevier BV. (2009)

[67] KRONMÜLLER, H.; SCHREFL, T.. Interactive and cooperative magnetization processes in hard magnetic materials. Journal Of Magnetism And Magnetic Materials, v. 129, n. 1, p. 66-78, Elsevier BV (1994)

[68] MINOWA, T.. Rare Earth Magnets: conservation of energy and the environment. Resource Geology, v. 58, n. 4, p. 414-422, Wiley. (2008)

[69] RADEMAKER, J. H.; KLEIJN, R.; YANG, Y.. Recycling as a Strategy against Rare Earth Element Criticality: a systemic evaluation of the potential yield of NdFeB magnet recycling. Environmental Science & Technology, v. 47, n. 18, p. 10129-10136, American Chemical Society (ACS). (2013)

[70] ITOH, M.; MASUDA, M.; SUZUKI, S.; MACHIDA, K.-I. Recycle for sludge scrap of Nd-Fe-B sintered magnet as isotropic bonded magnet. (2004)

[71] SAGUCHI, A.; ASABE, K.; FUKUDA, T.; TAKAHASHI, W.; SUZUKI, R.O.. Recycling of rare earth magnet scraps: carbon and oxygen removal from Nd magnet scraps. Journal Of Alloys And Compounds, v. 408-412, p. 1377-1381, Elsevier BV. (2006)

[72] CUI, X. G.; YAN, M.; MA, T. Y.; LUO, W.; TU, S. J. Fabrication of low-cost Nd–Fe–B sintered magnets reusing ultrafine powders. Materials Science And Technology, v. 26, n. 2, p. 193-196, Informa UK Limited. (2010)

[73] LI, X.T.; YUE, M.; LIU, W.Q.; LI, X.L.; YI, X.F.; HUANG, X.L.; ZHANG, D.T.; CHEN, J.W.. Large batch recycling of waste Nd–Fe–B magnets to manufacture sintered magnets with improved magnetic properties. Journal Of Alloys And Compounds, v. 649, p. 656-660 Elsevier BV. (2015)

[74] ÖNAL, M.; JÖNSSON, C.; ZHOU, W.; VAN GERVEN, T.; GUO, M.; WALTON, A.; BLANPAIN, B.. Comparative oxidation behavior of Nd-Fe-B magnets for potential recycling methods: effect of hydrogenation pre-treatment and magnet composition. Journal Of Alloys And Compounds, v. 728, p. 727-738, Elsevier BV. (2017)

[75] PROSPERI, D.; BEVAN, A.I.; UGALDE, G.; TUDOR, C.O.; FURLAN, G.; DOVE, S.; LUCIA, P.; ZAKOTNIK, M.. Performance comparison of motors fitted with magnet-to-magnet recycled or conventionally manufactured sintered NdFeB. Journal Of Magnetism And Magnetic Materials, v. 460, p. 448-453, Elsevier BV. (2018)

[76] LALANA, E. H.; DEGRI, M. J. J.; BRADSHAW, A.; WALTON, A. Recycling of Rare Earth Magnets by Hydrogen Processing and Re-Sintering European Congress and Exhibition on Powder Metallurgy. European PM Conference Proceedings; Shrewsbury, (2016).

[77] GUTFLEISCH, O.; GÜTH, K.; WOODCOCK, T.; SCHULTZ, L.. Recycling Used Nd-Fe-B Sintered Magnets via a Hydrogen-Based Route to Produce Anisotropic, Resin Bonded Magnets. Advanced Energy Materials, v. 3, n. 2, p. 151-155, Wiley. (2012)

[78] IKRAM, A.; MEHMOOD, M. F.; PODLOGAR, M.; ELDOSOUKY, A.; SHERIDAN, R.; AWAIS, M.; WALTON, A.; KRžMANC, M.; TOMSE, T.; KOBE, S.. The sintering mechanism of fully dense and highly coercive Nd-Fe-B magnets from the recycled HDDR powders reprocessed by spark plasma sintering. Journal Of Alloys And Compounds, v. 774, p. 1195-1206, Elsevier BV. (2019)

[79] NOH, T.; CHA, H.; KIM, Y.; LEE, J.. High Coercive RE-Fe-B Powders Recycled via HD and HDDR Process from Waste Magnets. Journal Of Magnetics, v. 27, n. 2, p. 117-122, The Korean Magnetics Society. (2022)

[80] LIXANDRU, A.; VENKATESAN, P.; JÖNSSON, C.; POENARU, I.; HALL, B.; YANG, Y.; WALTON, A.; GÜTH, K.; GAUß, R.; GUTFLEISCH, O.. Identification and recovery of rare-earth permanent magnets from waste electrical and electronic equipment. Waste Management, v. 68, p. 482-489, Elsevier BV. (2017)

[81] DIEHL, O.; SCHÖNFELDT, M.; BROUWER, E.; DIRKS, A.; RACHUT, K.; GASSMANN, J.; GÜTH, K.; BUCKOW, A.; GAUß, R.; STAUBER, R.. Towards an Alloy Recycling of Nd–Fe–B Permanent Magnets in a Circular Economy. Journal Of Sustainable Metallurgy, v. 4, n. 2, p. 163-175, Springer Science and Business Media LLC. (2018)

[82] YUE, M.; YIN, X.; LIU, W.; LU, Q.. Progress in recycling of Nd–Fe–B sintered magnet wastes. Chinese Physics B, v. 28, n. 7, p. 077506, IOP Publishing. (2019)

[83] SCHULTZ, L; EL-AZIZ, A.M; BARKLEIT, G; MUMMERT, K. Corrosion behaviour of Nd–Fe–B permanent magnetic alloys. Materials Science And Engineering: A, v. 267, n. 2, p. 307-313, Elsevier BV. (1999)

[84] KUMAR, M B.; SATHIYA, P. Methods and materials for additive manufacturing: a critical review on advancements and challenges. Thin-Walled Structures, v. 159, p. 107228, Elsevier BV. (2021)

[85] GAO, W.; ZHANG, Y.; RAMANUJAN, D.; RAMANI, K.; CHEN, Y.; WILLIAMS, C. B.; WANG, C.C.L.; SHIN, Y.C.; ZHANG, S.; ZAVATTIERI, P. D.. The status, challenges, and future of additive manufacturing in engineering. Computer-Aided Design, v. 69, p. 65-89, Elsevier BV. (2015)

[86] WANG, H.; LAMICHHANE, T.N.; PARANTHAMAN, M.P. Review of additive manufacturing of permanent magnets for electrical machines: a prospective on wind turbine. Materials Today Physics, v. 24, p. 100675, Elsevier BV. (2022)

[87] PPEYRE, P.; ROUCHAUSSE, Y.; DEFAUCHY, D.; RÉGNIER, G.. Experimental and numerical analysis of the selective laser sintering (SLS) of PA12 and PEKK semi-crystalline polymers. Journal Of Materials Processing Technology, v. 225, p. 326-336,. Elsevier BV. (2015).

[88] GIBSON, I.; ROSEN, D.; STUCKER, B.. Additive Manufacturing Technologies: 3d printing, rapid prototyping, and direct digital manufacturing. 2. ed. New York: Springer, (2015)

[89] ZAKOTNIK, M.; DEVLIN, E.; HARRIS, I. R.; WILLIAMS, A. J. Hydrogen decrepitation and recycling of NdFeB-type sintered magnets. Proceedings of the 19th International Workshop on Rare Earth Permanent Magnets & Their Applications, p. 289-295, (2006)

[90] ZAKOTNIK, M.; WILLIAMS, A. J.; HARRIS, I. R. Possible methods of recycling NdFeB-type sintered magnets using the HD/Degassing or HDDR processes. Paper presented at the 18th International Workshop on High Performance Magnets and their Applications, pp. 267-274, (2004)

[91] PÉRIGO, E. A.; SILVA, S. C.; MARTIN, R. V.; TAKIISHI, H.; LANDGRAF, F. J. G. Properties of hydrogenation-disproportionation-desorption-recombination NdFeB powders prepared from recycled sintered magnets. Journal of Applied Physics, 111, 07A725 (2012)

[92] BALDISSERA, A. B.; PAVEZ, P.; WENDHAUSEN, P. A. P.; AHRENS, C. H.; MASCHERONI, J. M.. Additive Manufacturing of Bonded Nd–Fe–B—Effect of Process Parameters on Magnetic Properties. Ieee Transactions On Magnetics, v. 53, n. 11, p. 1-4, Institute of Electrical and Electronics Engineers (IEEE). (2017).

[93] FIM, R.G.T.; MASCHERONI, A.A.; ANTUNES, L.F.; ENGERROFF, J.B.e.; AHRENS, C.H.; WENDHAUSEN, P.A.P.. Increasing packing density of Additively Manufactured Nd-Fe-B bonded magnets. Additive Manufacturing, v. 35, p. 101353. Elsevier BV. (2020)

[94] 3D SYSTEMS "DuraForm PA Datasheet" Available in: https://www.3dsystems.com/materials/duraform-gf. Acessed in December 2022

[95] MCGUINESS, P. J.; DEVLIN, E.; HARRIS, I. R.; ROZENDAAL, E.; ORMEROD, J.. A study of Nd-Fe-B magnets produced using a combination of hydrogen decrepitation and jet milling. Journal Of Materials Science, v. 24, n. 7, p. 2541-2548, Springer Science and Business Media LLC. (1989)

[96] GUTFLEISCH, O. Controlling the properties of high energy density permanent magnetic materials by different processing routes. Journal Of Physics D: Applied Physics, v. 33, n. 17, p. 157-172, IOP Publishing. (2000)

[97] GUTFLEISCH, O.; HARRIS, I. R. In-situ electrical resistivity measurements: study of magnetic and phase transitions and solid-hddr processes in nd-fe-b-type alloys. Journal Of Materials Science, v. 30, n. 6, p. 1397-1404, Springer Science and Business Media LLC. (1995)

[98] GUTFLEISCH, O.; MATZINGER, M.; FIDLER, J.; HARRIS, I.R. Characterization of solid-HDDR processed Nd16Fe76B8 alloys by means of electron microscopy. Journal Of Magnetism And Magnetic Materials, v. 147, n. 3, p. 320-330, Elsevier BV. (1995)

[99] RÖHRIG, M.; FIM, R. G. T.; QUISPE, L. T.; LANDGRAF, F. J. G.; AHRENS, C. H.; PLA CID, C. C.; WENDHAUSEN, P. A. P. On the feasibility of using Sm2Fe17Nx powders obtained via HDDR process for laser powder bed fusion of bonded permanent magnets. Journal Of Magnetism And Magnetic Materials, v. 565, p. 170273, Elsevier BV. (2023).

[100] SCHÄFER, K.; BRAUN, T.; RIEGG, S.; MUSEKAMP, J.; GUTFLEISCH, O.. Polymer-bonded magnets produced by laser powder bed fusion: influence of powder morphology, filler fraction and energy input on the magnetic and mechanical properties. Materials Research Bulletin, v. 158, p. 112051, Elsevier BV. (2023)

[101] SILVA, M. R. M. Aplicação de Pós Nanocristalinos à base de Sm-Fe-N em Manufatura Aditiva de Ímãs Compósitos. 2023. 100 f. Tese (Doutorado) - Universidade Federal de Santa Catarina, Florianópolis, (2023)

[102] MA, Q.; ZHANG, Z.; HU, Z.; ZHANG, X.; YUE, M.; LIU, Y.; LIU, F.; JU, X.; ZHANG, J.. Magnetic Domain Evolution in Sintered Nd–Fe–B Magnet during Magnetization Process. Journal Of Superconductivity And Novel Magnetism, v. 31, n. 6, p. 1665-1668, Springer Science and Business Media LLC. (2018)

[103] SODERžNIK, M.; SEPEHRI-AMIN, H.; SASAKI, T.T.; OHKUBO, T.; TAKADA, Y.; SATO, T.; KANEKO, Y.; KATO, A.; SCHREFL, T.; HONO, K.. Magnetization reversal of exchange-coupled and exchange-decoupled Nd-Fe-B magnets observed by magneto-optical Kerr effect microscopy. Acta Materialia, v. 135, p. 68-76, Elsevier BV. (2017)

[104] LOPES, L.; CARVALHO, M.; CHAVES, R.; TREVISAN, M.; WENDHAUSEN, P.A.P.; TAKIISHI, H.. Study of Carbon Influence on Magnetic Properties of Metal Injection Molding Nd-Fe-B Based Magnets. Materials Science Forum, v. 727-728, p. 124-129, Trans Tech Publications, Ltd.. (2012)

[105] LOPES, L.; FOOK, P.; OWCZARZAK, A.; UENAL, N.; HARTWIG, T.; WENDHAUSEN, P.. Feasibility Study for Feedstock Recycling on PIM Nd-Fe-B Permanent Magnets. Materials Science Forum, v. 802, p. 574-578, Trans Tech Publications, Ltd.. (2014)

[106] MO, W.; ZHANG, L.; LIU, Q.; SHAN, A.; WU, J.; KOMURO, M.. Dependence of the crystal structure of the Nd-rich phase on oxygen content in an Nd–Fe–B sintered magnet. Scripta Materialia, v. 59, n. 2, p. 179-182, Elsevier BV. (2008)

[107] SHINBA, Y.; KONNO, T. J.; ISHIKAWA, K.; HIRAGA, K.; SAGAWA, M.. Transmission electron microscopy study on Nd-rich phase and grain boundary structure of Nd–Fe–B sintered magnets. Journal Of Applied Physics, v. 97, n. 5, p. 12-17, AIP Publishing. (2005)

[108] HARRIS, I.R.; MCGUINESS, P.J.. Hydrogen: its use in the processing of ndfeb-type magnets. Journal Of The Less Common Metals, v. 172-174, p. 1273-1284. Elsevier BV. (1991)

[109] KOBAYASHI, K.; SKOMSKI, R.; COEY, J.M.D. Dependence of coercivity on particle size in Sm2Fe17N3 powders. Journal Of Alloys And Compounds, v. 222, n. 1-2, p. 1-7, Elsevier BV. (1995)

[110] SCHÄFER, K.; FIM, R.G.T; MACCARI, F.; BRAUN, T.; RIEGG, S.; SKOKOV, K.P.; KOCH, D.; BRUDER, E.; RADULOV, I.; AHRENS, C.H.. Laser powder bed fusion of anisotropic Nd-Fe-B bonded magnets utilizing an in-situ mechanical alignment approach. Journal Of Magnetism And Magnetic Materials, v. 583, p. 171064, Elsevier BV. (2023)

[111] FIM, R. G. T. Técnicas de Aumento de Remanência em Ímãs Compósitos de Nd-Fe-B obtidos por Manufatura Aditiva. 2023. 100 f. Tese (Doutorado) - Universidade Federal de Santa Catarina, Florianópolis, (2023)

[112] CHUN-LIN, T.; SHU-XIN, B.; HONG, Z.; KE, C.; JIA-CHUN, Z.; XUN, C.. Effects of hydrogen on the oxidation of coarse decrepitated powder of Nd–Dy–Fe–B alloy. Journal Of Alloys And Compounds, v. 368, n. 1-2, p. 333-336, Elsevier BV. (2004)

[113] BALDISSERA, A. B. Ímãs compósitos à base de Nd-Fe-B e PA-12 obtidos por manufatura aditiva. 2018. 100 f. Tese (Doutorado) - Universidade Federal de Santa Catarina, Florianópolis, (2018)

[114] ENGERROF, J. A. B. Manufatura Aditiva de Ímãs Compósitos à base de Sm-Fe-N via Fusão em Leito de Pó a Laser. 2020. 100 f. Tese (Doutorado) - Universidade Federal de Santa Catarina, Florianópolis, (2020)

[115] KRUTH, J. P.; MERCELIS, P.; VAN VAERENBERGH, J.; FROYEN, L.; ROMBOUTS, M. Binding mechanisms in selective laser sintering and selective laser melting, Rapid Prototyp. J., vol. 11, no. 1, pp. 26–36, (2005).

[116] MAPLEY, M.; PAULS, J..; TANSLEY, G.; BUSCH, A.; GREGORY, S.D.. Selective laser sintering of bonded magnets from flake and spherical powders. Scripta Materialia, v. 172, p. 154-158, Elsevier BV. (2019)

[117] NLEBEDIM, I.C.; UCAR, Huseyin; HATTER, Christine B.; MCCALLUM, R.W.; MCCALL, Scott K.; KRAMER, M.J.; PARANTHAMAN, M. Parans. Studies on in situ magnetic alignment of bonded anisotropic Nd-Fe-B alloy powders. Journal Of Magnetism And Magnetic Materials, v. 422, p. 168-173, Elsevier BV. (2017)